



**HAL**  
open science

## Periodate oxidation of cellulose for internal plasticization and materials design

Julien Leguy

► **To cite this version:**

Julien Leguy. Periodate oxidation of cellulose for internal plasticization and materials design. Material chemistry. Université Grenoble Alpes, 2018. English. NNT : 2018GREAV010 . tel-01852166

**HAL Id: tel-01852166**

**<https://theses.hal.science/tel-01852166>**

Submitted on 1 Aug 2018

**HAL** is a multi-disciplinary open access archive for the deposit and dissemination of scientific research documents, whether they are published or not. The documents may come from teaching and research institutions in France or abroad, or from public or private research centers.

L'archive ouverte pluridisciplinaire **HAL**, est destinée au dépôt et à la diffusion de documents scientifiques de niveau recherche, publiés ou non, émanant des établissements d'enseignement et de recherche français ou étrangers, des laboratoires publics ou privés.

## THÈSE

Pour obtenir le grade de

### **DOCTEUR DE LA COMMUNAUTE UNIVERSITE GRENOBLE ALPES**

Spécialité : **Science des Polymères**

Arrêté ministériel : 25 mai 2016

Présentée par

**Julien LEGUY**

Thèse dirigée par **Yoshiharu NISHIYAMA**, Chargé de Recherche, CNRS, et codirigée par **Laurent HEUX**, Directeur de Recherches, CNRS et **Bruno JEAN**, Chargé de Recherche, CNRS

préparée au sein du **Centre de la Recherche sur les  
Macromolécules Végétales (CERMAV)**  
dans l'**École Doctorale Chimie et Sciences du Vivant**

## **Periodate oxidation of cellulose for internal plasticization and materials design**

Thèse soutenue publiquement le **30 mars 2018**,  
devant le jury composé de :

**Monsieur Naceur BELGACEM**

Professeur, Pagora, Président, Examinateur

**Monsieur Wim THIELEMANS**

Professeur, KU Leuven, Rapporteur

**Monsieur Gilles SEBE**

Maître de Conférences, Université de Bordeaux, Rapporteur

**Madame Emily CRANSTON**

Maître de Conférences, Mc Master University, Examinatrice

**Monsieur Yoshiharu NISHIYAMA**

Chargé de Recherches, CERMAV, Directeur de thèse

**Monsieur Laurent HEUX**

Directeur de Recherches, CERMAV, Co-directeur de thèse

**Monsieur Bruno JEAN**

Chargé de Recherches, CERMAV, Co-directeur de thèse, invité

**Monsieur Nathanaël GUIGO**

Maître de Conférences, Université de Nice Sophia Antipolis, Invité









J'aimerais tout d'abord remercier mes directeurs de thèse, Yoshiharu NISHIYAMA, Laurent HEUX et Bruno JEAN pour leurs aides, les discussions scientifiques animées et leur soutien moral durant les mois de rédaction, sans qui ce travail n'aurait pas abouti.

Je remercie également Caroll VERGELATI de la société Solvay pour sa gestion du projet PLACELMAT, ainsi que tous les autres membres du projet pour leurs conseils techniques.

Je remercie l'équipe SPG du CERMAV pour son accueil pendant ces trois ans et particulièrement Marie-France METRAL, Stéphanie PRADEAU et Pierre SAILLIER pour l'aide et la gestion quotidienne de l'équipe.

Je tiens également à remercier personnellement Isabelle JEACOMINE pour sa gestion de la RMN, Henry CHANZY pour son aide à la rédaction et Bruno JEAN pour ces conseils en photographie, ainsi que pour mes innombrables défaites au squash.

Enfin je tiens à remercier Cloé et toute ma famille pour le soutien qu'ils m'ont apporté pendant ces trois années.



<b>List of abbreviations</b>	<b>7</b>
<b>Preface</b>	<b>9</b>
1. <i>The PLACELMAT project</i>	9
2. <i>Thermoplastic context</i>	10
3. <i>Objectives</i>	10
<b>Chapter 1: Literature review</b>	<b>13</b>
1. <i>Cellulose</i>	13
1.1. Structure and microfibrillar organization	14
1.2. Thermo-mechanical properties	14
1.3. Chemical modifications of cellulose	16
1.3.1. Hydrolysis and substitutions	16
1.3.2. Oxidation reactions	17
2. <i>Cellulose acetate</i>	18
2.1. Overview	18
2.2. Industrial uses	19
2.3. Thermal properties	19
3. <i>Plasticizers</i>	20
3.1. External plasticizers	20
3.2. Internal plasticization	21
4. <i>Plasticizers in the case of CAC</i>	22
4.1. Plasticization effects on CAC	22
4.2. Chemical hazards of external plasticizers for CAC	22
5. <i>Periodate oxidation</i>	23
5.1. Periodate oxidation substrates	24
5.2. Cellulose periodate oxidation protocols	24
5.3. Historical use: polysaccharides characterization	26

5.4. Current uses: a platform for functional material	26
5.4.1. Direct uses of POC	27
5.4.2. Reduction	27
5.4.3. Post-oxidation	29
5.4.4. Grafting	32
5.4.4.1. Imination/reductive amination protocols	33
5.4.4.2. Properties of amine-grafted-POC materials	34
6. Colloidal suspensions	36
6.1. Preparation of stable CNC suspensions	37
6.1.1. Direct electrostatic stabilization	37
6.1.2. Indirect stabilization	38
6.1.2.1. Electrostatic stabilization	38
6.1.2.2. Steric stabilization	38
6.2. Properties of materials made from colloidal suspensions	40
<b>Chapter 2: Accurate degree of oxidation measurement of periodate oxidized cellulose by CP-MAS <sup>13</sup>C NMR</b>	<b>43</b>
1. Introduction	43
2. Materials and methods	47
2.1. Materials	47
2.2. MFC oxidation to POC	47
2.3. Measuring the degree of oxidation (DO)	48
2.3.1. Periodate consumption monitored by UV-visible spectroscopy, yielding DO <sub>UV</sub>	48
2.3.2. Aldehyde amount deduced from the quantitative reaction with hydroxylamine hydrochloride	49
2.3.2.1. Titration of released HCl (DO <sub>t-NaOH</sub> )	49
2.3.2.2. Titration of consumed base (DO <sub>t-HCl</sub> )	49
2.3.3. <sup>13</sup> C CP-MAS solid-state NMR spectroscopy	50
2.3.3.1. DO estimation from NMR spectra (DO <sub>NMR</sub> )	50

3. <i>Results and discussion</i>	52
3.1. Obtaining DOs from NaOH oxime titration ( $DO_{t-NaOH}$ ):	52
3.2. Comparison of the titration protocols ( $DO_{t-NaOH}$ and $DO_{t-HCl}$ ):	54
3.3. Obtaining DOs from titration with UV-Visible Spectroscopy ( $DO_{UV}$ ):	55
3.4. Obtaining DOs from CP-MAS $^{13}C$ NMR spectroscopy ( $DO_{NMR}$ ):	55
3.5. Heterogeneous reaction leading to $DO_{UV} > DO_{NMR}$	58
3.6. Agreement between $DO_{NMR}$ and $DO_{t-HCl}$	61
4. <i>Conclusions</i>	61
<b>Chapter 2: Supporting information</b>	<b>63</b>
<b>Chapter 3: Synthesis and characterization of all-cellulose thermoplastics</b>	<b>73</b>
1. <i>Introduction</i>	73
2. <i>Materials and methods</i>	76
2.1. Materials	76
2.2. Periodate modification of MFC	76
2.3. Reduction of POC	77
2.4. Film casting	78
2.5. CP-MAS solid-state NMR	78
2.6. Thermogravimetric analysis (TGA)	78
2.7. Differential scanning calorimetry (DSC)	78
2.8. Dynamic mechanical analysis (DMA)	79
2.9. X-Ray Diffraction (XRD)	79
3. <i>Results and discussion</i>	80
3.1. Ultrastructural characterization	80
3.2. Thermal properties	83
3.3. Dynamic mechanical analysis	86
3.4. Wideline separation NMR (WISE)	87

3.5. Discussion	91
4. Conclusions	95
<b>Chapter 3: Supporting information</b>	<b>97</b>
<b>Chapter 4: Periodate oxidation followed by NaBH<sub>4</sub> reduction converts microfibrillated cellulose into sterically-stabilized neutral cellulose nanorod suspensions</b>	<b>101</b>
1. Introduction	101
2. Materials and methods	104
2.1. Materials	104
2.2. MFC oxidations to POC	104
2.3. POC reduction by NaBH <sub>4</sub> (rPOC)	105
2.4. <sup>13</sup> C CP-MAS solid-state NMR	105
2.5. Carbonyl group content: degree of oxidation (DO)	106
2.6. Dynamic light scattering (DLS)	106
2.7. ζ-potential measurements	107
2.8. Turbidimetry measurements	107
2.9. Transmission electron microscopy (TEM)	108
2.10. Small-angle X-ray scattering (SAXS)	108
3. Results and discussion	109
3.1. POC and rPOC synthesis	109
3.2. Suspension stability and nanoparticles dimensions	111
3.3. Core-shell structure	117
4. Conclusions	121
<b>Chapter 4: Supporting information</b>	<b>123</b>
<b>Chapter 5: Cellulose-based thermoplastics through periodate cleavage and amine grafting</b>	<b>127</b>
1. Introduction	130

2. <i>Materials and methods</i>	131
2.1. Materials	131
2.2. MFC oxidations to POC	132
2.3. POC grafting via reductive amination	132
2.4. <sup>13</sup> C CP-MAS solid-state NMR	133
2.5. Two-dimensional wide-line separation nuclear magnetic resonance (WISE NMR)	133
2.6. Carbonyl group content: degree of oxidation (DO)	134
2.7. Degree of substitution (DS)	134
2.8. Thermogravimetric analysis (TGA)	135
2.9. Differential Scanning calorimetry (DSC)	135
2.10. Dynamic mechanical analysis (DMA)	135
3. <i>Results and Discussion</i>	136
3.1. POC synthesis and amine grafting	136
3.2. Characterization of thermal properties	141
3.3. Mechanical properties of amine-grafted samples films	144
3.4. Mobile versus rigid components from 2D WISE NMR	147
4. <i>Conclusions</i>	150
<b>Conclusions and perspectives</b>	<b>153</b>
<i>Conclusions</i>	153
<i>Perspectives</i>	157
<b>Résumé étendu en français</b>	<b>161</b>
<b>References</b>	<b>171</b>



# List of abbreviations

---

AGU: anhydroglucose unit

BBP: benzyl butyl phthalate

CAC: cellulose acetate

CESA: cellulose synthase

CMC: carboxymethyl cellulose

CNC: cellulose nanocrystals

CAB: cellulose acetate butyrate

CAP: cellulose acetate propionate

CBu: cellulose butyrate

CP-MAS NMR: cross-polarized/magic angle spinning NMR

CPr: cellulose propionate

DAC: dialdehyde cellulose

DAMC: dialdehyde-modified cellulose

DCC: dicarboxylic acid cellulose

DEHP: bis (2-ethylhexyl) phthalate

DMA: dynamic mechanical analysis

DO: degree of oxidation

DO<sub>max</sub>: maximum theoretical reachable DO

DO<sub>t-HCl</sub>: DO measured by the oxime titration at pH 5

DO<sub>t-NaOH</sub>: DO measured by the oxime titration at pH<3.2

DO<sub>UV</sub>: DO measured by the UV method

DS: degree of substitution

DSC: differential scanning calorimetry

MFC: microfibrillated cellulose

NMR: nuclear magnetic resonance

PEG: polyethylene glycol

PET: polyethylene terephthalate

PLACELMAT: plasticized cellulose materials

PMMA: poly(methyl methacrylate)

POC: periodate oxidized cellulose

PS: polystyrene

rPOC: reduced periodate oxidized cellulose

TEMPO: (2,2,6,6-tetramethylpiperidin-1-yl)oxyl

T<sub>g</sub>: glass transition temperature

T<sub>m</sub>: melting temperature

UV: ultra-violet

XRD: X-ray diffraction

# Preface

## 1. The PLACELMAT project

This PhD work is part of the “Agence Nationale pour la recherche (ANR)”-funded **PL**asticized **CELL**ulose **MAT**erials (PLACELMAT) project, which gathers three academic laboratories (the “Institut National des Sciences Appliquées” – INSA – and the “Institut de recherches sur la catalyse et l’environnement” – IRCE – in Lyon and the Centre de recherche sur les macromolécules végétale” – CERMAV – in Grenoble) and the Solvay Company, former owner of the historical cellulose acetate company (Acetow) and 3<sup>rd</sup> biggest producer of cellulose acetate in the world, each partner having a specific role as specified in Figure 1.

The goal of this PhD is to make an experimental proof of concept in the investigation of a new chemical modification of cellulose that can compete with, or replace cellulose acetate as thermoplastic.



Figure 1. Partners of the PLACELMAT project, and their respective task

## 2. Thermoplastic context

Many materials used in day-to-day life are thermoplastics:<sup>1</sup> polyethylene terephthalate (PET) for plastic bottles, polystyrene (PS) for pens and packaging foams, or poly(methyl methacrylate) (PMMA) for plastic windows are some examples.

The term thermoplastic implies these polymers have a characteristic temperature called the glass transition temperature ( $T_g$ ), above which they soften and easily flow, but recover their rigidity when cooled down.<sup>2</sup> This property allows industrial shaping of polymers with a large variety of thermo-forming processes:<sup>1</sup> the polymers are heated above their  $T_g$ , shaped and then cooled down to keep their final shape. Injection or compression molding and vacuum forming are some examples of these shaping processes.

The general industrial practice is to work at  $T_g + 50^\circ\text{C}$  to have viscosities as low as possible, which facilitate the shaping processes described above. Alternatively, the processing temperature can also be above the melting temperature,  $T_m$ , if the polymers are semi-crystalline (the  $T_g$  being lower than  $T_m$ , all the amorphous and crystalline regions of the polymer would then have a low viscosity).

## 3. Objectives

Cellulose, as the most abundant polymer on earth,<sup>3</sup> appears to be one of the best raw material to potentially replace the oil-based polymers and especially thermoplastics. As a linear polymer with a glass transition temperature, and by definition, cellulose is a semi-crystalline thermoplastic. However, cellulose cannot easily be used in the industry: its high  $T_g$  and its melting temperature beyond its degradation temperature<sup>4-5</sup> would

lead to degradation if submitted to a thermo-forming process. Cellulose acetate (CAc), one of the most used cellulose derivative in the industry, shows better thermoplastic properties but still requires the use of plasticizers, which can exude after migrating out of the polymer matrix overtime leading to a loss of the ductility of the material and to potential environmental issues in the case of molecules of high concern.

The goal of the present project is to design and develop internally plasticized cellulose-based polymers (without any added plasticizer) and investigate their thermo-mechanical properties. Internal plasticization should result in equivalent properties as adding external plasticizers, but would prevent any diffusion of plasticizers out of the polymer matrix. It would lead to more stable polymers regarding aging, and more environmentally-friendly compounds regarding release of toxic substances.

The cellulose (and CAc) chain is intrinsically rigid, which is one of the causes of its high  $T_g$  and  $T_m$ .<sup>4-8</sup> Consequently, an alternative way to decrease the  $T_g$  of either cellulose or CAc is to increase their backbone mobility. Since in both cases the macromolecule's lack of flexibility is mainly due to the glycosyl ring, cleaving one of its bonds should provide the desired flexibility, while keeping the backbone integrity (Figure 2a). Additionally, the cleavage of the glycosyl ring would remove the numerous H-bonds in which the anhydroglucose units (AGU) are involved and induce a major release of molecular motions within the chains and between the chains. Furthermore, the grafting of bulky side groups using controlled reactions should further increase the free volume, contributing to the internal plasticization (Figure 2b).

This innovative two-steps strategy depicted in Figure 2 should lead to internally-plasticized cellulose derivatives.

The present thesis will be composed of a literature survey and four chapters, each one is intended to be the manuscript of a scientific publication, and divided as follows:

- The first chapter will be a literature review;
- The second chapter will detail the cleavage reaction of cellulose namely the periodate oxidation, and the ways to precisely characterize it (Submitted to ACS Sustainable Chemistry and Engineering);
- The third chapter deals with the molecular structure and the thermomechanical properties of all-cellulose films obtained by casting of oxidized cellulose suspensions having undergone a reduction reaction;
- The fourth chapter explores the properties of oxidized then reduced suspensions in terms of colloidal stability and the structures and dimensions of the obtained nanoparticles;
- Finally, the fifth chapter will review the preparation and properties of thermoplastic materials obtained after grafting of amines on periodate-oxidized substrates.

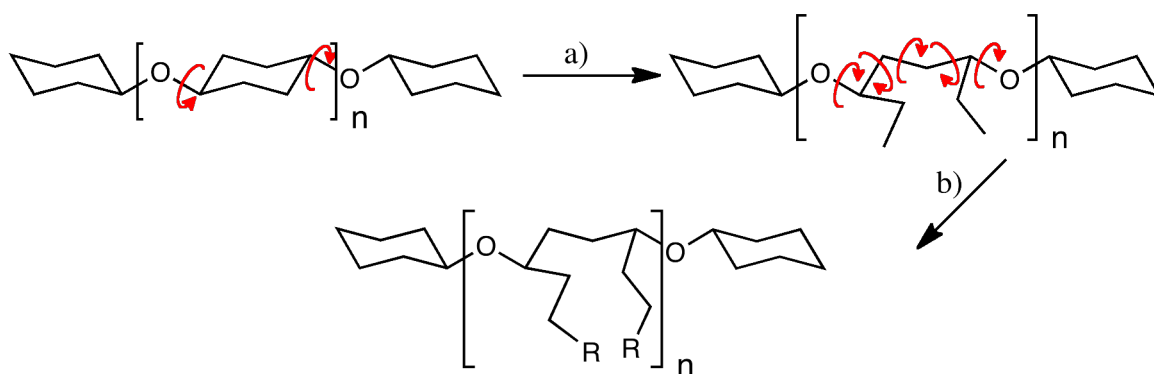


Figure 2. Schematic representation of the increased chain mobility after cleaving a bond of some AGU along the macromolecule (cellulose or CAC). Red arrows represent the degrees of freedom of the chain before and after the cleavage (a). Grafting on the cleaved AGU to increase the free volume between chains (b).

# Chapter 1: Literature review

## 1. Cellulose

Cellulose is a natural polymer mainly synthesized by plants, trees and algae but also by some bacteria and sea animals such as tunicate. Cellulose is synthesized at the plasma membrane by cellulose synthases (CESA).<sup>9</sup> In higher plants, the CESAs are organized in rosette. Each CESA protein synthesizes a cellulose chain, which collapses into a microfibril with other chains synthesized in the same rosette. The secondary cell walls are produced when the cell expansion is finished and thickening occurs. The secondary cell walls account for the majority of the biomass. The primary cell walls that are produced in the expanding cells are important in morphogenesis of plants, but have less importance in terms of biomass. Secondary plant cell walls can be seen as nanocomposites: the cellulose is organized in the form of slender nanometric rods (called cellulose microfibrils) that act as fillers, while the other components like hemicellulose and lignin act as the matrix (Figure 3).

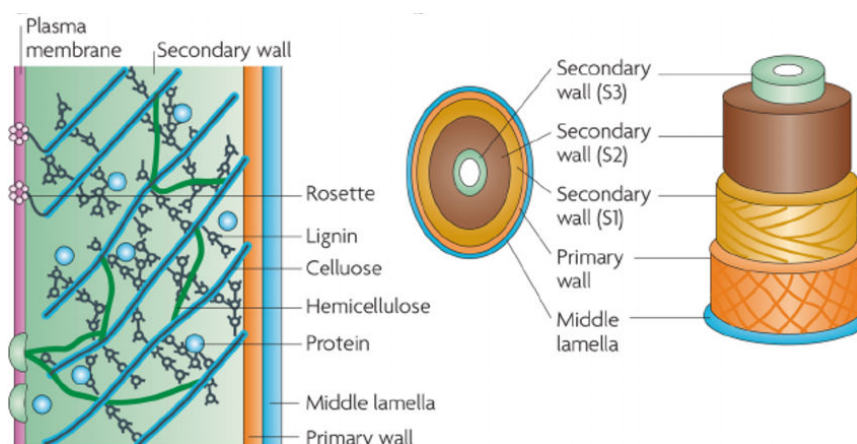


Figure 3. Schematic representation of plant cell walls<sup>10</sup>

## 1.1. Structure and microfibrillar organization

Cellulose is a linear homopolysaccharide of D-anhydroglucopyranose unit (AGU) connected by  $\beta$ -1,4 linkages, which tends to organize into crystalline fibrils (Figure 4a-b).

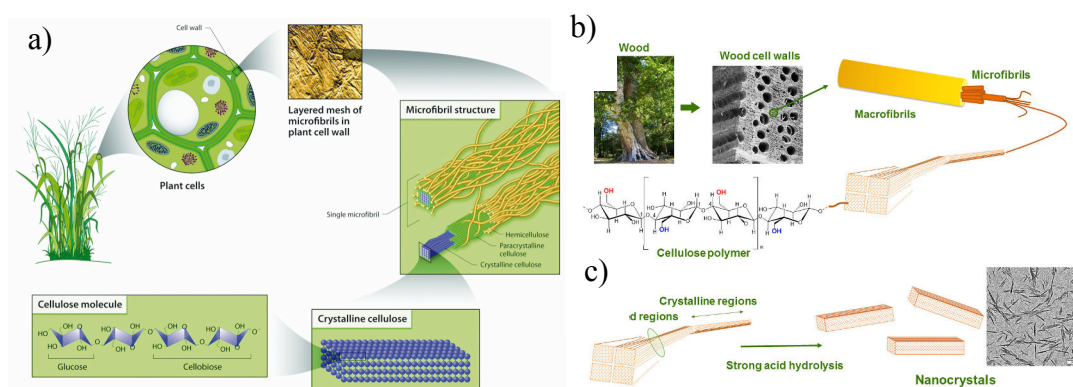


Figure 4. Origin, composition and structure of cellulose microfibrils (a and b) and cellulose nanocrystals synthesis from microfibrils (c).<sup>11-12</sup>

The microfibrils are not perfect: some defects are present along the chain direction. These defects can be used to cleave the fibers by acid hydrolysis leading to smaller objects of high crystallinity called cellulose nanocrystals (CNCs) (Figure 4c).

## 1.2. Thermo-mechanical properties

The high Young's modulus of cellulose crystals estimated to 137 GPa<sup>13</sup> in the longitudinal direction makes it an attractive reinforcing material. Since the 90's, when Favier *et al.*<sup>14</sup> showed that cellulose nanocrystals, also called whiskers for the ones with high aspect ratio, could be used as fillers in nanocomposites to improve the mechanical properties, a wide range of nanocomposite materials incorporating cellulose crystals have been studied.<sup>15-19</sup>

Given its linear structure, cellulose can theoretically be processed like any semi-crystalline thermoplastic. The glass transition temperature,  $T_g$ , of dry cellulose is

estimated to be at around 220 °C<sup>4-5</sup> and the melting temperature,  $T_m$ , is estimated at around 450 °C,<sup>8</sup> though no direct measurements have been reported. The experimental difficulty in evaluating these values comes from the small difference in heat capacity and the overlap with the thermal degradation. The thermal degradation temperature is reported to be around 300 °C but starts at 220 °C with a heating speed of 1.25 °C/min.<sup>5</sup> These high transition temperatures are mainly due to the structure of cellulose: a stiff macromolecule, which organizes in highly crystalline domains. In fact, Gibbs and DiMarzio and later Chee<sup>6-7</sup> demonstrated that the  $T_g$  of a macromolecule is directly linked to its flexibility. As seen in Figure 5, each glucosyl monomer of cellulose is involved in three hydrogen bonds, and the glycosyl ring itself is bulky,<sup>20</sup> resulting in steric hindrance that allows little freedom of rotation around the glycosidic linkages and leading to the reported high  $T_g$  and  $T_m$  values.

These properties make the industrial transformation of neat cellulose as a thermoplastic unfeasible. Therefore, chemical modification and/or plasticization are required to overcome this difficulty.

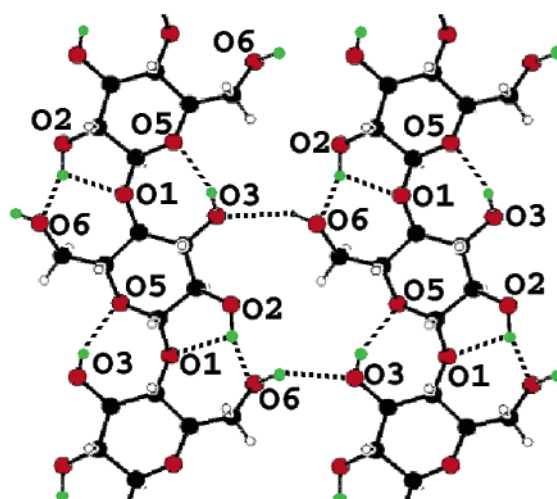


Figure 5. Crystalline structure of cellulose. Dashed lines represent the H-bonds between AGUs.<sup>21</sup>

### 1.3. Chemical modifications of cellulose

Thanks to the three hydroxyl groups present on each AGU, cellulose can easily be chemically modified in several ways as shown in Figure 6.

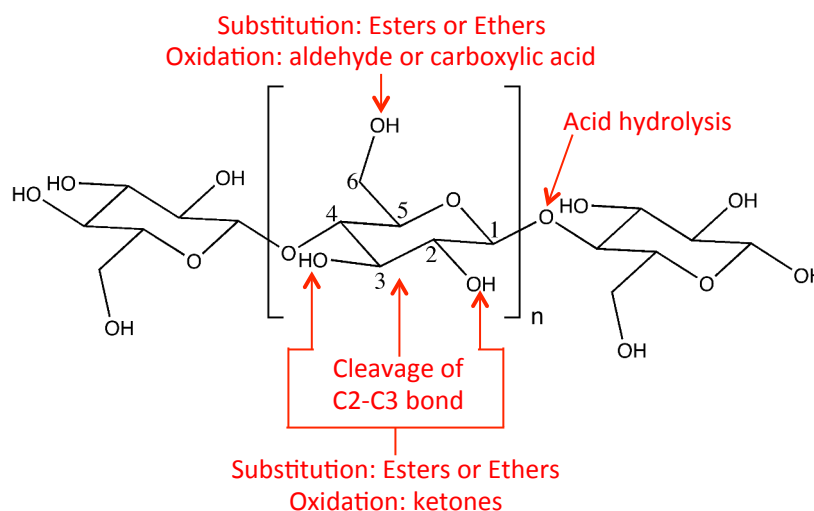


Figure 6. Potential chemical modifications of cellulose

#### 1.3.1. Hydrolysis and substitutions

Among the chemical modification categories presented in Figure 6, the acid hydrolysis is the reaction used to cleave cellulose fibers in order to synthesize CNCs,<sup>22-24</sup> as shown in Figure 4c. This reaction will be further described in section 6.

Cellulose acetate is the result of the partial or full esterification of the three hydroxyl groups with acetyl.<sup>25-26</sup> Cellulose acetate and other cellulose esters will be discussed in section 2.

Other modifications include etherifications. Usually etherification is carried out in alkali-swollen state to obtain block-copolymer-like substitution patterns, but regio-selective homogeneous substitution can also be done in some solvents.<sup>27-29</sup>

### 1.3.2. Oxidation reactions

The hydroxyl groups of cellulose can be oxidized to different states, namely aldehyde, ketone or carboxylic acid, depending on type of alcohol (primary or secondary) and the type of reagent selected.

Oxidizing cellulose with  $\text{NO}_2$  results in the oxidation of the C6 into a carboxylic group (Figure 7). This reaction is industrially used to confer bioresorbability for wound dressing: the materials do not need any mechanical removal, but is broken down by the body tissues. However, different side reactions such as oxidation of the secondary alcohols into ketones, the cleavage of the C2-C3 bond and the formation of aldehyde groups or an incomplete oxidation of the C6 to the aldehyde stage also occur.<sup>30</sup> The  $\text{NO}_2$ -oxidized products are used in the biomedical field for their biocompatibility and bioresorbability.

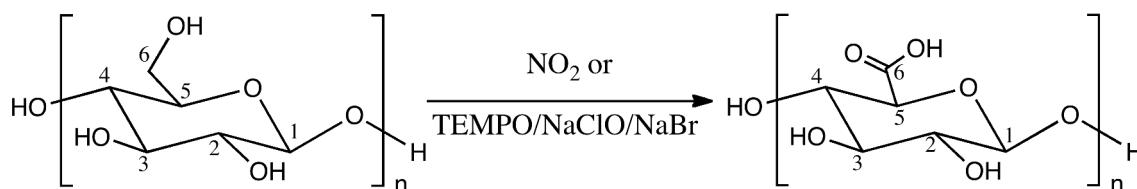


Figure 7. Oxidation of the primary alcohol on the C6 position of the AGU into carboxylic acid, as a result of  $\text{NO}_2$ - or TEMPO-mediated oxidations

In contrast to  $\text{NO}_2$  oxidation, TEMPO-mediated oxidation<sup>31-32</sup> is strictly limited to the primary alcohol at the C6 position (Figure 7). When performed under basic conditions, some cellulose depolymerization can occur by  $\beta$ -elimination.<sup>32-34</sup> This oxidation, widely studied over the last two decades,<sup>35-36</sup> is able to turn fibers, microfibrils or CNCs into negatively charged nano-objects. This reaction is especially suitable for the individualization of cellulose microfibrils facilitated by the electrostatic repulsion induced by the surfaces charges.<sup>37</sup> Additionally, the introduced carboxylic acid is a

convenient intermediate for the subsequent grafting of functional molecules or macromolecules.<sup>38-39</sup>

Another possible route for the oxidation of cellulose is periodate oxidation, which will be described in details in section 5.

## 2. Cellulose acetate

### 2.1. Overview

Until now, one of the most developed cellulose-based polymers used in industry is cellulose acetate (CAc). Invented at the end of the 19<sup>th</sup> century, it is synthesized by reacting acetic anhydride with cellulose, which converts the hydroxyl groups into acetyl groups (Figure 8).<sup>26, 40</sup> The characteristics of CAc vary with its degree of substitution (DS), which is the average number of acetyl groups present on one AGU. This DS can take any value from 0 (for cellulose) to 3 for the cellulose triacetate. The DS of CAc for fiber and filter applications are around 2.45 (arbitrarily called cellulose diacetate). In a standard industrial process, cellulose triacetate is first obtained in the form of a solution in acetic acid. Triacetate is then hydrolyzed in homogeneous conditions by addition of water to decrease its DS to a desired value.<sup>26</sup>

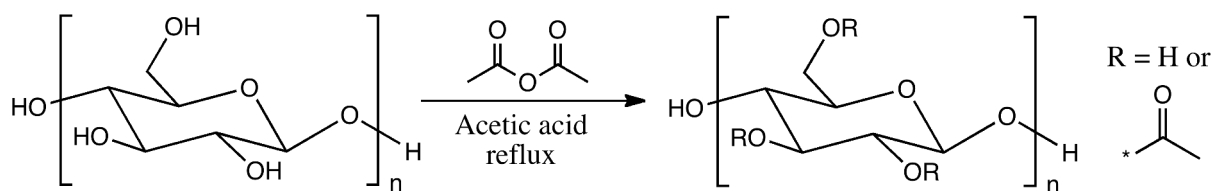


Figure 8. Synthesis of Cellulose Acetate (CAc)

## 2.2. Industrial uses



Figure 9. Time line of the historical uses of cellulose acetate.

The diversification of CAC's industrial applications started about a decade before World War I. At that time CAC was used as films and lacquers (due to its solubility in solvents such as acetone). From there, CAC applications expanded to a large variety of domains such as fibers, frames for glasses, textiles, or tapes (Figure 9). CAC main use was as textile fibers until the 60's when cheaper oil-based fibers arrived on the market (namely polyamides and polyesters). Today, Solvay's diacetate is mainly used as tow for air filters and in particular for cigarette filters.

## 2.3. Thermal properties

CAC has a DS-dependent  $T_g$ , as described by Kamide and Saito<sup>25</sup> and presented in Figure 10: for cellulose tri-acetate, the  $T_g$  is around 190°C,<sup>4, 25</sup> and is around 210 °C for a degree of substitution of 2.5.<sup>25</sup> Other ester substituents like propionate (CPr) or butyrate (CBu) can be grafted instead of acetate.<sup>41-45</sup> Butyrate and propionate derivatives and their combination with acetate (cellulose acetate propionate, CAP, and cellulose acetate butyrate, CAB) have lower  $T_g$  compared to CAC with identical DS (Figure 10),<sup>25, 44-52</sup> and

exhibit better flow properties above  $T_g$ , hence need less plasticizers<sup>43</sup> (see section 3.1) but are more expensive.

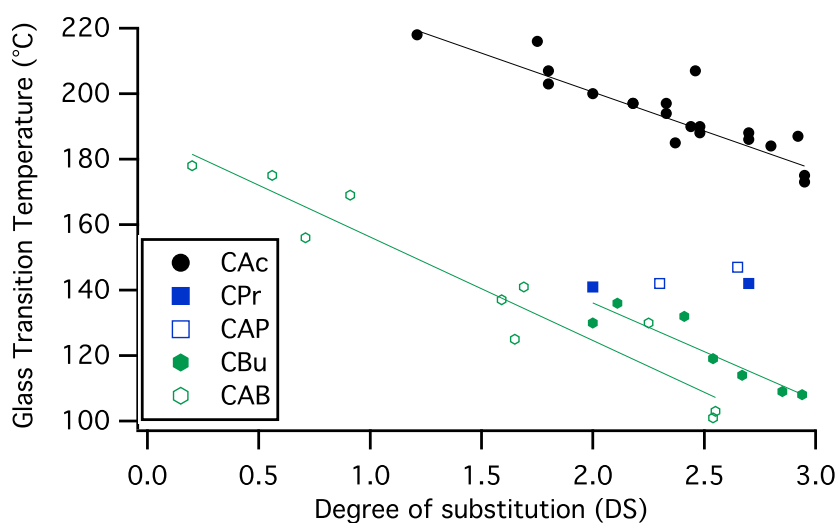


Figure 10. Glass transition temperatures of different cellulose esters as a function of their degree of substitution (CAc: cellulose acetate, CPr: cellulose propionate, CAP: cellulose acetate propionate, CBu: cellulose butyrate, CAB; cellulose acetate butyrate). (The DS of acetate groups is not taken in account for CAP and CAB).<sup>25, 44-52</sup>

## 3. Plasticizers

### 3.1. External plasticizers

External plasticizers are low molecular weight molecules that are added into polymer formulations to act as lubricants between the amorphous polymeric chains. They increase the free volume between the macromolecules, facilitating their reptation. They are expected to decrease the  $T_g$  and the  $T_m$  of the material, hence to facilitate the polymer processing and modify the overall thermo-mechanical properties,<sup>53</sup> leading to higher flexibility and reduced brittleness for specific material applications.<sup>43</sup>

Plasticizers are cheap molecules (cheaper than polymers) used in significant amount in polymer formulations (several tens of %). Thus, in addition to the improvement of

thermo-mechanical properties, they also contribute to reduce the price of the final material.

The problem of these small molecules is that they can easily migrate through the polymer matrix over time until reaching the surface of the material and being expelled. This phenomenon is called exudation.<sup>43, 54</sup> The proportion of plasticizer inside the polymer matrix decreases and, as a consequence, the material loses its thermo-mechanical properties.<sup>54</sup>

In addition to the loss of mechanical properties, depending on the toxicity of the plasticizers, exudation might cause environmental issues. In fact, as the exudation brings the plasticizer from inside of the polymer matrix to the surface, the end users might be in direct contact with the plasticizer, which can be problematic in the case of bioactive or toxic substances.

### **3.2. Internal plasticization**

Internal plasticizers have the exact same roles and uses as external plasticizers. The only difference is that they are chemically bound to the polymer, hence free of any exudation issues compared to classical external plasticizers. Since internal plasticizers are part of the polymer, internally plasticized macromolecules are in fact self-plasticized polymers. This type of plasticization is rarely used due to its high cost related to the need for chemical modifications steps. Furthermore, substantial R&D efforts need to be undertaken to obtain a self-plasticized polymer to meet the precise industrial requirements.

Nevertheless, internal plasticizing would lead to more stable and durable polymers and solve some environmental issues, which is worth the effort.

## 4. Plasticizers in the case of CAC

### 4.1. Plasticization effects on CAC

Even if CAC exhibits thermoplastic properties, it cannot be directly used as a thermoplastic: its melting temperature is still too close to its degradation temperature<sup>25</sup> (Figure 11a-b), which, as in the case of cellulose, would lead to thermal degradation in real situation of thermo-forming. The effects on  $T_g$ ,  $T_m$  and  $T_{deg}$  of acetylation of cellulose into CAC and then the effect of plasticization of CAC are described in Figure 11.

To further decrease the glass transition temperature, large amounts of plasticizer (30 to 50%) need to be incorporated into CAC formulations.<sup>26, 43</sup>

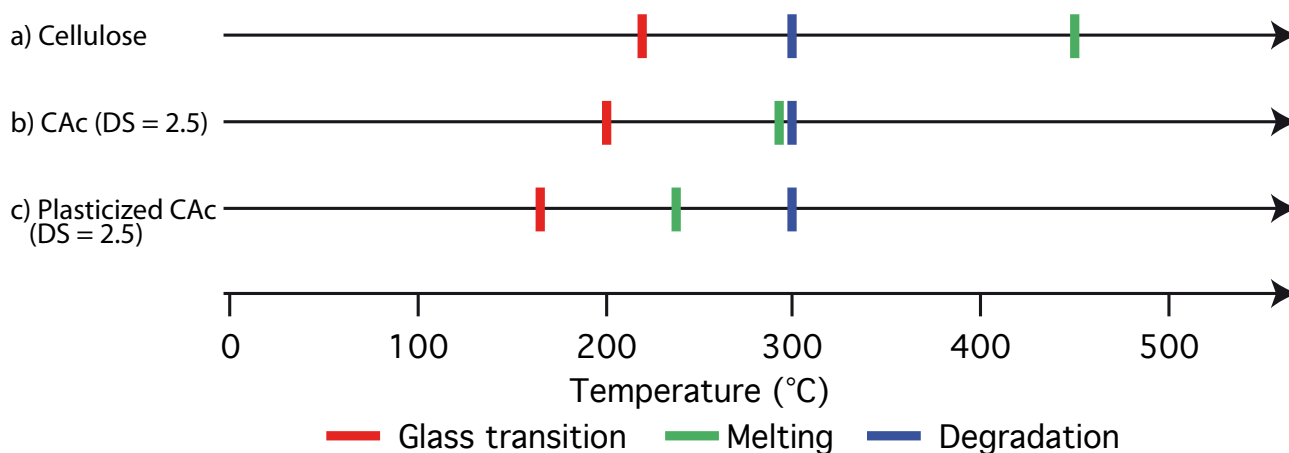


Figure 11.  $T_g$ ,  $T_m$  and  $T_{deg}$  modifications after acetylation of cellulose (a), cellulose acetate (b) and cellulose acetate with plasticizer (c)<sup>4-5, 8, 26, 43</sup>

### 4.2. Chemical hazards of external plasticizers for CAC

Nowadays the most frequently used external plasticizers, in the case of CAC and also in the general thermoplastic industry, are phthalates (Figure 12a). Some are suspected to

be carcinogenic.<sup>55-56</sup> Some are also REACH restricted like the benzyl butyl phthalate (BBP) or the bis (2-ethylhexyl) phthalate (DEHP), for example.<sup>57</sup>

In the case of CAc, more and more benign plasticizers are used such as triacetin (used as food additive)<sup>58</sup> (Figure 12b). But even if the use of those molecules prevents the environmental issues, CAc formulations still require large proportions of plasticizers and their exudation is still a problem.

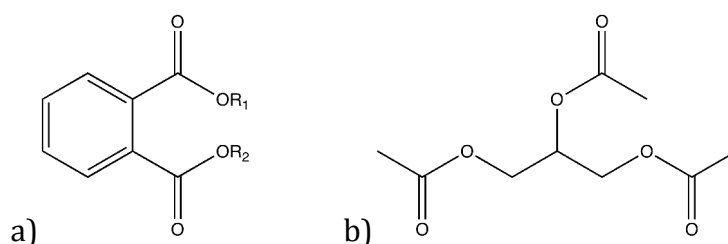


Figure 12. General structure of phthalates (A) and triacetin (B), standard plasticizers of CAc formulations

## 5. Periodate oxidation

As discussed in section 1.4, among the available cellulose chemical modification routes only the periodate oxidation selectively opens the glucose ring.

The periodate oxidation cleaves bonds between vicinal diols following the general mechanism described in Figure 13 and transforms primary alcohols into formaldehyde and secondary ones into aldehyde groups.<sup>59</sup>

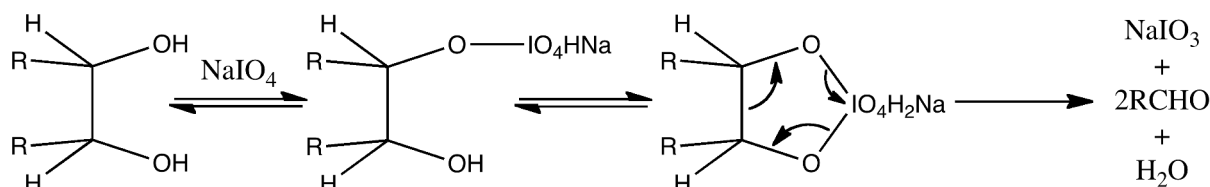


Figure 13. General periodate oxidation mechanism.<sup>59</sup>

The vicinal diols are present on the glucose monomer of cellulose between the C2 and C3 positions (Figure 14).<sup>59</sup> The periodate oxidation of cellulose is a heterogeneous

reaction since the sodium (meta)periodate salt is soluble in water but cellulose is not. The product of this reaction is called periodate oxidized cellulose (POC).

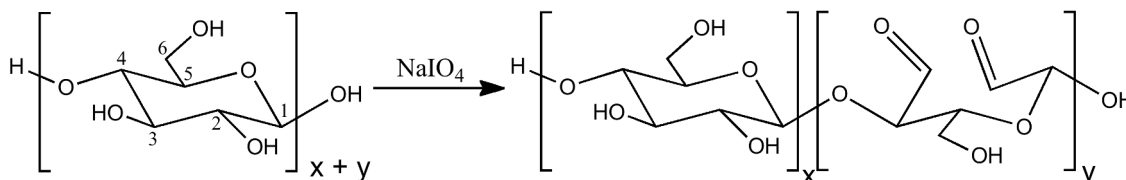


Figure 14. Synthesis of periodate oxidized cellulose.

This reaction is characterized by the degree of oxidation (DO), which represents the average number of aldehyde groups introduced per AGU. The DO can then vary from 0 for cellulose to 2 for fully oxidized POC (all the AGU are oxidized and display 2 aldehyde groups).

### 5.1. Periodate oxidation substrates

Since the periodate oxidation selectively cleaves vicinal diols and nothing else on polysaccharides, this reaction will limit the number of available substrates. This reaction could be carried out on CAC or cellulose. For the case of industrial CAC with DS around 2.5, only a statistical presence of vicinal hydroxyl groups (the DS is an average on all the AGUs) randomly distributed along the chain will be present. Their cleavage could result in an increased mobility downshifting the  $T_g$  but with a lack of reproducibility due to the statistical character of the acetylation. In this work, cellulose was preferred as a working substrate since it exhibits vicinal diols on each AGU.

### 5.2. Cellulose periodate oxidation protocols

A large variety of protocols are reported in the literature to oxidize cellulose with  $\text{NaIO}_4$ . They correspond to variations in the parameters that can influence the DO, namely, temperature, amount of  $\text{NaIO}_4$ , reaction time, cellulose concentration and to a lesser

extent, the cellulose source. The only commonality to the experimental procedures reported is that the reaction must be performed in the dark to avoid the UV decomposition of  $\text{NaIO}_4$ .<sup>60-61</sup>

Most of the time, an empirical combination of parameters leading to a defined DO is reported but no systematic study has been made to understand the evolution of the final DO after varying the parameters. Still, the effect of reaction time at a defined periodate and cellulose concentration has been investigated.<sup>62-63</sup> These studies made at room temperature with 1.0<sup>62</sup> or 1.3<sup>63</sup> eq of periodate per AGU, show that the DO increases in the first 50 hours of the reaction then levels off before reaching a plateau corresponding to almost full consumption of periodate or to full oxidation of cellulose, when an excess of periodate is used.

Most of the time reactions have been performed on a single cellulose source, making conclusions about the influence of the substrate difficult. Maekawa *et al.*<sup>63</sup> showed that cellulose II reacts faster than cellulose I, due to the difference in crystallinity. Accordingly, Kim *et al.*<sup>64</sup> showed that *Cladophora* cellulose, which has a high crystallinity, was less oxidized than commercial cotton cellulose powder with reduced crystallinity.

Previously, reactions have been carried out at low temperatures, which slows down the kinetics and the oxidation process could take up to weeks.<sup>65-67</sup> Today, many authors seem to work at room temperature (20-25°C) in which case a full oxidation is achieved within days: Lindh *et al.* report DO close to 1.70 or 2 within 10 to 13 days using 5  $\text{NaIO}_4$  equivalents per AGU<sup>68-69</sup> while Kim *et al.* reached the same DO within only 3 days with 1.3 eq per AGU.<sup>70</sup> Some studies report reactions at elevated temperatures, 55-75 °C,<sup>71-77</sup> to reduce the reaction time while preventing thermal decomposition of the periodate.<sup>78</sup>

In the literature, the amount of periodate varies from 0.05<sup>79</sup> to 6.5 equivalents of oxidant per AGU.<sup>68-69, 80-81</sup> Typically 0.6 equivalent is used to reach intermediate DO values<sup>72-77, 82</sup> or 1.3 equivalent to achieve a full oxidation.<sup>63-64, 70, 82-85</sup>

Finally, the reaction time can vary from a few hours to several days or even weeks.<sup>69-70, 73</sup> The reaction time is empirically adjusted depending on the desired DO, temperature and the amount of periodate.

### **5.3. Historical use: polysaccharides characterization**

Periodate oxidation of cellulose has been known for almost a century<sup>86</sup> and was first extensively used in the polysaccharide field for analytic purposes.<sup>87-88</sup> The characterization of polysaccharides by periodate oxidation is not based on the fact that periodate can oxidize polysaccharides into their dialdehyde form, but on the fact that the oxidation can be carried to the over-oxidation step leading to a complete degradation of the polysaccharides into formic acid, formaldehyde and other small molecular weight molecules.<sup>89</sup> Using this over-oxidation, and by following the periodate consumption and measuring the amount of formic acid generated during the reaction, it is possible to obtain information about the type of linkage between sugars (1-2, 1-3, 1-4 or 1-6), the degree of polymerization of linear polysaccharides, or the amount of branching in the case of branched polymers.<sup>65-67, 89-92</sup>

### **5.4. Current uses: a platform for functional material**

Today, periodate oxidation is increasingly used as a way to modify cellulose owing to its selectivity towards secondary alcohols and to the reactivity of the generated aldehyde groups. A large variety of compounds can be further obtained by different chemical reactions, leading to a broad range of materials and properties. Some of these compounds and the materials made out of them are listed below.

### 5.4.1. Direct uses of POC

Many studies on dialdehyde cellulose involve a post modification. However, materials can be made directly from POC. For example, Codou *et al.*<sup>93</sup> made all cellulose thermosets by hot pressing periodate oxidized microcrystalline cellulose (Figure 15). They used the spontaneous formation of hemiacetal groups between alcohols and aldehyde as crosslinks. Henschen *et al.*<sup>94</sup> similarly used the POC crosslinking property to make TEMPO/periodate oxidized films covered with polyvinylamine and study their bactericide effect as a function of the charge density for medical and hygiene products such as wound dressing. The TEMPO oxidized and POC crosslinked films perform better, meaning that fewer bacteria develop on such films compared to the only TEMPO oxidized ones. Hollertz *et al.*<sup>95</sup> used periodate-oxidized CMC and other polymers as additives for paper. With such formulations, Hollertz *et al.*<sup>95</sup> obtained stronger films even with low (2 or 5 wt% and up to 15 wt%) amount of additives, in both dry and wet states.

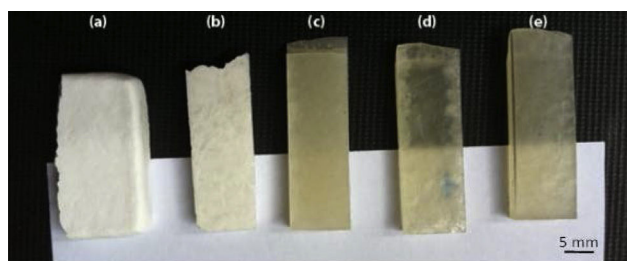


Figure 15. POC thermosets: (a) pristine powder, (b) DO=0.2, (c) DO=0.4, (d) DO=0.65, (e) DO=0.75.<sup>93</sup>

### 5.4.2. Reduction

The aldehyde groups of the POC can simply be reduced into primary alcohols<sup>96-100</sup> leading to a stereo-regular polymer with an enhanced flexibility<sup>96</sup> and well defined crystal structures.<sup>97</sup> This reduction is carried out by mixing the POC product with 2 eq of NaBH<sub>4</sub>, or more, per AGU<sup>101</sup> (Figure 16) leading to reduced periodate oxidized cellulose

(rPOC). The oxidized then reduced part of rPOC samples is a poly-(primary)alcohol, which can be further modified by esterification<sup>97</sup> for example, in the same way cellulose can be modified (cf section 1.4). rPOC can be used as additives in paper formulations to improve the overall ductility<sup>100</sup> or to add an oxygen-barrier property.<sup>99</sup> López Durán *et al.*<sup>102</sup> studied both POC and rPOC to improve paper properties. Both modifications were beneficial for the paper properties in term of strength, stiffness or ductility.<sup>102</sup>

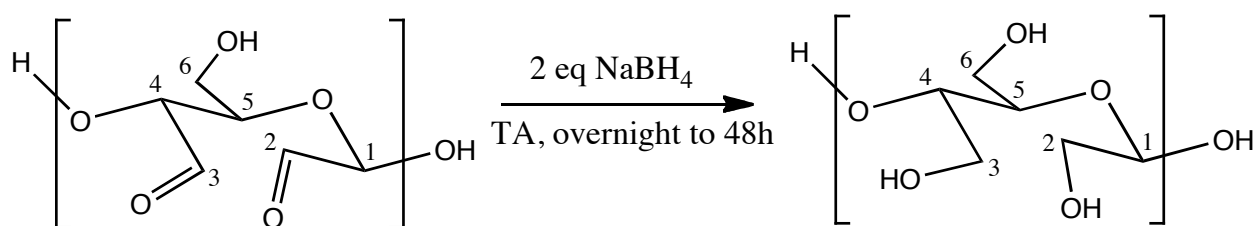


Figure 16. Sodium borohydride reduction of POC to its reduced counterpart.<sup>101</sup>

Kasai *et al.*<sup>98</sup> carried out homogeneous periodate oxidation of cellulose with a pre-modification of cellulose into a soluble hydroxymethyl cellulose, followed by a NaBH<sub>4</sub> reduction. In these homogeneous conditions, a full oxidation was performed within only 12 hours at room temperature. The films made from this reduced POC show thermoplastic properties with a DO-dependent T<sub>g</sub>: the T<sub>g</sub> decreases proportionally to the DO as seen in Figure 17 ranging from 170 to 75 °C for DO between 0.5 and 1.8 respectively. Additionally, the product showed plasticization by water, meaning their thermo-mechanical properties are humidity dependent.<sup>98</sup>

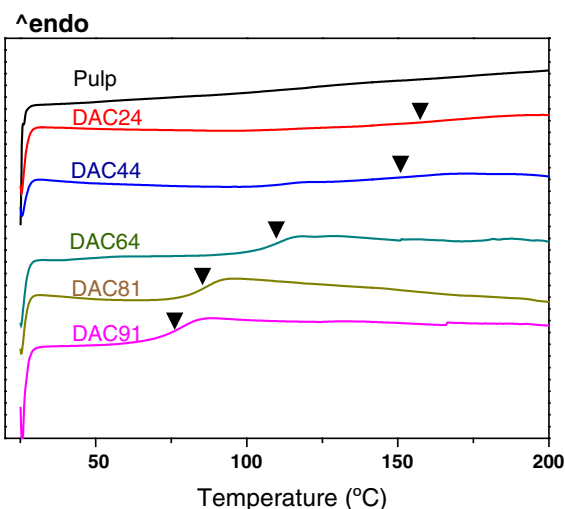


Figure 17. DSC thermograms of reduced POC (named DAC by Kasai *et al.*) in homogeneous conditions, showing the DO dependency of the  $T_g$  (legend in the figure: DACXX corresponds to a POC film with percentage of oxidation of XX%, its DO is  $2XX/100$ ).<sup>98</sup>

Larsson and Wågberg<sup>103</sup> showed that reduced POC in heterogenous synthesis also showed thermoplastic properties in DMA analysis. The details of such materials will be discussed in Chapter 4.

### 5.4.3. Post-oxidation

In contrast to the reduction treatment, the POC can be post-oxidized into what is usually called dicarboxylic acid cellulose (DCC)<sup>79, 83, 104-107</sup> following a treatment with sodium chlorite in an acetic acid solution<sup>101</sup> (Figure 18). This sodium chlorite *post-oxidation* has to be distinguished from the sodium periodate side reactions that can happen during the synthesis of the POC, and referred as *over-oxidation*.<sup>89</sup>

One of the potential use of DCC is to complex heavy metallic ions by the two COOH groups on each AGU that probably act like clamps to complex ions.<sup>83</sup> Varma *et al.* studied DCC by XRD and NMR, showing that the crystallinity decreases proportionally to the increase in DO.<sup>104-105</sup> This material can also be used for its high charge density, which

can be valuable for creating new column packing materials for ion-exchange chromatography.<sup>79</sup>

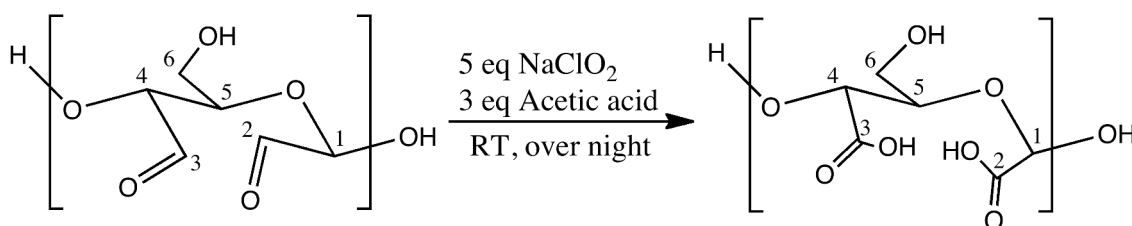


Figure 18: Post-oxidation of POC into DCC<sup>101</sup>

Recently, Plappert *et al.*<sup>108</sup> synthesized DCC from sulfite dissolving pulp. They showed that the DCC with a charge content of about 1 mmol/g (corresponding to a DO of about 0.16) needed less energy to defibrillate than the TEMPO-oxidized cellulose from the same source with the same charge density. When concentrated, the never-dried DCC suspensions could self-organize into nematic phases. This nematic phase was preserved when the suspensions were dried with supercritical CO<sub>2</sub> into aerogels and after uniaxial compression as shown in Figure 19. Furthermore, the compression allowed a tuning of the pore size distribution inside the aerogel.

López Durán *et al.*<sup>109</sup> studied the influence of pulp modification by TEMPO-mediated oxidation, periodate oxidation, periodate oxidation followed by either NaBH<sub>4</sub> reduction or chlorite post oxidation or a mix of some of these reactions, as presented in Figure 20, on paper properties. These reactions only corresponded to low levels of modifications. They showed that depending on the charge density and the chemical modification(s) the pulp water retention was different: TEMPO oxidized + reduced POC samples (number 8 in Figure 20) have the same water retention as DCC samples (number 5 in Figure 20) but with a three times lower charge density. In terms of mechanical properties, papers

modified by DCC are stiff, while ductile when partially periodate oxidized and further reduced.

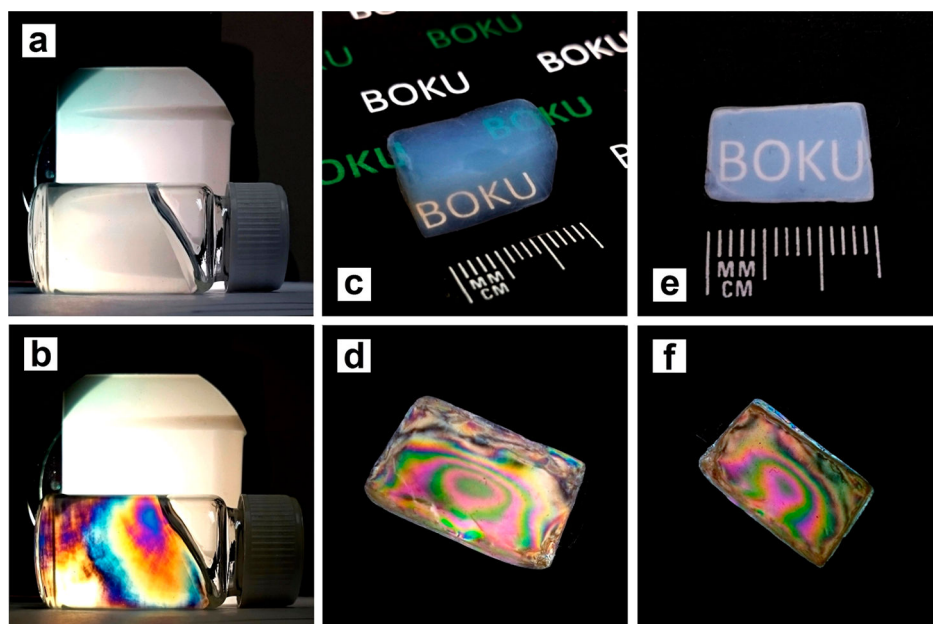


Figure 19. (a) DCC suspensions at 1.5 w/v%, (c) DCC aerogel ( $18 \text{ mg/cm}^3$ ), (e) compressed DCC aerogel ( $160 \text{ mg/cm}^3$ ), (b)(d) and (f) same materials under polarized light.<sup>108</sup>

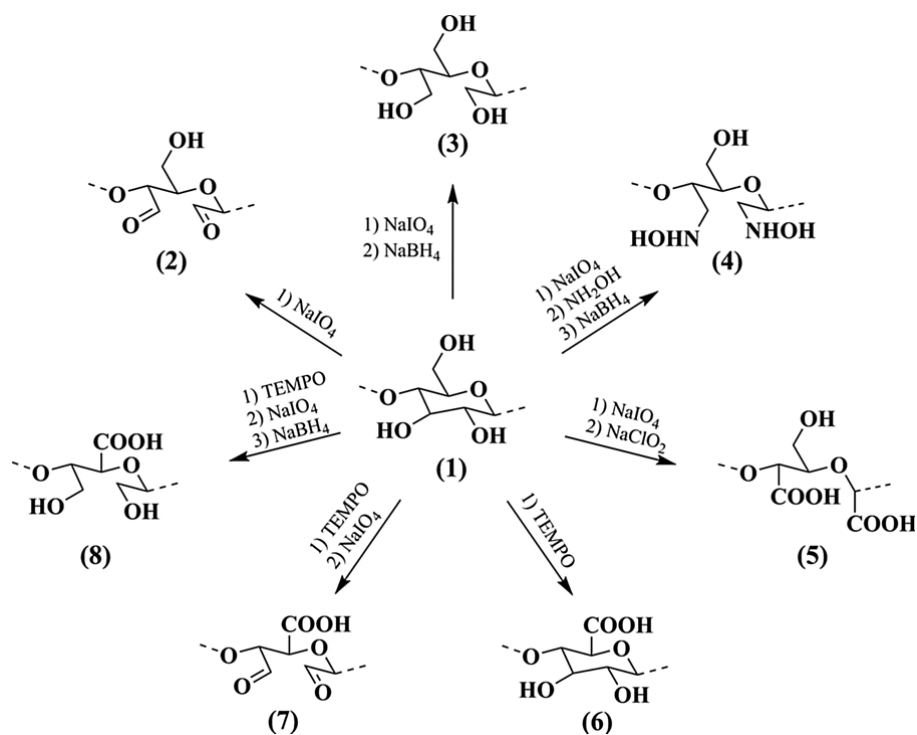


Figure 20. Schematic representation of the modifications made by López Durán *et al.*<sup>109</sup>

### 5.4.4. Grafting

Among the possible post-modifications of POC, the grafting of amines has been extensively studied.<sup>62, 68-69, 72-77, 84-85, 94, 110-115</sup> In contrast to the borohydride reduction or the chlorite oxidation that both lead to only one type of product, grafting allows a large variety of modifications by changing the amine.

The grafting can be achieved either by a one step reaction like imination (Figure 21a)<sup>62</sup> or by a two steps mechanism, as in the case of reductive amination (Figure 21a and b).<sup>72, 111</sup> The mechanism of the reaction is described Figure 21c. The imination consists of the condensation of the amine on the aldehyde, while the reductive amination adds a reduction step with a reductive agent such as NaBH<sub>3</sub>CN, leading to secondary amines.

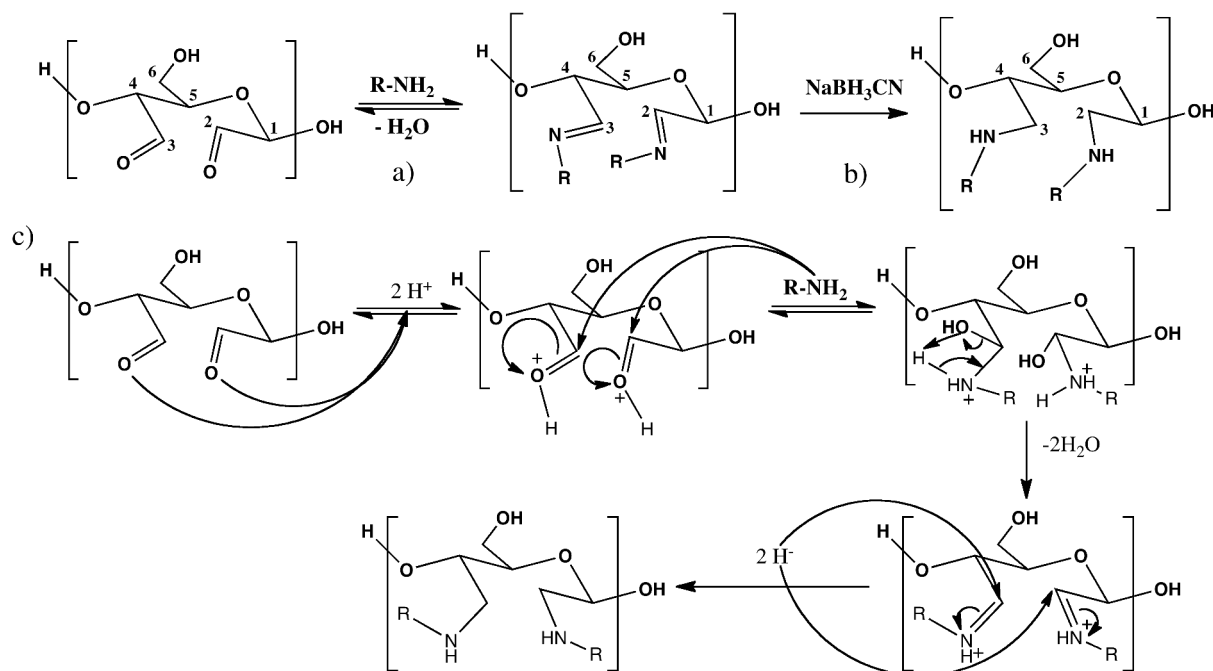


Figure 21. Grafting of POC by reductive-amination: imination (a) followed by reduction (here with NaBH<sub>3</sub>CN) The second part of the figure describe the mechanism of the reaction (c).

#### 5.4.4.1. Imination/reductive amination protocols

Depending on the reaction (imination or reductive amination) considered, different protocols are reported. Some examples are listed below:

- Sabzalian *et al.*<sup>62</sup> performed a simple imination using 1.3 eq of n-butylamine in toluene on a DO=1.8 POC sample at room temperature for 24 to 72 hours. Since the imination is an equilibrium between the condensed form (with release of a water molecule) and the free forms of amine and aldehyde, changing the solvent from water to toluene would push the equilibrium toward the formation of the imine group. But Sabzalian *et al.*<sup>62</sup> only justified their solvent choice by explaining that the hydrophobic products would be better dispersed in toluene.
- Kim *et al.*<sup>85</sup> also performed a simple imination but in an acetate buffer at pH 4.4 with 16 eq of amine per carbonyl group. In this case the equilibrium is pushed toward the formation of the imine due to the large excess of reagent.
- Lindh *et al.*<sup>68</sup> or Jin *et al.*<sup>112</sup> first did the imination (24h at room temperature or 6h at 30°C) followed by a NaBH<sub>4</sub> reduction. This protocol seems to have some drawbacks: the NaBH<sub>4</sub> can reduce the imine, but it can also reduce the unreacted aldehyde into primary alcohol. Additionally, as already stated, the imine is in equilibrium with its free form (amine + aldehyde). So this method would probably decrease the efficiency of the grafting. In fact Jin *et al.*<sup>112</sup> reported a grafting of 1.3 mmol/g of amine while the initial DO was of almost 9 mmol/g, corresponding to a 15% grafting efficiency only.
- Guigo *et al.*<sup>111</sup> and Azzam *et al.*<sup>110</sup> did the reductive amination in one step by performing a reduction of the imine that forms *in situ* using NaBH<sub>3</sub>CN. The reactions were performed at pH 6 in buffered conditions since the NaBH<sub>3</sub>CN

requires neutral to slightly acidic conditions to reduce exclusively imine, letting the aldehyde intact. Sirviö *et al.*<sup>76</sup> describe similar reductive amination protocols with picoline borane as reductive agent and control the pH by the addition of diluted HCl.

#### 5.4.4.2. Properties of amine-grafted-POC materials

Yang *et al.*<sup>113</sup> prepared injectable hydrogels with a double-barrel syringe loaded with periodate-oxidized dextran, periodate-oxidized CNCs and hydrazide-modified CMC (Figure 22). When mixed, aldehyde and hydrazide groups react, forming crosslinks leading to stable hydrogels. It is also possible that hemiacetal crosslinking is part of the hydrogel stability as seen in previous studies.<sup>93-95</sup> The CNCs also help, as fillers, to hold the structure like a scaffold.

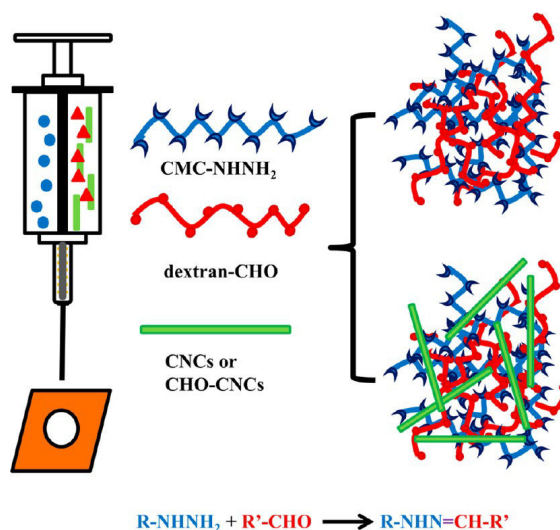


Figure 22. Schematic illustration of the injectable hydrogels crosslinked by aldehyde/hydrazide condensation<sup>113</sup>

Yang *et al.* used the same crosslinking method between periodate-oxidized CNCs and hydrazide-modified CNCs to make ultra-light-weighted aerogels with shape recovery and superabsorbent properties<sup>114</sup> and supercapacitor aerogels.<sup>115</sup> The superabsorbent properties come from the cryo-templated porosity,<sup>114</sup> (Figure 23) while the super

capacity comes from the capacitor nanoparticles (polypyrrole nanofibers, polypyrrole-coated carbon nanotubes or manganese dioxide nanoparticles) trapped inside the crosslinked CNC network.<sup>115</sup>

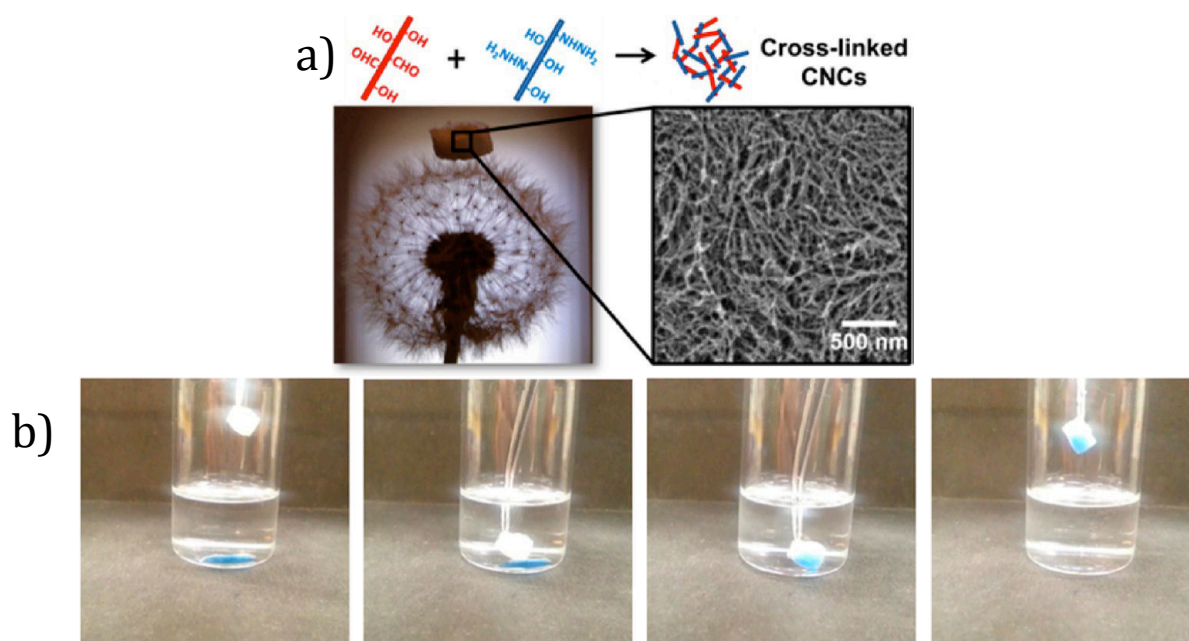


Figure 23. Aerogels from crosslinked CNCs with superabsorbent properties (a-b) absorption of water dyed in blue from dodecane/water mixture (b).<sup>114</sup>

Suopajarvi *et al.*<sup>77</sup> grafted charged amines on POC to make flocculating materials for water purification. Other groups made flocculating agents by either grafting amines with thiol groups that can complex metals such as palladium<sup>69</sup> or aliphatic amines for a selective flotation of aluminium.<sup>74</sup> In the same perspective, Jin *et al.*<sup>112</sup> crosslinked POC with ethylenediamine and used these materials to adsorb dyes.

The same materials grafted with aliphatic amines also displayed hydrophobic properties.<sup>76</sup> Sabzalian *et al.*<sup>62</sup> grafted aliphatic amines with or without a combination with diamines, which provided the same hydrophobization but the diamine products showed additional crosslinking leading to higher yields than the same materials without crosslinking.

Sirviö *et al.*<sup>75</sup> grafted aromatic amines on oxidized CNCs and used them as fillers: the materials proved to be UV-absorbing without interfering in the transparency of the materials (Figure 24). Such materials could be used in medical applications, such as ophthalmic materials.

Similar to the case of reduced POC, some oxygen barrier films can be obtained by reductive amination of taurine.<sup>72</sup>

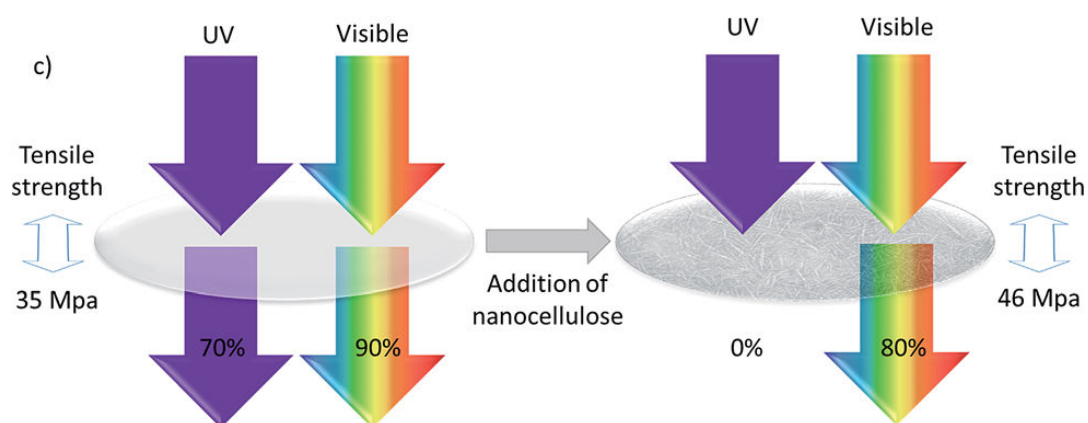


Figure 24. Schematic description of the UV-filtering property and the reinforcing effect of CNCs in PVA films with aminobenzoic acid modified CNCs fillers.<sup>75</sup>

## 6. Colloidal suspensions

Van de Ven *et al.*<sup>106, 116-120</sup> showed that stable suspensions of hairy cellulose nanocrystalloids can be obtained by periodate oxidation of cellulose and further modification to DCC,<sup>106, 116-117</sup> grafting<sup>118</sup> or simple washing of the oxidized shell.<sup>119-120</sup> As described in Chapter 4, stable suspensions of core-shell cellulosic nanorods were also produced in this work from a periodate oxidation of microfibrils followed by a reduction step. As an introduction to such results, this section will briefly describe the preparation and properties of stable colloidal suspensions from cellulose reported in the literature without providing an exhaustive review on the topic.

Colloidal suspensions are stable dispersions of insoluble nano/micro particles. The particles can be organic or inorganic materials<sup>121</sup> and their stabilization can be due to electrostatic or steric repulsion forces or their combination.<sup>38, 122</sup> In the case of electrostatic stabilization, particles are considered stable when their zeta-potential is above 30 mV in absolute value<sup>123</sup> while steric stabilization will depend on several parameters: the density of the adsorbed/grafted polymer on the CNC surface and the polymer chain length are most important.<sup>124</sup>

In the case of cellulose, CNCs and in particular sulfuric acid hydrolyzed CNCs can form stable suspensions by electrostatic repulsion due to the sulfate half-ester groups introduced on the surface of the crystals during the hydrolysis. They were first described by Rånby in 1949.<sup>22</sup>

## **6.1. Preparation of stable CNC suspensions**

### **6.1.1. Direct electrostatic stabilization**

CNCs are extracted/synthesized from cellulose fibers by acid hydrolysis. While several aqueous acid media can be used for converting cellulose fibers into CNCs, the acid selection is a key parameter for the quality of the colloidal stability. In fact, performing acid hydrolysis of cellulose fibers with HCl leads to poorly-stable dispersions with significant inter-particle agglomeration, due to the absence of stabilizing forces.<sup>125</sup> In contrast, sulfuric acid hydrolysis directly leads to suspensions of individualized nanoparticles, which are stable over time.<sup>126-127</sup> In this case the stability is provided by the introduction of sulfate half-ester groups during the H<sub>2</sub>SO<sub>4</sub> hydrolysis, which induces electrostatic repulsion between the particles, preventing them from flocculating.

### 6.1.2. Indirect stabilization

After acid hydrolysis using HCl, for example, or other non-stabilizing CNC isolation processes, CNCs can be post modified to form stable suspensions. This stabilization can be either electrostatic, steric or a combination of both.<sup>38, 122</sup>

#### 6.1.2.1. Electrostatic stabilization

Since the HCl hydrolysis does not introduce any new groups, all the surface hydroxyl groups are available for further chemistry. Hasani *et al.*<sup>128</sup> grafted epoxy molecules with an ammonium positive charge leading to non-conventional cationic stabilization.

Some authors hydrolyzed cellulose fibers with HCl to obtain CNC and treated them with sulfuric acid in order to introduce sulfate half-ester groups to provide an electrostatic stability with anionic charge. This process has the advantage to lead to the same CNCs than with the direct H<sub>2</sub>SO<sub>4</sub> hydrolysis in terms of CNCs sizes, but with less sulfate half-ester groups on the surface, providing a better thermal stability.<sup>129-130</sup> With the same idea, Araki *et al.*<sup>38</sup> and others<sup>131-133</sup> performed a TEMPO-mediated oxidation on HCl hydrolyzed CNCs in order to introduce negatively charged carboxylic acids on the CNC surface.

#### 6.1.2.2. Steric stabilization

A steric stabilization can be induced either by polymer adsorption or polymer grafting (Figure 25) on the surface of the particles.<sup>124</sup>

The surface TEMPO-mediated oxidation is sufficient to provide electrostatic stability. It is also possible to switch from electrostatic to steric stabilization by grafting polymers like PEG on the newly formed COOH groups.<sup>38</sup> More recently, Azzam *et al.*<sup>39, 134</sup> did the same with thermo-sensitive polymers providing reversible temperature-induced

aggregation and gelation properties that can further be tuned by the pH of the medium (Figure 26).

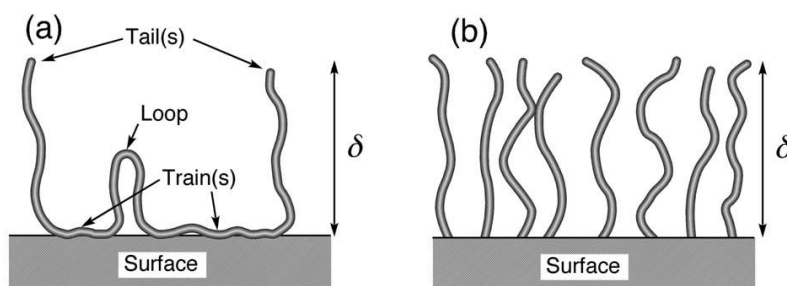


Figure 25. Schematic steric stabilization by adsorption (a) or grafting (b) of polymer chains.<sup>124</sup>

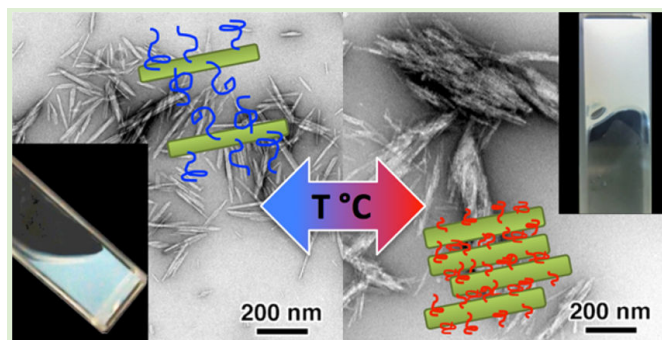


Figure 26. Thermo-reversible aggregation and gelation of thermo-sensitive polymer modified CNCs.<sup>134</sup>

After classical  $\text{H}_2\text{SO}_4$  hydrolysis, CNCs can be covered by surfactants (Beycostat NA for example) in order to convert the electrostatic stability into a steric one. In doing so, colloidal CNC suspensions can be produced in organic solvents such as toluene instead of water, leading to new properties and applications.<sup>135-137</sup>

Interestingly it was shown by van de Ven's group that sterically stabilized CNCs can be obtained after periodate oxidation of cellulose paper pulp, and further solubilization of the oxidized part in solvents.<sup>116, 119-120</sup> The proposed schematic structure model of the stable CNCs is depicted in Figure 27.

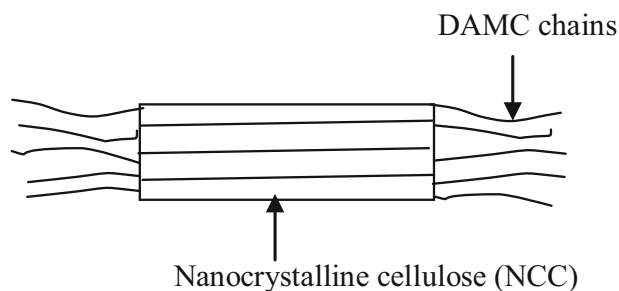


Figure 27. Schematic representation of the sterically stabilized CNCs obtained after periodate oxidation and further solubilization of the oxidized parts (DAMC stands for dialdehyde-modified cellulose).<sup>119</sup>

## 6.2. Properties of materials made from colloidal suspensions

Kept never dried or incorporated in materials, CNCs exhibit specific properties. Favier *et al.*<sup>14</sup> demonstrated that sulfuric acid hydrolyzed CNCs could be introduced as fillers in polymer matrix, drastically increasing the modulus especially above the glass transition temperature of the matrix with small amount of particles (Figure 28). Since then, CNC fillers are of great interest in materials research.<sup>138-139</sup>

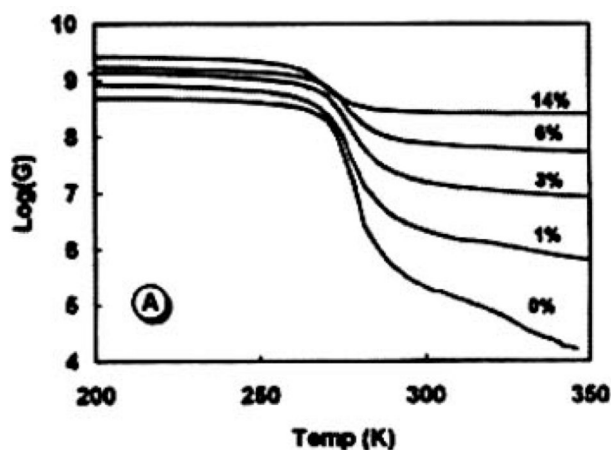


Figure 28. Storage modulus from DMA measurements, showing the reinforcing effect of CNC fillers in a thermoplastic matrix as function of the filler content.<sup>14</sup>

CNCs in suspension self-organize when a critical concentration is reached leading to chiral-nematic liquid crystals (organization of CNCs into helicoidal structures). These

liquid crystals became a subject of interest in the scientific community since it can lead to highly textured materials<sup>24, 126, 140-141</sup> displaying remarkable optical properties. This phenomenon is called iridescence and can lead to pigment-free colored materials.<sup>18, 142</sup> The liquid crystal organization can be enhanced and controlled by orienting CNCs using magnetic fields<sup>143-144</sup> or electric fields<sup>135, 145-146</sup> (Figure 29).

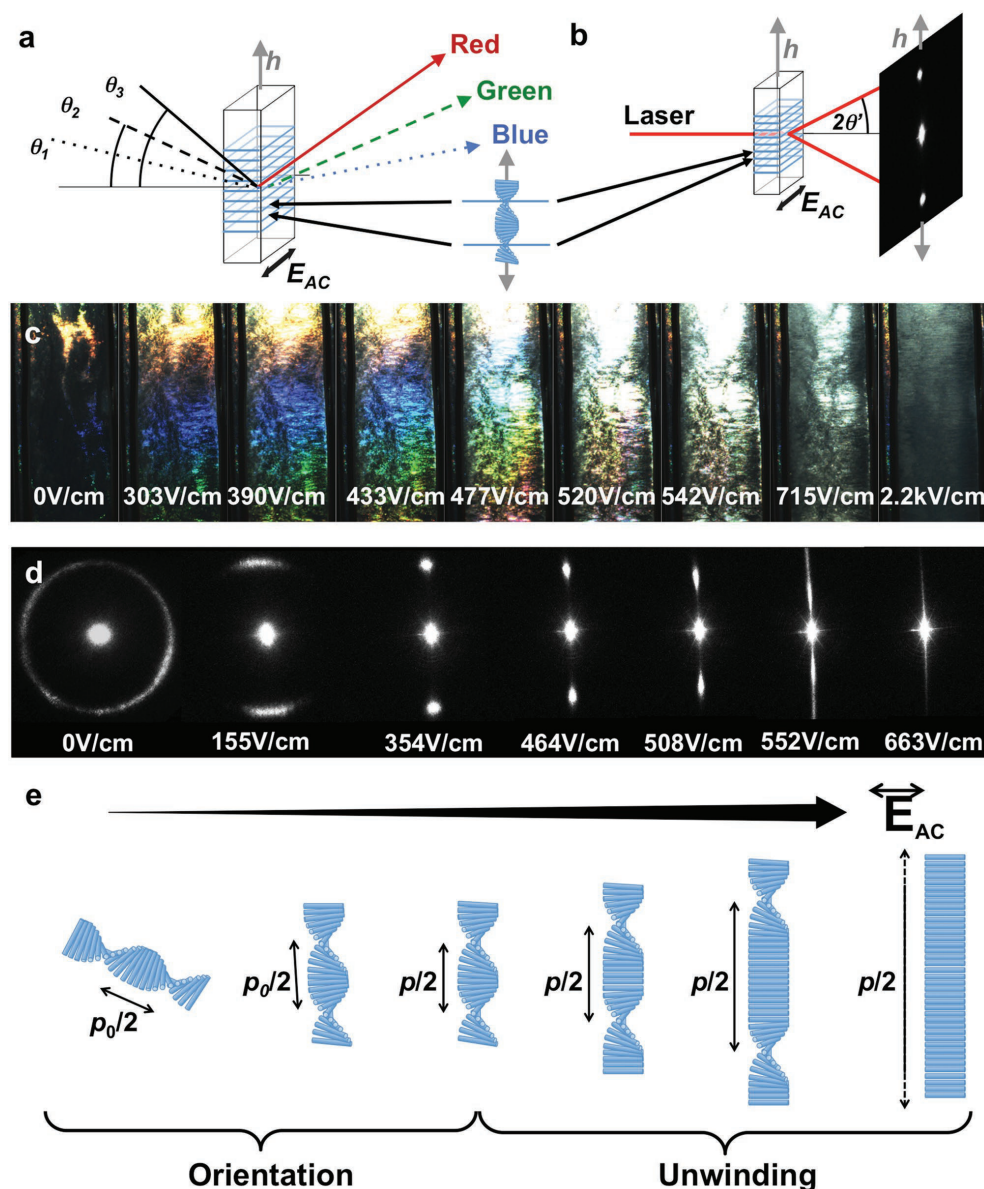


Figure 29. Schematics illustrating a) iridescence and b) the laser diffraction pattern of a cholesteric phase. c) controlled iridescence by applying an increasing electric field, d) corresponding laser diffraction pattern and e) schematic of the sequential cholesteric orientation and unwinding upon electric field increase.<sup>146</sup>



# Chapter 2: Accurate degree of oxidation measurement of periodate oxidized cellulose by CP-MAS $^{13}\text{C}$ NMR

---

The first step of this project was to determine the conditions that lead to a specific DO in order to be able to synthesize any desired DO for the next material preparation steps. Moreover, an accurate way to characterize the DO had to be determined in order to be able to accurately understand the structure/property relationships of the materials that will be obtained from POC.

## 1. Introduction

Chemical modifications of cellulose have been the subject of intense research to widen the properties and uses of this naturally ubiquitous product. Among the broad variety of chemical pathways that can be envisaged, periodate oxidation stands as a unique reaction as it is able to drastically modify the cellulose backbone under mild conditions, while keeping the original cellulose stereoregularity. Periodate oxidation selectively cleaves the cellulose glucosyl rings between the C2 and C3 carbons and converts the two associated alcohols moieties into two aldehyde groups, leading to the so-called periodate oxidized cellulose (POC). Initially, the periodate oxidation of polysaccharides

was used for structural analysis purpose,<sup>87-88</sup> but more recently it has been revived as a way to prepare a new class of cellulose-based products. For example, POC can be used as a component in the processing of all-cellulose thermosets,<sup>93</sup> and also as a potential intermediate for the creation of a large variety of bio-based products.<sup>62, 69, 72, 74-77, 79, 96-97, 99-100, 106-107, 112</sup> When reduced with sodium borohydride, POC gets converted into an acyclic stereoregular polyalcohol of enhanced flexibility,<sup>96-97</sup> which can be used to increase the ductility of paper<sup>100</sup> or to make oxygen-barrier films.<sup>99</sup> In other systems, the grafting of amines on the created aldehyde groups is a way to obtain flocculating agents,<sup>69, 74, 77</sup> hydrophobized cellulose,<sup>62, 76</sup> materials reacting to light,<sup>75, 112</sup> or oxygen-barrier films.<sup>72</sup> Periodate oxidation followed by post-oxidation to dicarboxylic acid cellulose (DCC) leads to highly charged anionic cellulose that finds applications in ion exchange chromatography.<sup>79, 106-107</sup> A prerequisite for a rational use of these reactions is a precise control of the amount of created aldehyde groups to properly identify the structure/properties relationship of the desired products.

The aldehyde amount in a POC sample can be expressed in different ways: (i) the number of moles of aldehyde per gram of product (a fully oxidized sample would reach 12.5 mmol/g), which is the most popular unit,<sup>70, 147</sup> (ii) the percentage of oxidation representing the ratio of oxidized units over the total number of anhydroglucose units (AGU) (a fully oxidized sample would have an oxidation percentage of 100%)<sup>83, 98</sup> and finally (iii) the degree of oxidation (DO) defined as the average number of aldehyde groups introduced per AGU (a fully oxidized sample would have a DO of 2 since two aldehyde groups are created when one AGU is oxidized).<sup>110-111</sup> This last unit will be used in the present study.

Different methods to measure the DO exist. The first method, the aldehyde moieties can be further oxidized into carboxylic acid groups using acidified sodium chlorite and these groups can in turn be titrated with NaOH.<sup>88, 148-149</sup> However, the use of this method in the literature was limited to low amounts of aldehydes groups (less than 8% oxidized units),<sup>88, 149</sup> and was mostly used for cellulose reducing-end characterization.<sup>148</sup>

The second method is to follow the periodate consumption. The DO can be deduced from monitoring of the periodate concentration in the reaction medium by the UV absorbance. The expected amount of aldehyde groups introduced on a cellulose substrate should be proportional to this consumption since one mole of periodate should lead to two moles of aldehyde groups.<sup>63, 70, 83, 98, 150-152</sup> This method has been widely used since it is simple and straightforward.<sup>19, 21, 22, 27-30</sup>

In a third method - the most popular for polysaccharide and especially for cellulose - POC is subjected to a reaction with hydroxylamine hydrochloride, leading to the conversion of aldehyde moieties into oximes, while liberating HCl molecules, which can be titrated by NaOH. The protocol, initially proposed by Zhao and Heindel,<sup>153</sup> involves, after the reaction between the POC and hydroxylamine, a titration of the released HCl with NaOH back to an initial pH of 3.2.<sup>111</sup> The net alkali consumption to recover the pH of 3.2 is expected to correspond to the aldehyde content. In similar protocols, Yang *et al.*<sup>120</sup> used an initial pH of 3.5, while Larsson *et al.*,<sup>154</sup> Cervin *et al.*<sup>155</sup> and Lopez Duran *et al.*<sup>102</sup> used a pH of 4 and Kim *et al.*,<sup>64, 70</sup> and Lindh *et al.*,<sup>147</sup> used a pH of 4.5. Nitrogen elemental analysis after oximation was also used to quantify the aldehyde contents.<sup>19, 26</sup> Kim and Kuga<sup>85</sup> found an average match between the results of different DO measurements methods including nitrogen elemental analysis after reaction with hydroxylamine-hydrochloride or the periodate consumption, the periodate

consumption giving always higher DO. With the exception of the UV technique, these methods may suffer from the limited accessibility of the analytical reagents toward the aldehyde groups located within the cellulosic matrix and the possible titration of other aldehyde groups (e.g. those located at chain ends, resulting from over oxidation...).

In parallel to chemical titration methods, solid-state  $^{13}\text{C}$  NMR is a powerful tool to quantify functional groups in bulk material, as the entire content of the material under investigation is probed. However, in the case of POC, deducing DO values from NMR data is not straightforward since the created aldehyde groups are never observed in the carbonyl region of the POC spectra. Indeed, in these bulk samples the concentration of hydroxyl groups is high and the newly formed highly reactive aldehyde groups quickly interact with these hydroxyls to form various covalent hemiacetals or hemialdals,<sup>64, 110-111, 120, 147, 156-157</sup> whose carbon signals overlap with those of the intact glucosyl residues.

So far, solid-state  $^{13}\text{C}$  NMR has been mainly used for measuring the degree of crystallinity of cellulose before and after periodate oxidation.<sup>64, 104-105, 120, 147, 156</sup> However, as initially proposed by Guigo *et al.* in the study of the oxidation and benzylamination of microfibrillated cellulose,<sup>111</sup> this technique should also allow measuring DOs. In the present work, we address the question of the accurate quantitative measurement of the DO of POC samples by an NMR technique. For this, using microfibrillated cellulose as a starting material, we have devised various experimental conditions of periodate oxidation to obtain a series of POC products with DO values covering the entire achievable DO range. We have used these products to test a protocol leading to the calculation of DO values from  $^{13}\text{C}$  NMR CP-MAS data, and compared these values to those of conventional quantification methods.

## 2. Materials and methods

### 2.1. Materials

A batch of paste-like never dried microfibrillated cellulose (MFC) prepared by a mechano-enzymatic treatment<sup>158-159</sup> of spruce sulfite pulp, with a consistency of about 2%, was purchased from the Centre Technique du Papier (CTP), Grenoble, France. It contains less than 4% of hemicellulose. Sodium metaperiodate with purity  $\geq 99.8\%$  was acquired from Carl Roth (France).

### 2.2. MFC oxidation to POC

In a typical experiment, about 50 g of the 2% MFC suspension (equivalent to 1 g of dry cellulose) were inserted into a flask equipped with magnetic stirring. Periodate, from 0.2 to 1.3 equivalent of the total amount AGUs was dissolved in 40 mL deionized water and added to the MFC suspension. About 50 mL deionized water was further added to adjust the cellulose concentration to 7.2 g/L. The flask was wrapped with aluminum foils to avoid UV-light degradation of sodium metaperiodate.<sup>61</sup> The oxidation was carried out for reaction times ranging from 2 to 170 h at room temperature. At the end of the reaction, the mixture was centrifuged for 1 h at 20,000 g. The pellet was then redispersed in deionized water using an Ultra-Turrax double cylinder homogenizer. The centrifugation/redispersion process was repeated 3 to 4 times to remove any residual salts until the conductivity of the supernatant was below 30  $\mu\text{S}$ . The product was then freeze-dried and stored before use.

### 2.3. Measuring the degree of oxidation (DO)

#### 2.3.1. Periodate consumption monitored by UV-visible spectroscopy, yielding DO<sub>UV</sub>

The periodate concentration in the supernatant was deduced from the measurement of the absorbance at 290 nm measured using a Varian CARY 50 BIO UV-visible spectrometer, as first described by Maekawa *et al.*<sup>83</sup> This wavelength was preferred to the one corresponding to the maximum absorbance of periodate (223 nm) due to an absorbance linearity on a larger range of periodate concentration (0.02 – 0.2 mM, Supporting Information Figure SC2-1).<sup>63</sup> Briefly, an aliquot of the supernatant resulting from the centrifugation at the end of the reaction was immediately filtered through a 0.4 μm syringe filter, and the absorbance at 290 nm was measured after dilution with distilled water to reach a sample concentration in the 0.02 – 0.2 mM range. As each molecule of periodate oxidizes one AGU to give two aldehyde groups, the degree of oxidation extracted from the periodate consumption, DO<sub>UV</sub>, can be obtained from:

$$DO = 2 \frac{V([NaIO_4]_i - [NaIO_4]_f) \cdot M_{AGU}}{w} \quad (1)$$

where

$[NaIO_4]_i$  (mol.L<sup>-1</sup>) is the periodate concentration at the beginning of the reaction,

$[NaIO_4]_f$  (mol.L<sup>-1</sup>) is the periodate concentration at the end of the reaction measured by UV,

$V$  (L) is the volume of the reaction solution,

$M_{AGU}$  (160 g.mol<sup>-1</sup>) is the molar mass of an oxidized AGU,

and  $w$  (g) is the weight of dried cellulose used in the reaction.

### 2.3.2. Aldehyde amount deduced from the quantitative reaction with hydroxylamine hydrochloride

#### 2.3.2.1. Titration of released HCl (DO<sub>t-NaOH</sub>)

In a typical experiment,<sup>153</sup> a 100 mg POC sample was reacted with 25 mL of an aqueous 0.25 M hydroxylamine hydrochloride solution for 2 h at room temperature, which led to a minimum hydroxylamine/carbonyl ratio of 5 for fully oxidized samples. The pH of the hydroxylamine solution and the hydroxylamine solution with POC was initially around 3.2. After the 2 h reaction time, the pH of the whole sample decreased due to HCl release (sometimes below pH 1). The sample was then titrated with a NaOH solution (0.01 M) back to pH 3.2 and DO<sub>t-NaOH</sub> is calculated from:

$$DO_{t-NaOH} = \frac{V_{eq} \cdot [NaOH] \cdot M_{AGU}}{w} \quad (2)$$

where

V<sub>eq</sub> (L) is the volume of NaOH added to reach pH 3.2,

[NaOH] (mol.L<sup>-1</sup>, here 0.01 N) is the NaOH concentration.

#### 2.3.2.2. Titration of consumed base (DO<sub>t-HCl</sub>)

Alternatively, in a method described by Green,<sup>160</sup> the pH of the hydroxylamine hydrochloride solution can first be increased to pH 5.2 by a controlled addition of NaOH, and titrated to pH 3.2 by HCl addition after oxime formation, avoiding the strong acidic conditions of the previous protocol.<sup>160</sup> In a typical experiment, a 100 mg sample was reacted with 25 mL of an aqueous solution of hydroxylamine hydrochloride (0.72 M) and NaOH (0.12 M) for 2 h at room temperature, which led to a minimum hydroxylamine/carbonyl ratio of 14 for fully oxidized samples. With this protocol, the

pH never goes below 4.8 during the oxime formation and less HCl is needed to reach a pH of 3.2 when the oximation proceeds.

The  $\text{DO}_{t-\text{HCl}}$  is calculated from:

$$\text{DO}_{t-\text{HCl}} = \frac{(V_{\text{blank}} - V_{\text{eq}}) \cdot [\text{HCl}] \cdot M_{\text{AGU}}}{w} \quad (3)$$

where

$V_{\text{blank}}$  (L) is the volume of HCl needed to reach pH 3.2 on a blank sample without POC,

$V_{\text{eq}}$  (L) is the volume of HCl needed to reach pH 3.2 with the POC sample,

$[\text{HCl}]$  ( $\text{mol}\cdot\text{L}^{-1}$ , here 0.1 N) is the HCl concentration.

### 2.3.3. $^{13}\text{C}$ CP-MAS solid-state NMR spectroscopy

Solid-state  $^{13}\text{C}$  NMR spectra were acquired using a Bruker Avance III DSX 400 MHz spectrometer operating at 100.6 MHz for  $^{13}\text{C}$ , using the combination of the cross-polarization, high-power proton decoupling and magic angle spinning (CP-MAS) method. The spinning speed was set at 12,000 Hz. The  $^1\text{H}$  radio-frequency field strength was set to give a  $90^\circ$  pulse duration of 2.5  $\mu\text{s}$ . The  $^{13}\text{C}$  radio-frequency field strength was obtained by matching the Hartman-Hahn conditions at 60 kHz. At least 2,000 scans were integrated with a contact time of 2 ms using a ramp CP protocol and a recycle delay of 2 s. The acquisition time was 35 ms and the sweep width set at 29,400 Hz. The chemical shifts were calibrated with respect to the carbonyl peak of glycine (176.03 ppm).

#### 2.3.3.1. DO estimation from NMR spectra ( $\text{DO}_{\text{NMR}}$ )

After the reaction with periodate, the cellulose units exist in two forms: either oxidized, meaning that the glucosyl ring is open, or unmodified with intact sugar rings. This large difference in the chemical environment between the two forms makes the chemical shift of both C1 for intact sugar rings and C1 for oxidized moieties easily distinguishable. As a

first approximation, it was assumed that the signal of the unmodified remaining cellulose after periodate treatment was the same as that in the starting material, and that the sensitivity of each carbon did not change after oxidation.

The intensity of the C1 signal of cellulose at 105 ppm was then used to define the sub-spectra arising from the remaining intact cellulose (spectrum S0) in the POC sample (spectrum S) since it is the only region where the spectra of cellulose and the spectra of fully oxidized POC do not overlap, as shown in Supporting Information Figure SC2-2. As seen in this figure, the contribution due to the intact cellulose in the POC sample is assumed to be the S0 spectra, identical to that of the starting cellulose, but normalized by the intensity at 105 ppm. The fraction of carbon atoms belonging to the intact cellulose with respect to the total number of carbon atoms in the sample is obtained by dividing the integral of the normalized S0 sub-spectra with that of the whole S spectra, the integrations being done from 40 to 230 ppm.

If we assume that the oxidation is completely selective, giving two aldehyde groups for each oxidized glucosyl ring, the degree of oxidation (DO), as defined by the number of aldehyde groups per glycosyl residue, will be obtained from:

$$\text{DO} = 2 \frac{\text{number of oxidized AGU}}{\text{total number of AGU}} \quad (4)$$

$$= 2 \frac{\text{total number of AGU} - \text{number of unoxidized AGU}}{\text{total number of AGU}} \quad (5)$$

$$= 2 \left( 1 - \frac{\text{number of unoxidized AGU}}{\text{total number of AGU}} \right) \quad (6)$$

and thus from the normalized spectra,

$$\text{DO}_{\text{NMR}} = 2 \left( 1 - \frac{\int S_0}{\int S} \right) \quad (7)$$

Where  $\int S_0$  and  $\int S$  correspond to the integrated quantities of the  $S_0$  (initial cellulose) and  $S$  (analyzed POC sample) spectra, respectively.

### 3. Results and discussion

#### 3.1. Obtaining DOs from NaOH oxime titration ( $\text{DO}_{\text{t-NaOH}}$ ):

A first series of samples was produced from the periodate oxidation of MFC for 65 h with increasing amounts of periodate, from 0.2 to 1.3 equivalent of AGU. At first, we followed Zhao and Heindel's protocol<sup>153</sup> where the reaction time with the hydroxylamine solution was set to 2 h. To probe the completion of oxime formation, this reaction time was then increased to 24, 65 and 96 h. The DOs extracted from oxime titration, noted  $\text{DO}_{\text{t-NaOH}}$ , and corresponding to the various reaction times with hydroxylamine are shown in Figure 30 as a function of the periodate to AGU molar ratio.

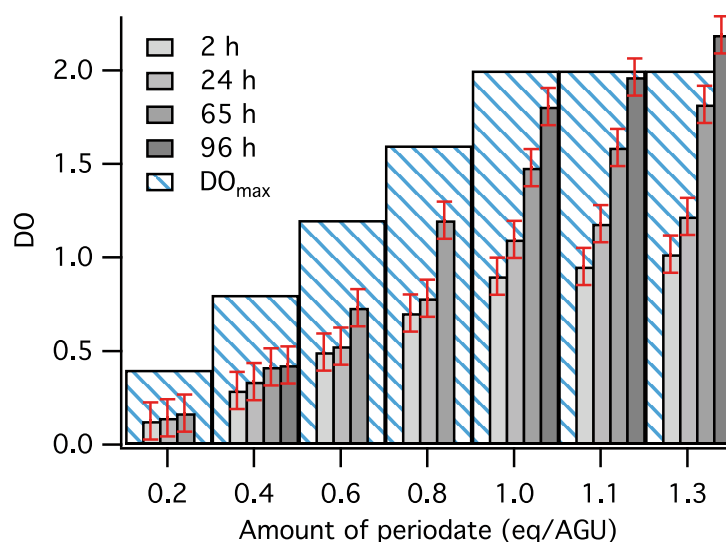


Figure 30.  $\text{DO}_{\text{t-NaOH}}$  of MFCs oxidized for 65 h measured by hydroxylamine titration as a function of the periodate to AGU molar ratio for variable reaction times with hydroxylamine. Hatched areas correspond to  $\text{DO}_{\text{max}}$ , the theoretical DO when all periodate input would have been consumed for oxidation.

Figure 30 shows that the  $\text{DO}_{\text{t-NaOH}}$  keeps increasing with the reaction time between the POC and the hydroxylamine, without any clear critical time or leveling off time. The oxime method to titrate the generated HCl by Zhao and Heindel<sup>153</sup> was originally used for oxidized dextran, a water-soluble polymer, *i.e.* under homogeneous conditions where the accessibility is maximized. Under these conditions, a 2 h reaction time with hydroxylamine was probably sufficient to achieve a full completion of the reaction. However, in the case of oxidized MFCs, a heterogeneous reaction takes place and the accessibility toward the reagent is strongly hampered, thus requiring longer reaction times to achieve completion of the reaction. For 1.3 equivalent periodate added,  $\text{DO}_{\text{t-NaOH}}$  even exceeds the theoretical maximum value of 2 after a 96 h reaction with hydroxylamine. The reason for this overestimation is probably due to the acid catalyzed hydrolysis of the sample as a result of the low pH. In fact, for highly oxidized samples, the pH decreases below 1 two hours after the mixing of the POC with the hydroxylamine solution. The extended reaction time in these highly acidic conditions can then lead to the hydrolysis of the POC as well as to that of unoxidized cellulose, thus liberating new reducing ends that also react with hydroxylamine. This contribution would be negligible as long as the degree of polymerization remains high, but when the number of short fragments increases, the contribution of the chain ends becomes significant, resulting in an overestimation of DOs that can even exceed the theoretical maximum. Additionally, heterogeneous conditions apparently led to slower oximation and the longer reaction time results in interference with acid hydrolysis.

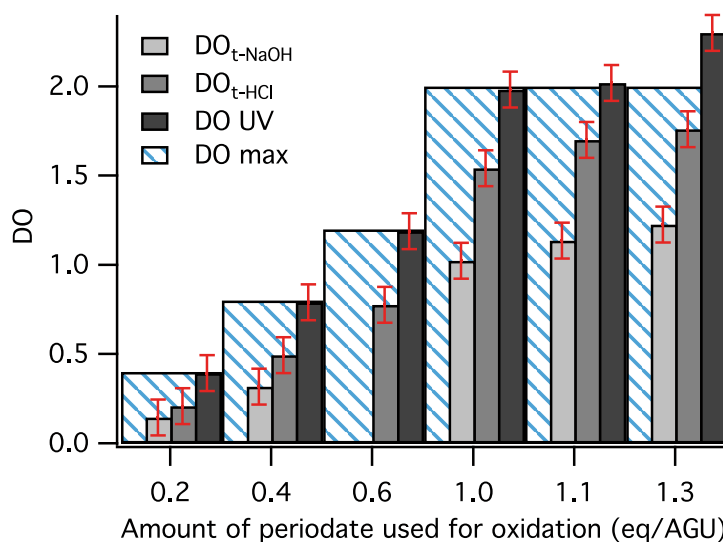
MAS  $^{13}\text{C}$  NMR

Figure 31. Comparison of the DO of MFCs oxidized for 170 h with periodate measured by the two hydroxylamine titration methods (after 2 h of reaction between POC and hydroxylamine),  $\text{DO}_{\text{t-NaOH}}$  and  $\text{DO}_{\text{t-HCl}}$ , and  $\text{DO}_{\text{UV}}$ , as a function of the periodate to AGU molar ratio. Hatched areas correspond to the maximum theoretical DO,  $\text{DO}_{\text{max}}$ .

### 3.2. Comparison of the titration protocols ( $\text{DO}_{\text{t-NaOH}}$ and $\text{DO}_{\text{t-HCl}}$ ):

A second series of periodate oxidation was carried out for 170 h with periodate to AGU molar ratio ranging from 0.2 to 1.3 and the DOs of the resulting POC samples were measured by the two aforementioned oxime titration methods, yielding  $\text{DO}_{\text{t-NaOH}}$  and  $\text{DO}_{\text{t-HCl}}$ . Results are reported in Figure 31. The high discrepancy between these two titrations methods is most probably the consequence of the fact that  $\text{DO}_{\text{t-NaOH}}$  is strongly affected by the sharp pH drop during the POC/hydroxylamine reaction. Compared to Zhao and Heindel protocol<sup>153</sup> made for soluble dextran, the alternative consumed base titration protocol, initially proposed for cellulosic samples, involves NaOH addition to achieve more buffered conditions, avoiding the sharp pH drop and thus results in much higher  $\text{DO}_{\text{t-HCl}}$  values for an identical reaction time (2 h) between the hydroxylamine and the POC. For  $\text{DO}_{\text{t-HCl}}$  measurements, the kinetics of oxime formation is probably faster due to the higher hydroxylamine concentration compared to that of Zhao and Heindel's

protocol and the excessive acid hydrolysis is avoided, as the medium is closer to neutrality (pH always higher than 4.8). This protocol also leads to more stable DOs over a period of 24 h of reaction between POC and hydroxylamine.<sup>161</sup>

### 3.3. Obtaining DOs from titration with UV-Visible Spectroscopy ( $\text{DO}_{\text{UV}}$ ):

The 170 h-oxidized samples were also characterized by UV-Visible spectroscopy (Figure 31).  $\text{DO}_{\text{UV}}$  was always close to the theoretical maximum after 170 h of oxidation, but had about twice the value of  $\text{DO}_{\text{t-NaOH}}$ . For the two samples with more than 1 equivalent of periodate,  $\text{DO}_{\text{UV}}$  was higher than  $\text{DO}_{\text{max}}$  (for example  $\text{DO}_{\text{UV}}$  with 1.3eq = 2.3 >  $\text{DO}_{\text{max}}= 2$ ), which means that in these cases, periodate is at least partly consumed by side reactions.<sup>162</sup> This extra consumption is obvious for samples with  $\text{NaIO}_4$  to AGU molar ratio larger than 1, and highly probable in the other cases. Thus, the UV method is likely to overestimate the dialdehyde production on the recovered products.

### 3.4. Obtaining DOs from CP-MAS $^{13}\text{C}$ NMR spectroscopy ( $\text{DO}_{\text{NMR}}$ ):

As shown above, the two classical methods, namely oxime titration and UV-absorbance, do not provide clear and reproducible DO values due to the inherent heterogeneous conditions that are used and the concomitant side reactions. Here, a new DO measurement approach based on CP-MAS  $^{13}\text{C}$  NMR is proposed. As a physical method, solid-state NMR is not sensitive to the heterogeneous reactivity limitations encountered with the oxime titration, and the analysis is directly made on the freeze-dried recovered substrate.

Figure 32 shows the CP-MAS NMR spectra of a series of 65 h-periodate oxidized MFC samples, identical to those tested in Figure 30. The spectra are normalized to have a constant total integrated area for each sample, as we expect the number of carbons to be constant (6 carbons on each glucosyl ring).

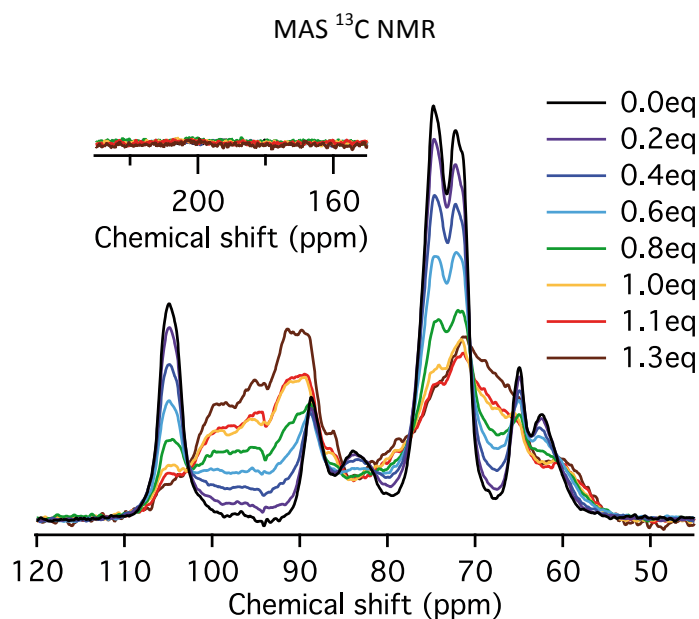


Figure 32. CP-MAS  $^{13}\text{C}$  NMR spectra in the dry state of MFCs oxidized for 65 h while varying the  $\text{NaIO}_4$  to AGU molar ratio (from 0.2 to 1.3 eq). For each spectrum, the total integrated area was normalized to 1.

As systematically reported, the absence of signals in the 160-200 ppm region indicates that the aldehyde groups do not exist in their free form but have readily recombined with neighboring hydroxyl groups to give various hemiacetal and/or hemialdal entities, which give rise to a broad signal in the 90-100 ppm region.<sup>93, 110-111, 120, 147, 152, 163</sup> In Figure 32, the resonance at 105 ppm assigned to the C1 of native cellulose decreases as a function of the periodate concentration, while the hemiacetal signals are increasing, which is consistent with an increase of the DO with the  $\text{NaIO}_4$  to AGU molar ratio.<sup>110-111</sup>

As described in the experimental part, the intensity of the signal from the C1 of cellulose at 105 ppm was used as an internal standard for the remaining amount of un-oxidized cellulose. By normalization of the C1 of the initial MFCs with the C1 of the remaining intact cellulose in the POC samples, and by integrating the whole spectra, the calculation of a percentage of oxidation or DO can be quantitatively extracted from a CP-MAS  $^{13}\text{C}$  NMR spectrum of any POC sample, using equation 7.

A series of periodate oxidation of MFC suspensions were also performed using 0.2 to 1.3 equivalent of periodate to AGU and increasing oxidation times from 2 to 170 h. The  $\text{DO}_{\text{NMR}}$  calculated from the spectral integration as a function of reaction time and the amount of periodate are shown in Figure 33. The corresponding series of spectra are available in Supporting Information Figures SC2-3 to SC2-6. For a given  $\text{NaIO}_4$  to AGU molar ratio, the  $\text{DO}_{\text{NMR}}$  clearly increases with the oxidation time until 65 h. In addition, for a given reaction time, the  $\text{DO}_{\text{NMR}}$  clearly increases with the  $\text{NaIO}_4$  to AGU molar ratio. These data show that a very precise control of the DO of oxidized MFC samples in the 0-1.9 range can be reached by varying the two reaction parameters, namely time and periodate concentration. Remarkably, solid-state NMR spectra indicate the presence of remaining native cellulose up to a  $\text{DO}_{\text{NMR}}$  of 1.9, indicating the heterogeneous character of the oxidation reaction.

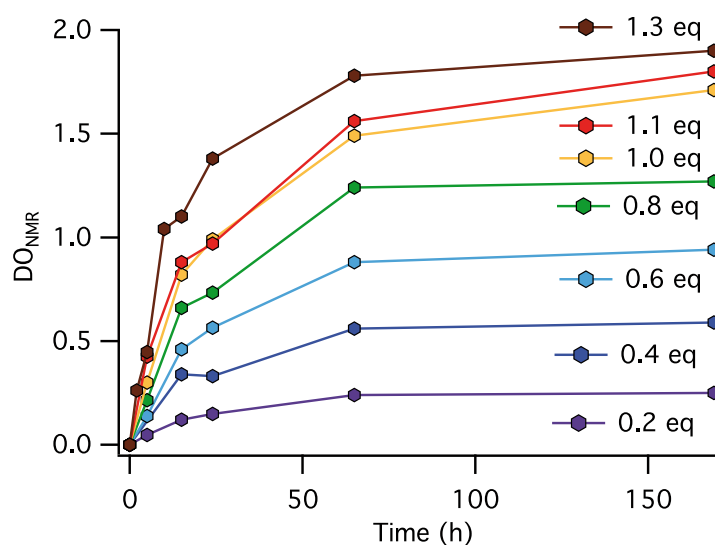


Figure 33. Evolution with reaction time of the DO measured by CP-MAS  $^{13}\text{C}$  NMR,  $\text{DO}_{\text{NMR}}$ , of periodate oxidized MFCs for variable amounts of  $\text{NaIO}_4$  to AGU molar ratio.

To evaluate the relevance of the NMR methods, NMR spectra of POC were reconstructed by a linear combination of the initial NMR spectrum of MFC and of the NMR spectrum of the most oxidized cellulose ( $\text{DO}=1.90$ ) (Figure SC2-7 to SC2-12). The resulting calculated

spectra are very close to the experimental ones, strongly supporting the idea that the oxidized samples are two-phase materials made of fully oxidized and unreacted native cellulose. However, there is still a systematic difference between the original and the reconstructed spectra, especially in the C4 region where the reconstructed spectra for intermediate DOs are slightly overestimated compared to the experiment. To account for this observation, one has to remember that the reaction most probably progresses from the surface to the interior of the microfibrils, leading to a heterogeneous core-shell structure, as already observed for the gas phase esterification of nanocelluloses.<sup>164-165</sup> For sufficiently high degrees of oxidation, the microfibrils are then partially consumed by the reaction and their dimensions and hence crystallinity should decrease concomitantly, explaining changes in the ratio of crystalline (near 90 ppm) and disordered / surface (around 85 ppm) contributions. The slight differences between experimental and reconstructed spectra would reflect this change in proportion of crystalline and surface fractions. Conversely, a minor contribution at high magnetic field is also always present for the C1 carbon resonance in the experimental spectra for the intermediate products, which can be due to chemically intact glucose residues with a slightly modified chemical shift due to a different environment. Altogether, these differences that reflect the ultrastructural modifications, account for less than 5% of the total area, making the evaluation of the oxidation degree by this technique quite robust and reproducible.

### 3.5. Heterogeneous reaction leading to $\text{DO}_{\text{UV}} > \text{DO}_{\text{NMR}}$

The oxidation mechanism implies that each periodate ion leads to a di-aldehyde unit and thus, the samples should reach a DO of 2 when 1 equivalent or more of periodate per AGU has been used. However, in this work, the final  $\text{DO}_{\text{NMR}}$  in the samples was

systematically lower than expected. For example, a sample oxidized for 170 h with 1.0 eq periodate per AGU had a  $\text{DO}_{\text{NMR}}$  of only 1.7, with significant amount of intact native cellulose, whereas  $\text{DO}_{\text{UV}}$  indicated that 99% of the introduced periodate had been consumed (*i.e.*  $\text{DO}_{\text{UV}}=1.98$ ).

To reconcile these discrepancies, we should keep in mind that the characterization is performed on the solid pellet recovered after extensive centrifugation, the reaction medium being discarded. Interestingly, Figure 34 shows that the mass yield of the recovered POC decreases linearly as oxidation proceeds, whatever the time and periodate conditions used for the experiments, reaching a final value of about 60% for almost fully oxidized cellulose (Figure 34). The discarded soluble fraction most probably consists of strongly oxidized chains that were solubilized before forming hemiacetal linkages with neighboring chains. This mechanism would be favored by the dilute conditions used (0.7%) and is in agreement with previous reports indicating that highly oxidized dialdehyde cellulose was soluble in hot water and remained stable in solution after cooling.<sup>70, 157</sup>

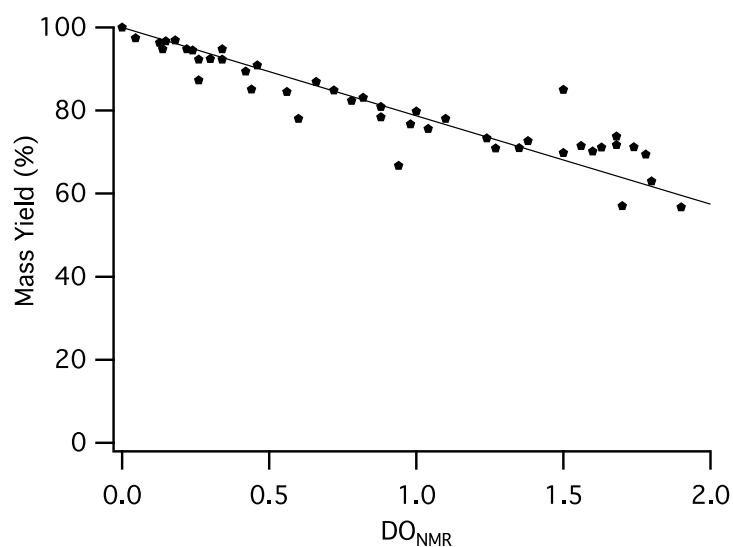


Figure 34. Mass yield evolution with the degree of oxidation of samples recovered after successive centrifugations at 20,000 g followed by freeze-drying.

In all these experiments the solubilized cellulose fraction is not recovered, but its DO is expected to be higher than that of the recovered solid due to higher accessibility. Two extreme scenarios could then be envisaged: (i) the DO of the solubilized part is the same as that of the recovered solid or (ii) the solubilized part has a DO of 2. To test these hypotheses, various presumed periodate quantities were calculated from  $\text{DO}_{\text{UV}}$  and  $\text{DO}_{\text{NMR}}$  data as well as from the mass yield after purification and freeze-drying. The UV-Vis measurements gives the total amount of periodate consumed during the oxidation reaction,  $P_{\text{total}}$ , while the NMR data combined with the mass yield values gives the amount of periodate necessary to oxidize the recovered solid POC fraction,  $P_{\text{solid}}$ . The amount of periodate consumed to oxidize the unrecovered fraction can be calculated from the mass yield but depends on the DO of the solubilized chains. On the one hand, if one assumes that the DO of these solubilized chains is the same as that of the recovered solid POC, the necessary consumed amount of periodate,  $P_{\text{soluble,DO=DO}_{\text{NMR}}}$  can be calculated and can be considered as the lowest reference. On the other hand, if the solubilized chains are considered to be fully oxidized, a consumed periodate amount,  $P_{\text{soluble,DO=2}}$  can be extracted.

Figure 35 compares the initial amount of periodate,  $P_{\text{initial}}$ , and the total periodate consumption,  $P_{\text{total}}$ , with  $P_{\text{solid}} + P_{\text{soluble,DO=DO}_{\text{NMR}}}$  (Straight black line) and with  $P_{\text{solid}} + P_{\text{soluble,DO=2}}$  (blue diamonds). It can be seen for the first four data points that  $P_{\text{total}}$  is significantly greater (from 10 to 50% greater) than  $P_{\text{solid}} + P_{\text{soluble,DO=DO}_{\text{NMR}}}$  but comparable to  $P_{\text{solid}} + P_{\text{soluble,DO=2}}$  indicating that the solubilized product is highly oxidized. These data therefore show that  $\text{DO}_{\text{UV}}$  and  $\text{DO}_{\text{NMR}}$  are comparable as long as the unrecovered soluble material is taken into account, at least for low DO values ( $\leq 1$ ).  $P_{\text{solid}} + P_{\text{soluble,DO=2}}$  data for

$1.5 < \text{DO}_{\text{NMR}} < 2$  cannot reproduce the over consumption of periodate indicating the presence of side reactions.<sup>162</sup>

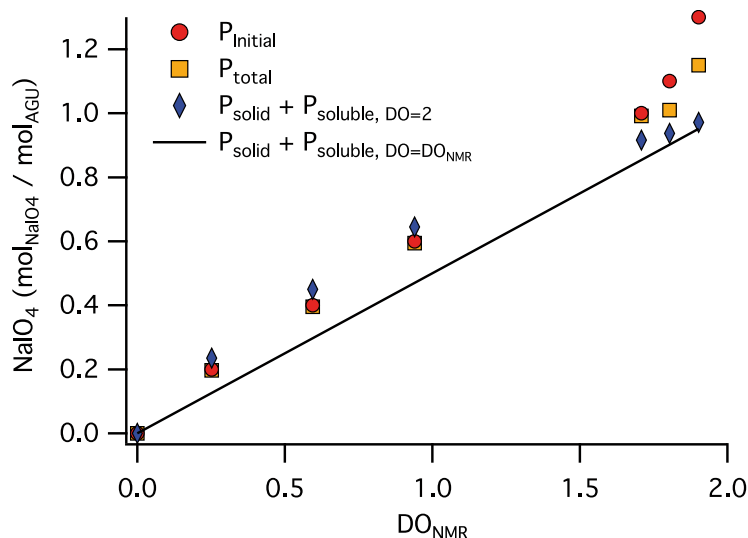


Figure 35. Various amounts of periodate measured or calculated from  $\text{DO}_{\text{UV}}$ ,  $\text{DO}_{\text{NMR}}$  and mass yield data. See text for details.

### 3.6. Agreement between $\text{DO}_{\text{NMR}}$ and $\text{DO}_{\text{t-HCl}}$

As aforementioned,  $\text{DO}_{\text{t-HCl}}$  are always higher than  $\text{DO}_{\text{t-NaOH}}$  after a conventional 2 h reaction time between POC and hydroxylamine. If we now compare these DO values with the results from NMR, the  $\text{DO}_{\text{t-NaOH}}$  and  $\text{DO}_{\text{t-HCl}}$  correspond to about 60% and 90% of the  $\text{DO}_{\text{NMR}}$  (see Supporting Information Figure SC2-13), respectively. This fairly good agreement between the proposed NMR quantification and Green's titration protocol suggests that these 2 methods measure the real DO of POC. Another aspect of the  $\text{DO}_{\text{t-HCl}}$  measurement is that they are not reaction time dependent.<sup>161</sup>

## 4. Conclusions

In this study, we have observed that in the  $^{13}\text{C}$  CP-MAS NMR spectra of the periodate oxidized cellulose, the resonances corresponding to the oxidized cellulose part always

have the same shape, independently of the DO. These resonances do not overlap with the peak attributed to the C1 of underivatized cellulose. This peak can be used to quantify the residual cellulose fraction and to deduce the degree of oxidation from NMR data. The periodate consumption monitored by UV absorption was always higher compared to the DO measured by the NMR spectrum of the recovered product, while the method based on oxime formation at a pH around 5 gave values close to the NMR method. At lower pH the oxime formation is slow and induces cellulose hydrolysis, leading to unreliable values. The DO of the recovered product estimated by solid-state NMR agrees with the periodate consumption from UV absorbance at 290 nm if we consider that the solubilized fraction is fully oxidized. Thus when a partial dissolution occurs, the UV absorbance can be used to follow the oxidation reaction, while the degree of oxidation of the solid phase has to be determined separately by solid state NMR or oxime formation in buffered conditions. Moreover, solid-state NMR gives information on the ultrastructure of the product, especially on the inherent heterogeneous character of the periodate oxidation, leading to a two-phase product made of a fully oxidized cellulose skin surrounding an intact but partially consumed native cellulose core. We provide here an accurate, simple and reproducible  $^{13}\text{C}$  NMR method that allows both DO measurements after periodate oxidation of cellulose and importantly the monitoring of its physical state, which could be extended to all types of cellulose.

## Chapter 2: Supporting information

Supporting Information contains a calibration curve of absorbance as function of the periodate concentration, the NMR spectra superposition protocol for DO calculation by  $^{13}\text{C}$  CP-MAS NMR, the  $^{13}\text{C}$  CP-MAS NMR spectra of periodate oxidized MFC series, reconstructed  $^{13}\text{C}$  CP-MAS NMR spectra of oxidized MFC, and the relationship between  $\text{DO}_{\text{NMR}}$  and the  $\text{DO}_{\text{titrations}}$ .

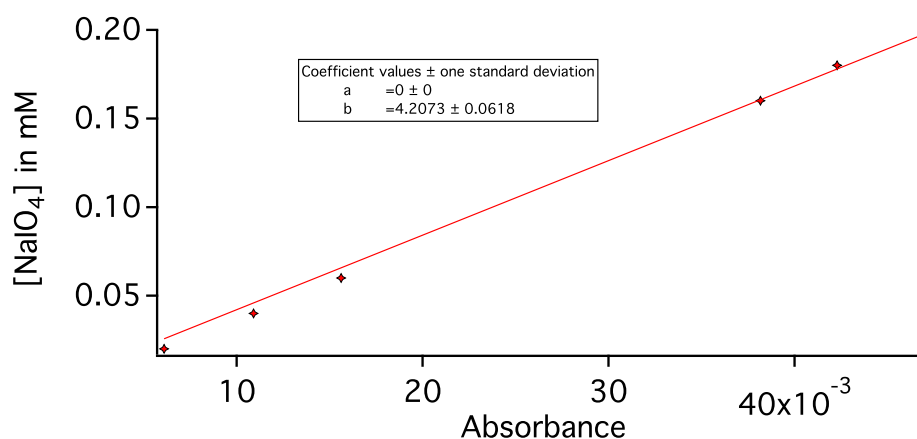


Figure SC2-1 Calibration curve for the determination of the remaining periodate concentration by UV-Visible spectroscopy at 290 nm.

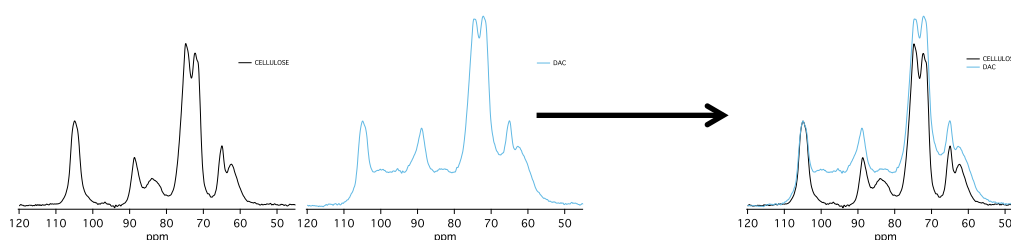


Figure SC2-2 Separated (left) and superimposed (right) CP-MAS NMR spectra from unmodified cellulose S0 (Black) and periodate oxidized cellulose S (Blue), normalized against the  $\text{C}_1$  signal at 105 ppm.

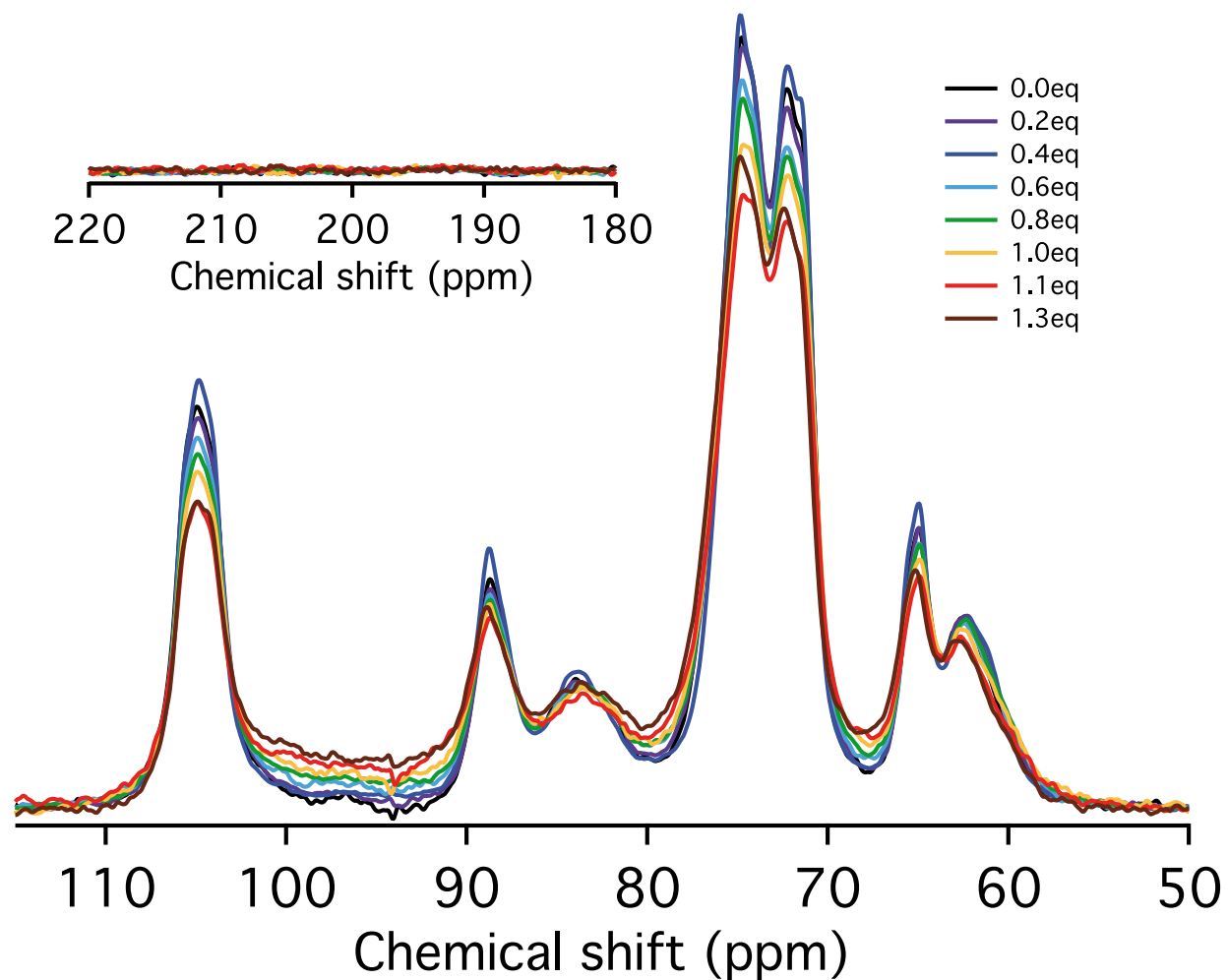


Figure SC2-3  $^{13}\text{C}$  CP-MAS NMR in the dry state of MFC oxidized 5 h with different amount of periodate (from 0.2 to 1.3eq). Spectra total area set to 1.

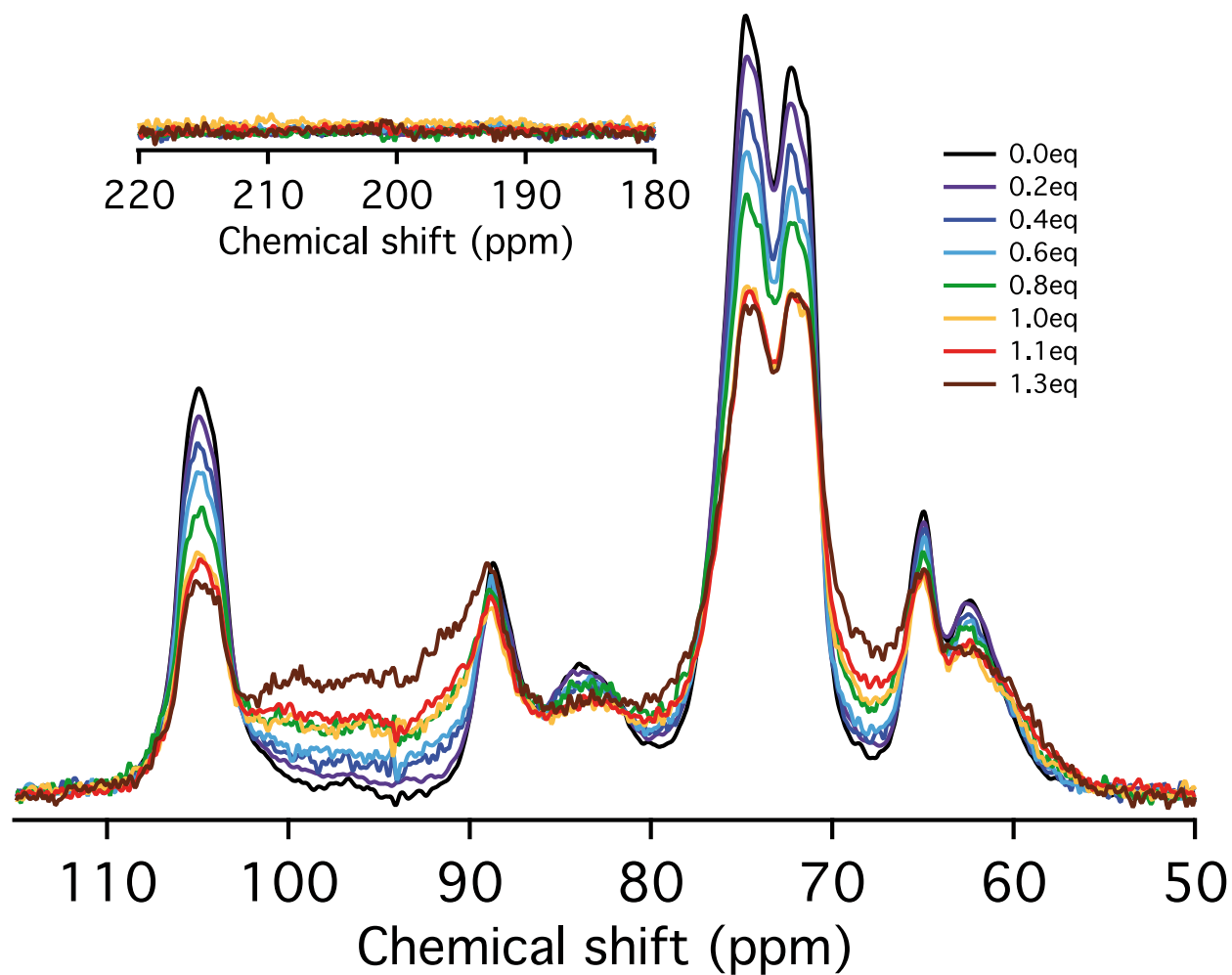


Figure SC2-4  $^{13}\text{C}$  CP-MAS NMR in the dry state of MFC oxidized 15 h with different amount of periodate (from 0.2 to 1.3eq). Spectra total area set to 1.

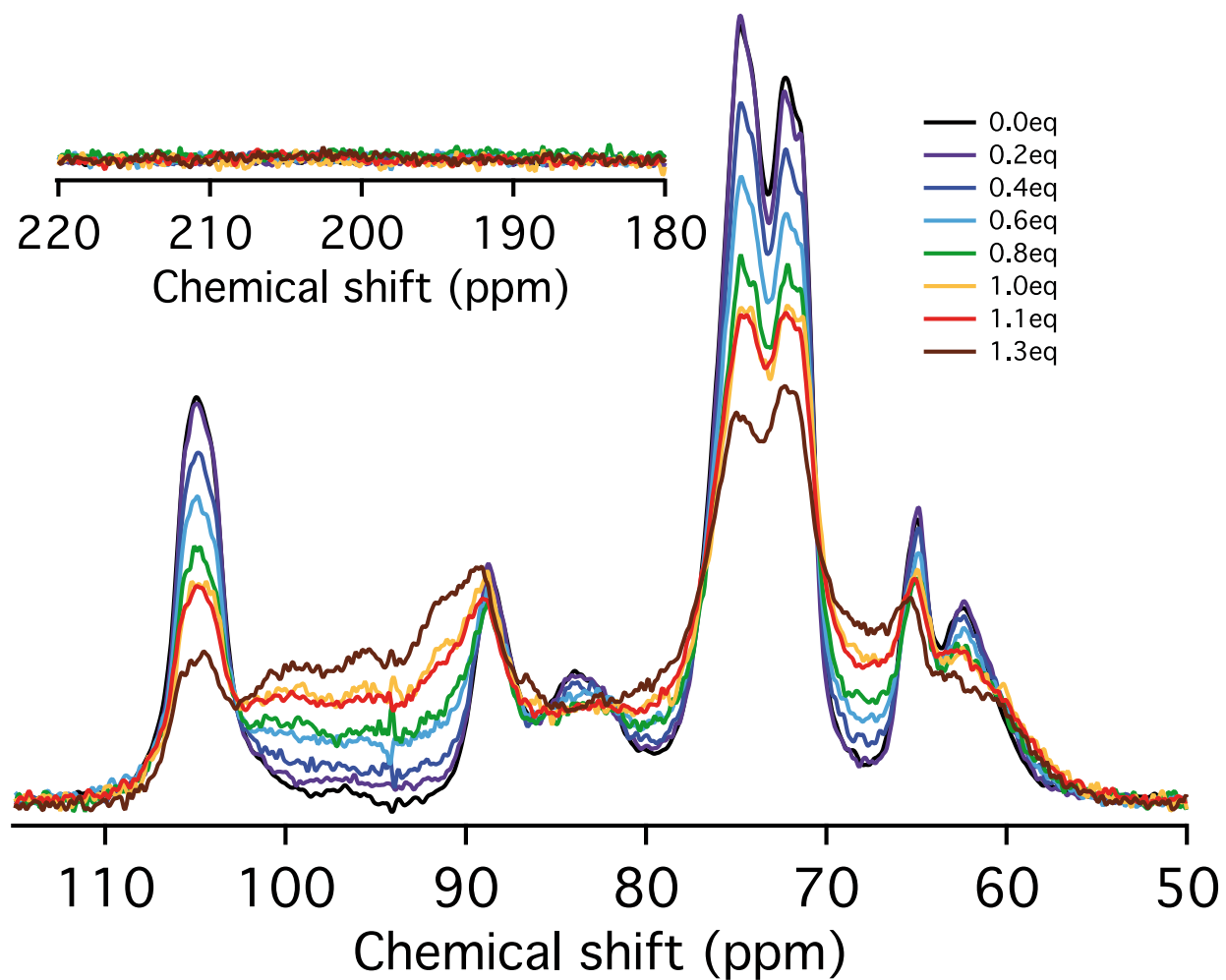


Figure SC2-5  $^{13}\text{C}$  CP-MAS NMR in the dry state of MFC oxidized 24 h with different amount of periodate (from 0.2 to 1.3eq). Spectra total area set to 1.

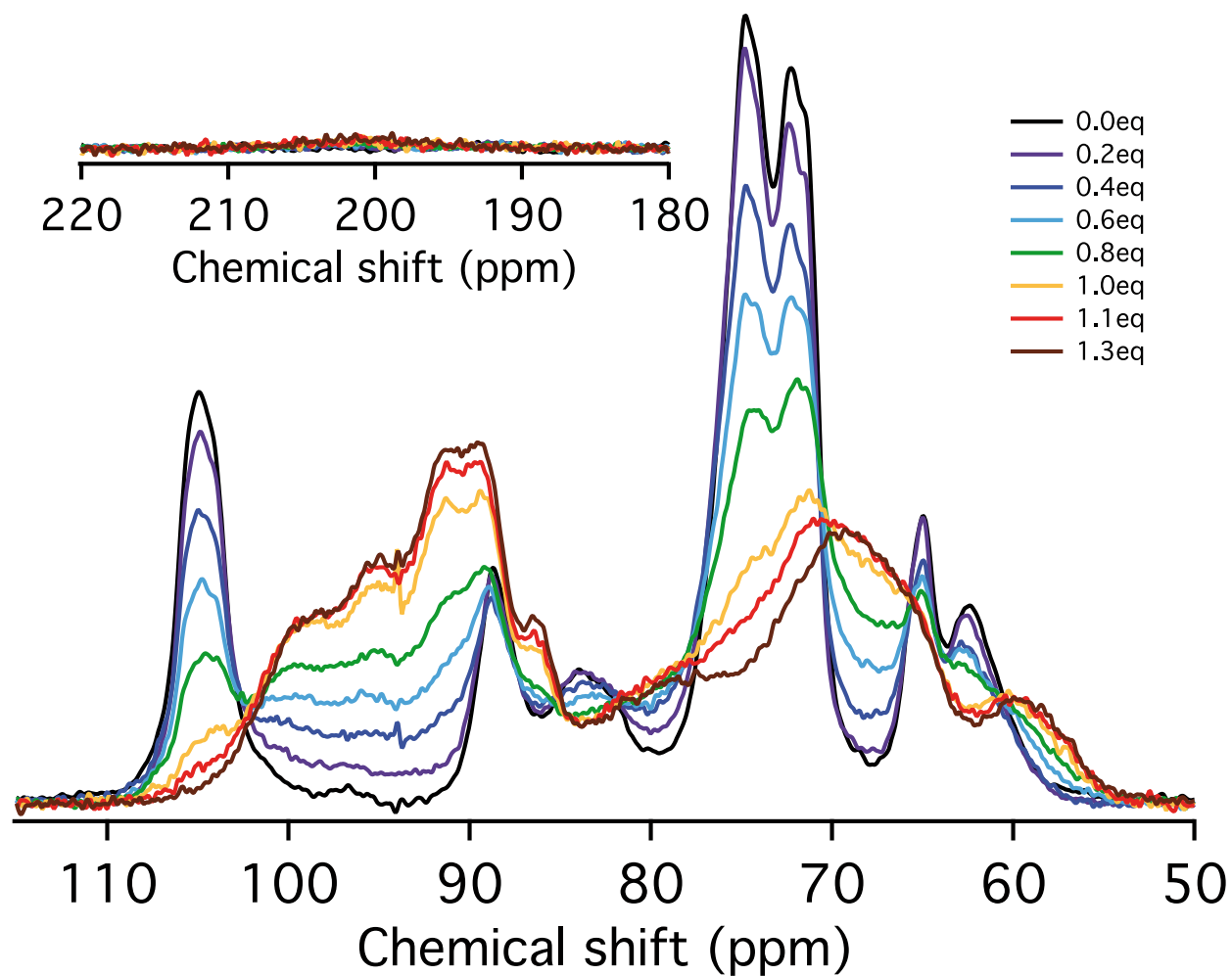


Figure SC2-6  $^{13}\text{C}$  CP-MAS NMR in the dry state of MFC oxidized 169 h with different amount of periodate (from 0.2 to 1.3eq). Spectra total area set to 1.

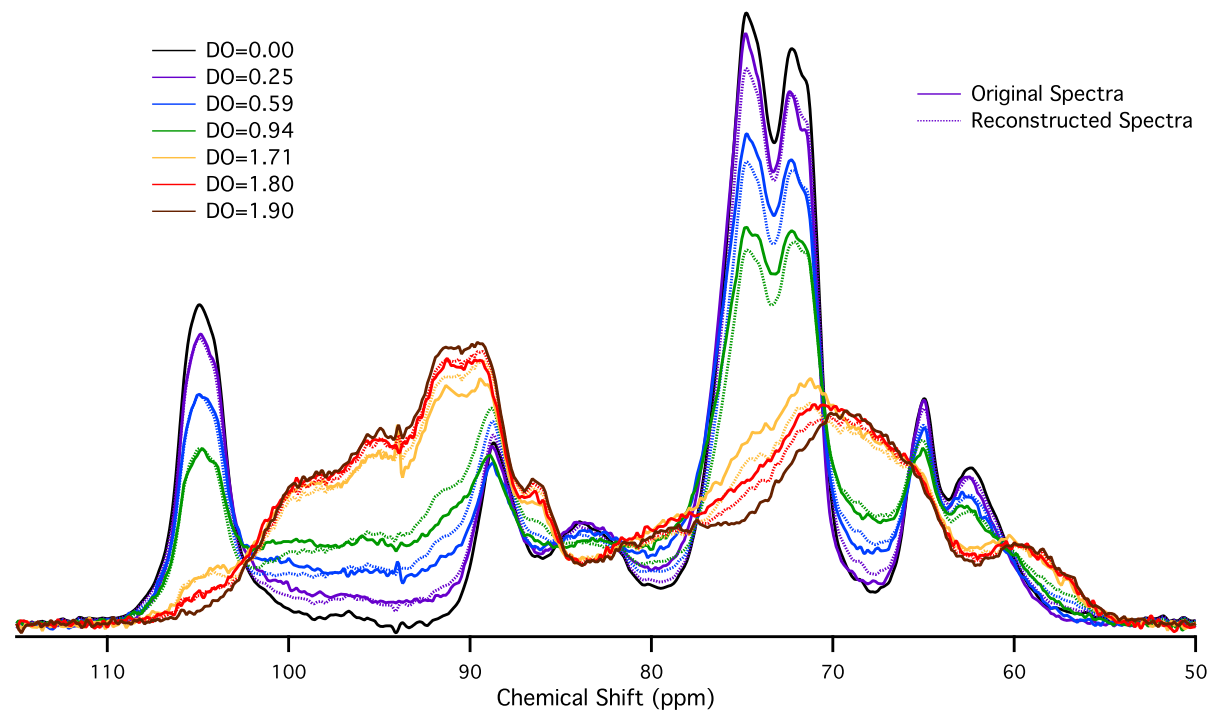


Figure SC2-7 Reconstruction of POC NMR spectra with intermediate DO from the spectrum of cellulose and the spectrum of fully oxidized cellulose ( $DO_{\text{NMR}}=1.90$ ).

$$DAC \text{ spectrum} = \frac{DO}{2} \cdot (DAC \text{ DO} = 2 \text{ spectrum}) + \left(1 - \frac{DO}{2}\right) \cdot (MFC \text{ spectrum})$$

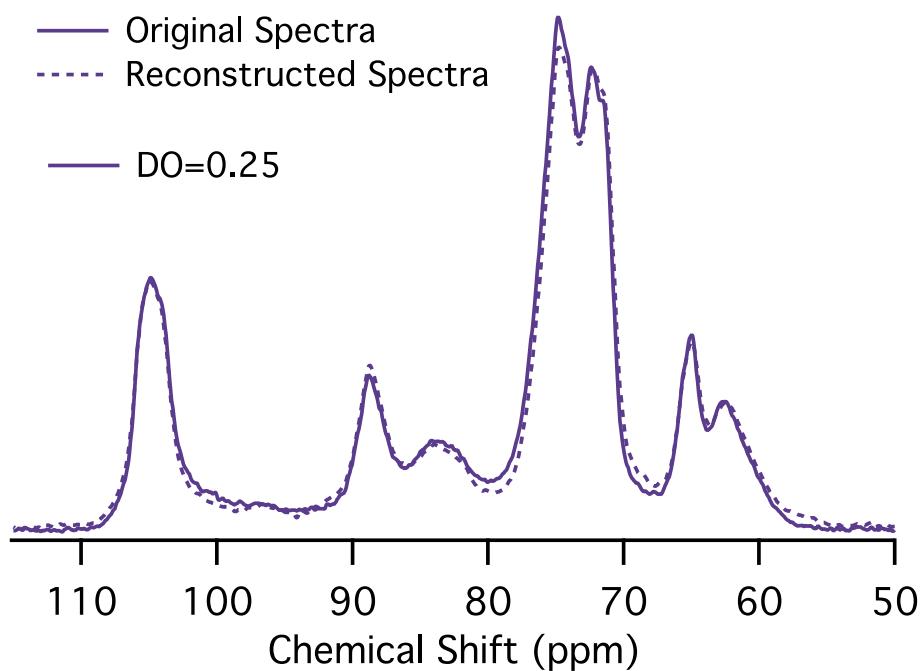


Figure SC2-8 Original and reconstructed NMR spectra of POC with  $DO_{NMR} = 0.25$  from the spectrum of cellulose and the spectrum of fully oxidized cellulose ( $DO_{NMR}=1.90$ ).

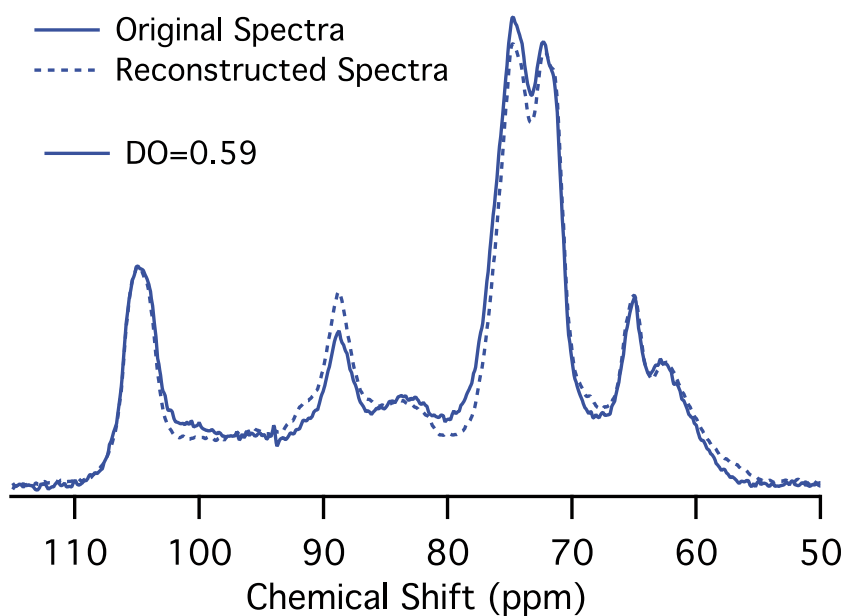


Figure SC2-9 Original and reconstructed NMR spectra of POC with  $DO_{NMR} = 0.59$  from the spectrum of cellulose and the spectrum of fully oxidized cellulose ( $DO_{NMR}=1.90$ ).

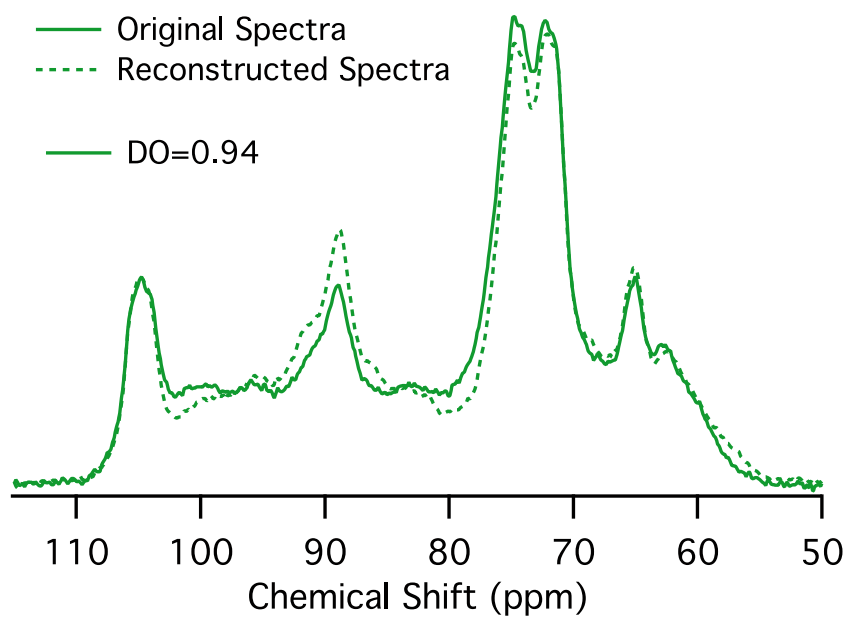


Figure SC2-10 Original and reconstructed NMR spectra of POC with  $DO_{\text{NMR}} = 0.94$  from the spectrum of cellulose and the spectrum of fully oxidized cellulose ( $DO_{\text{NMR}}=1.90$ ).

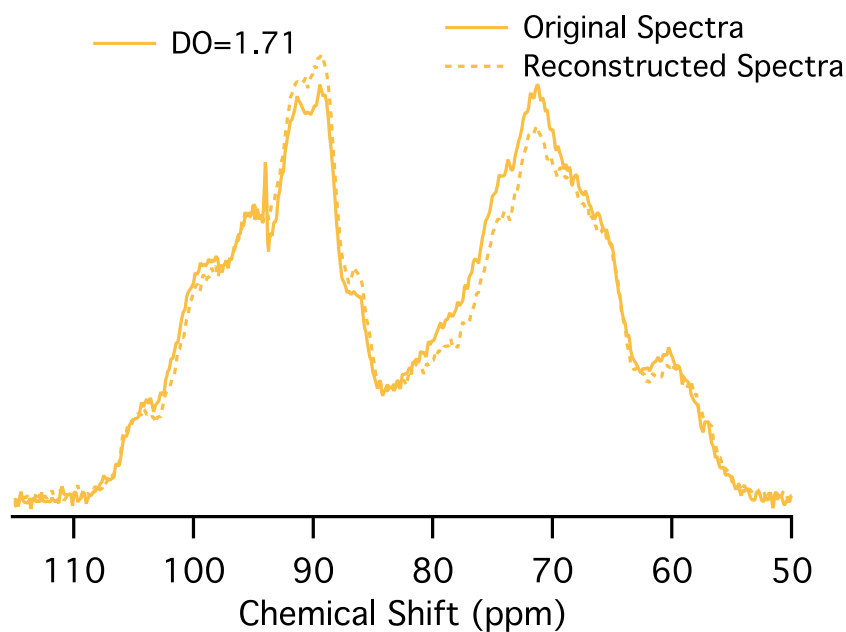


Figure SC2-11 Original and reconstructed NMR spectra of POC with  $DO_{\text{NMR}} = 1.71$  from the spectrum of cellulose and the spectrum of fully oxidized cellulose ( $DO_{\text{NMR}}=1.90$ ).

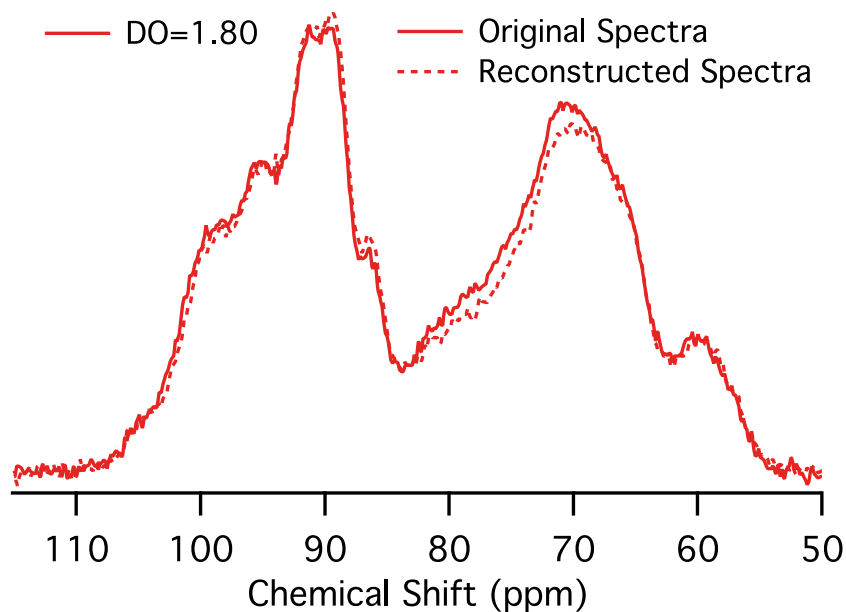


Figure SC2-12 Original and reconstructed NMR spectra of POC with  $DO_{NMR} = 1.80$  from the spectrum of cellulose and the spectrum of fully oxidized cellulose ( $DO_{NMR}=1.90$ ).

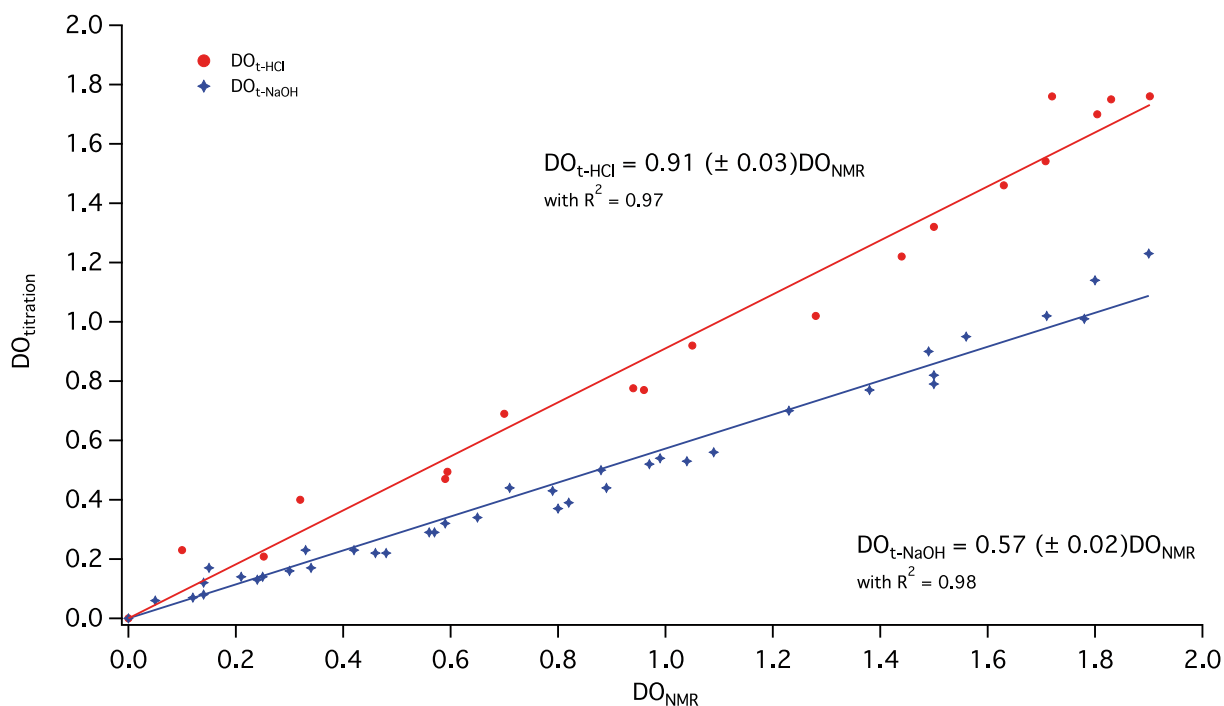


Figure SC2-13 Comparison of the  $DO_{NMR}$  with  $DO_{titration}$  from two different protocols:

Zhao *et al.*<sup>153</sup> ( $DO_{t-NaOH}$ ) and Green *et al.*<sup>160</sup> ( $DO_{t-HCl}$ ).



# Chapter 3: Synthesis and characterization of all-cellulose thermoplastics

---

In the previous chapter, POC samples were synthesized and the corresponding DOs were mapped as a function of the initial oxidation parameters. Additionally, accurate DO measurements protocols were set. Now that the synthesis of POC can be controlled, this chapter will use POC samples to prepare thermoplastic materials. In fact, POC samples were further reduced *in situ* with  $\text{NaBH}_4$  to produce materials with nanocomposite properties including a thermoplastic matrix.

## 1. Introduction

As a widely available and renewable material source, cellulose is one of the most promising candidates for the design of green materials. This ubiquitous polymer is already used in a great number of applications for which the processes are adapted to its fibrous form, typically forming non-wovens (paper) or yarns. The relatively recent renewed interest in what is currently called nanocellulose, including microfibrillated cellulose (MFC), also called cellulose nanofibrils (CNF), and cellulose nanocrystals (CNC) has revived the scientific activity around cellulose's use in nanopaper or nanocomposites.<sup>166</sup>

Cellulose in its native form suffers from a crucial limitation in that its degradation temperature is well below its glass transition or melting temperature, due to a very dense and organized network of hydrogen bonds between intrinsically rigid molecules. This major drawback, identified even before the beginning of polymer science, has been circumvented by substituting most of the hydroxyl groups, such as in the case of nitrocellulose or cellulose acetate which were discovered and have been produced since the nineteenth century. Such derivatives, however, necessitate the extensive use of plasticizers for optimal flowing properties. In addition to inherent drawbacks such as aging and exudation, the extended-chain structure of cellulose, which is at the origin of its outstanding mechanical properties, is lost during the homogenous derivatization process.

An alternative to the modification of hydroxyl groups is to directly cope with the problem of chain rigidity by introducing additional mobility to the backbone. Among the numerous possibilities of cellulose modification, the periodate oxidation is characterized by the selective oxidation of the hydroxyl groups in the C2 and C3 position into aldehydes accompanied by the opening the glucose ring. This reaction has been used since decades for the characterization of polysaccharides,<sup>59</sup> and continues to be used on cellulose.<sup>156</sup> The resulting products can be either post-oxidized by chlorite or reduced with sodium borohydride, resulting in dicarboxylic acid or dialcohol cellulose respectively.<sup>96-97</sup> In the field of materials development, periodate oxidized cellulose (POC) has been also proposed as a platform for further surface modification<sup>75-77, 111</sup> and hydrogel<sup>113</sup> or aerogel<sup>114</sup> cross-linking.

However, the generated aldehydes form hemiacetals and hemialdals resulting in new cyclic structures. This form of crosslinking hampers the benefit of the reaction in terms

of shaping possibilities. The resulting materials, which can be considered as all-cellulose composites, are much closer to thermoset materials than thermoplastic ones.<sup>93</sup> One of the possibilities to avoid the crosslinking due to the presence of aldehydes is to reduce them into alcohols. This reduction can be achieved either in homogeneous conditions after dissolution of cellulose<sup>98</sup> or in heterogeneous conditions in water suspension to improve the ductility of cellulose microfibril films,<sup>99</sup> or directly on cellulose fibers.<sup>103</sup>

The homogeneous reduction pathway leads to a material with a glass transition temperature that decreases with increasing degree of oxidation, the fibrillar structure is lost during the dissolution process.<sup>98</sup> This material can in principle be used as a conventional thermoplastic. In the heterogeneous reduction case, the reaction results in a core-shell structure of an intact crystalline cellulose core surrounded by a thermoplastic layer. A similar situation can be found in the case of heterogeneous esterification of cellulose fibers<sup>167</sup> or of nanocellulose aerogels,<sup>164-165</sup> for which the core-shell structure has been clearly demonstrated. For moderate degree of oxidation, the fibrillar morphology is preserved and conventional papermaking processes can be used to obtain ductile cellulose nanofibrils films<sup>99</sup> or fibre-based thermoplastic materials.<sup>103</sup>

In a preceding work, we used different techniques to carefully characterize a whole set of materials, from native cellulose to highly oxidized cellulose compounds, produced by the periodate oxidation of microfibrillated cellulose under various conditions. Solid-state <sup>13</sup>C CP-MAS NMR was shown to be a powerful tool to follow the progress of the reaction from the surface of the microfibrils to the core of the crystals, decrystallizing them progressively.

In order to systematically investigate the role of this core-shell structure on the properties of these oxidized then reduced materials over a wide range of oxidation

degree, we reduced these samples to obtain rPOC (reduced periodate-oxidized cellulose) samples with initial DO values ranging between 0 and 1.8. We characterized the ultrastructure of the rPOC by using  $^{13}\text{C}$  CP-MAS NMR and X-ray diffraction and the thermo-mechanical properties by differential scanning calorimetry, thermogravimetric analysis and dynamic mechanical analysis on thin films obtained by casting. Additional two-dimensional wideline separation NMR (WISE) experiments designed to probe local mobility have also been performed in order to relate the ultrastructure to the dynamic behavior.

## 2. Materials and methods

### 2.1. Materials

A batch of paste-like never dried microfibrillated cellulose (MFC) prepared by a mechano-enzymatic treatment<sup>158-159</sup> of spruce sulfite pulp, with a consistency of about 2%, was purchased from the Centre Technique du Papier (CTP), Grenoble, France. It contains less than 4% of hemicellulose. Sodium metaperiodate ( $\text{NaIO}_4$ ) with purity  $\geq 99.8\%$  and sodium borohydride with purity  $\geq 96\%$  were acquired from Carl Roth and Sigma Aldrich (France), respectively.

### 2.2. Periodate modification of MFC

For a typical experiment, about 1 g on dry basis of the 2 wt % MFC suspension was put in a flask with a magnetic stirrer. The right amount of periodate (from 0.2 to 1.3 equivalent of the total amount of AGU) was dissolved in 40 mL of deionized water and added to the MFC suspension. Another 50 mL of deionized water was added to adjust the cellulose concentration to around 7 g/L. The flask was covered with aluminum foils

to avoid the UV-light degradation of the sodium metaperiodate.<sup>61</sup> The oxidation was carried out at room temperature from 24 to 170 h based on the reaction conditions previously described.<sup>168</sup> The mixture was then dialyzed against deionized water with a 14 kDa cutoff membrane, until the conductivity was close to the conductivity of deionized water (less than 30  $\mu\text{S}$ ). The products, with a final consistency of about 5.5 g/L, were kept never-dried at 4 °C. Aliquots were freeze-dried for analysis purposes. The yield of the reaction was calculated from the ratio of final and initial dry mass. The theoretical maximum yield is 98.8% since the molecular weight of each AGU changes from 162 to 160 g.mol<sup>-1</sup>. Such samples will be referred to as periodate oxidized cellulose (POC). Due to the heterogeneous reaction, it is believed that these POC samples are composed of 2 distinct components: native non-oxidized cellulose and fully oxidized chains, the latter being designated as dialdehyde cellulose (DAC).

### 2.3. Reduction of POC

For a typical experiment, the 5.5 g/L suspension corresponding to about 1 g of a POC dry base was put in a 250 mL flask with a magnetic stirrer. NaBH<sub>4</sub> (2 eq per AGU – the maximum DO of 2 is never reached with the oxidation conditions used above so there is always an excess of NaBH<sub>4</sub> with the 2 eq per AGU) was added to the POC suspension. The mixture was stirred at room temperature for 24 to 48 h. Purifications were made by dialysis (14 kDa cutoff membrane) against deionized water until a conductivity around 30  $\mu\text{S}$  was reached. The products with final consistency of about 4.5 g/L were then stored at 4 °C before further use. Similarly to the denomination of oxidized samples, these products will be referred to as reduced periodate oxidized cellulose (rPOC), and the fully modified chains as dialcohol cellulose (DALC).

#### **2.4. Film casting**

After purification, 80mL samples with a consistency of about 4.5 g/L were film cast in polystyrene petri dishes under ambient conditions to obtain free-standing solid films. Solvent casting took on average 2 weeks.

#### **2.5. CP-MAS solid-state NMR**

Solid-state  $^{13}\text{C}$  NMR spectra were acquired using a Bruker Avance III DSX 400 MHz spectrometer operating at 100.6 MHz for  $^{13}\text{C}$ , using the combination of the cross-polarization, high-power proton decoupling and magic angle spinning (CP-MAS) methods. The spinning speed was set at 12,000 Hz. The  $^1\text{H}$  radio-frequency field strength was set to give a  $90^\circ$  pulse duration of 2.5  $\mu\text{s}$ . The  $^{13}\text{C}$  radio-frequency field strength was obtained by matching the Hartman-Hahn conditions at 60 kHz. At least 2,000 scans were integrated with a contact time of 2 ms using a ramp CP protocol and a recycle delay of 2 s. The acquisition time was 35 ms and the sweep width set at 29,400 Hz. The chemical shifts were calibrated with respect to the carbonyl peak of glycine (176.03 ppm).

#### **2.6. Thermogravimetric analysis (TGA)**

About 20 mg of sample was heated from 20 to 400  $^\circ\text{C}$  at a rate of 5  $^\circ\text{C}/\text{min}$  under nitrogen flow using a SETARAM TGA 92 instrument.

#### **2.7. Differential scanning calorimetry (DSC)**

The DSC measurements were made with a Q200 apparatus from TA instruments. The following procedure was used: the sample in a 40  $\mu\text{L}$  pan with a hole in the lid was first cooled to  $-80^\circ\text{C}$ , heated at 5  $^\circ\text{C}/\text{min}$  to 200  $^\circ\text{C}$  to erase the thermal history of the sample and to evaporate the adsorbed water, cooled down to  $-80^\circ\text{C}$  at  $-10^\circ\text{C}/\text{min}$  and then

reheated to 200 °C at 5 °C/min for the effective measurement. All the analyses were carried out under a 50 mL/min nitrogen flow.

### **2.8. Dynamic mechanical analysis (DMA)**

The DMA analyses were performed with a DMA50 apparatus from Metravib. The sample dimensions were approximately 15 (H) × 15-20 (W) × 0.04-0.15 (T) mm<sup>3</sup> (the effective span was 6 mm). The samples were tested at 1 Hz. Since the samples have adsorbed water and get brittle once dry, the samples were installed on the instrument without being fully dried (5 to 10 % remaining adsorbed water), and then dried *in situ*. To do so, a 2 hour drying protocol was performed: the temperature was raised from room temperature to 100 °C at 5 °C/min, under 1 N static tensile load, while the dynamic tensile force under 3 μm dynamic displacement was monitored to ensure the sample was not flowing. Immediately after the drying process, the DMA measurement was performed with a 2 N static force and a 5 μm dynamic movement from the equilibrium position. The temperature was first decreased from 100 to -125 °C at -5 °C/min with a 15 min plateau at -125 °C. Then the temperature was raised at 3 °C/min to 270 °C (usually the sample breaks before that temperature). All the drying and measurement procedures were carried out under nitrogen flow to avoid any water uptake during analysis. Storage and loss moduli as well as tangent delta were recorded. The T<sub>α</sub> values were measured at the onsets of the storage moduli.

### **2.9. X-Ray Diffraction (XRD)**

X-ray diffractograms of rPOC films were recorded overnight in vacuum using a Philips PW383 generator operating at 30 kV and 20 mA (Ni-filtered Cu K<sub>α</sub> radiation, λ = 0.1542 nm). Two-dimensional scattering patterns were recorded on Fujifilm imaging

plates read with a Fujifilm BAS-1800II bioimaging analyzer. Diffractograms were obtained by integration of the whole scattering patterns.

### 3. Results and discussion

#### 3.1. Ultrastructural characterization

Before reduction, the samples exhibited solid-state NMR spectral characteristics typical of the periodate oxidized cellulose (POC) with the formation of hemiacetal bonds upon drying, as evidenced by the increasing amount of spectral contributions within the 90-100 ppm<sup>168-169</sup> region as the oxidation proceeds (Supporting Information Figure SC3-1). Figure 36a shows the solid state NMR spectra recorded on the same series of samples after reduction and casting. The characteristic peaks of hemiacetal groups disappeared during the reduction step and the baseline of the spectra went back to zero between 90 and 100 ppm, indicating a total completion of the reduction. The borohydride reduction converts the aldehyde groups into alcohol, which breaks all the hemiacetals present in the POC samples. A progressive transformation of the spectral characteristics occurred with increasing degree of modification. Interestingly, the contribution of the C4 signal near 90 ppm assigned to the crystalline part of native cellulose continuously decreases with increasing DO. This observation further supports the progressive and heterogeneous transformation of the microfibrils upon periodate oxidation. Concomitantly, the signal intensity in the 70-80 ppm region, assigned to the C2, C3, C5 contribution of the anhydroglucose unit, decreases while the 55-70 ppm typical of alpha carbon of primary alcohol, increases. The two aldehydes at C2 and C3 form hemiacetals giving rise to the intensity at 90-100 ppm should indeed become two primary alcohols after reduction. The decrease of the signals for the C2, C3, C5 contribution accounts for

the opening of the sugar rings (Figure 36b). The results thus clearly show that the dialdehyde cellulose (DAC) is fully transformed into dialcohol cellulose (DALC).

Supplementary contributions arise between 80 and 85 ppm, which turn into a sharp defined doublet for the highest degree of oxidation. The contribution of the C1 (at 105 ppm) carbon does not drastically change, as its chemical environment is rather conserved. However, the shape of the signal evolves, becoming broader with increasing DO, with even noticeable sharp peaks for the most oxidized sample (DO = 1.8) at 101 and 108 ppm.

The evolution of the spectra is in good agreement with the description of these samples as core-shell structured materials<sup>168, 170</sup> comprising a core of intact crystalline cellulose that decreases when the DO increases, and a shell of a pure dialcohol cellulose crystallizing for the highest degree of substitution, as attested by the presence of sharp signals at 59, 80, 101 and 108 ppm on the DO=1.8 sample in Figure 36b.

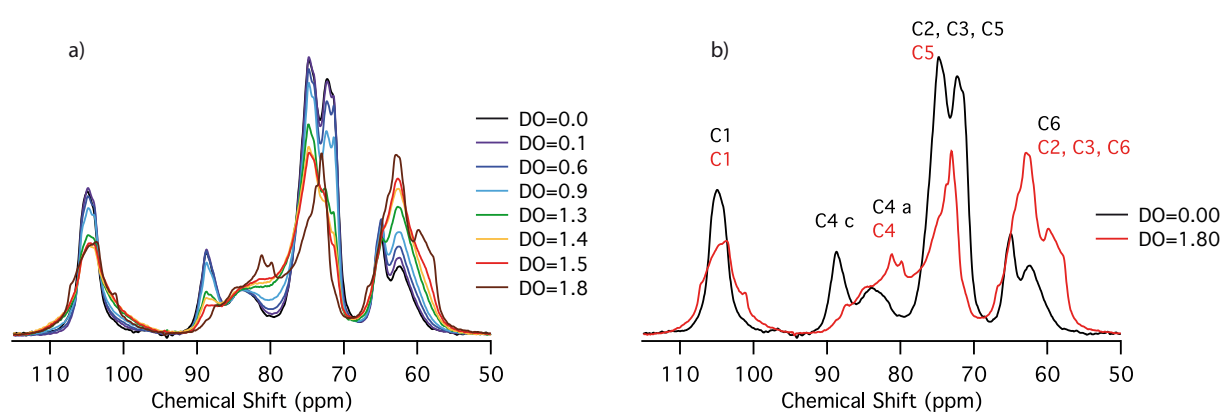


Figure 36:  $^{13}\text{C}$  CP-MAS NMR of freestanding rPOC films (a) and shift comparison between cellulose (DO=0.00) and the rPOC film DO=1.80 (b).

The diffraction profiles of the same rPOC films are shown in Figure 37.

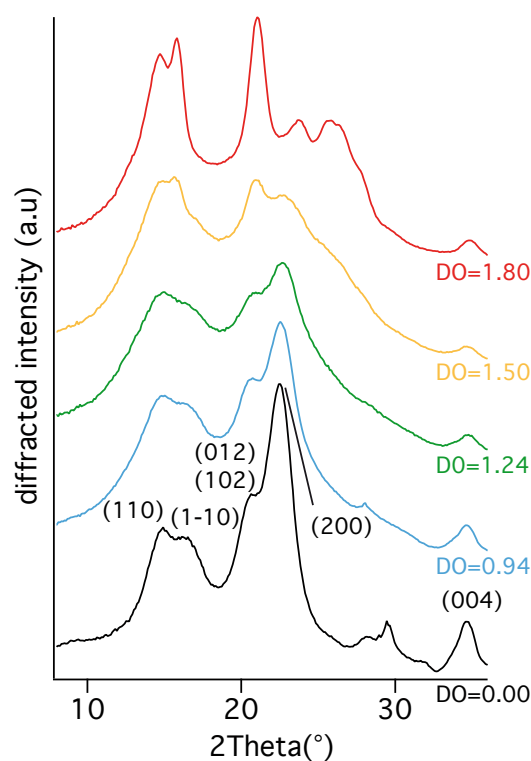


Figure 37. XRD measurements on rPOC films.

The sample crystallinity decreases as the DO of the parent POC sample increases, as shown by the increase in the broad halo centered at around  $20^\circ$ . Another highly crystalline structure is found for the sample with the highest DO (1.8) which corresponds to the pure pattern reported by Casu *et al.*<sup>97</sup> on a similar system. However, in their publication, the diffraction pattern of the periodate oxidized and reduced products of cellulose and amylose were probably interchanged since our pattern exactly fits to the one reported as a product from amylose. At lower degree of oxidation, the crystalline structure is less developed and is only slightly visible for the DO=1.5. This tendency corroborates with the NMR data where sharp peaks at around 80 ppm are only visible for the highest degree of oxidation. The presence of small amounts of residual

cellulose might impede the crystal growth of the fully oxidized dialcohol cellulose chains.

### 3.2. Thermal properties

The thermogravimetric curves of rPOC films and their derivatives with temperature are plotted in Figure 38a and 38b, respectively. With the exception of the sample with the lowest DO, for which the thermal stability did not vary much from the initial cellulose, all the other samples tested exhibited two clear maxima in the mass loss derivative traces. The second one around 360 °C corresponds to pure cellulose, and the first one is observed at 310 °C. The intensities of both vary with increasing DO: the one of cellulose decreases while the one at 310 °C increases. Therefore, the peak at 310 °C can be attributed to dialcohol cellulose segments (DO=2). This clear separation between two different degradation phenomena strongly supports the heterogeneous character of the oxidation with coexistence of two distinct phases of both intact and oxidized cellulose. Interestingly, at small oxidation degree (DO = 0.1) the yield at 400 °C jumps to 30% compared with the 15% value for pure cellulose. The yield then decreases with the degree of oxidation, reaching 5% for the highest DO of 1.8.

However, the thermograms of freeze-dried samples of rPOC showed completely different tendencies, suggesting that microstructure is also playing an important role (Supporting information SC3-2) – both cast films and freeze-dried samples being heated at 5 °C/min, the difference does not seem to be a kinetic effect.

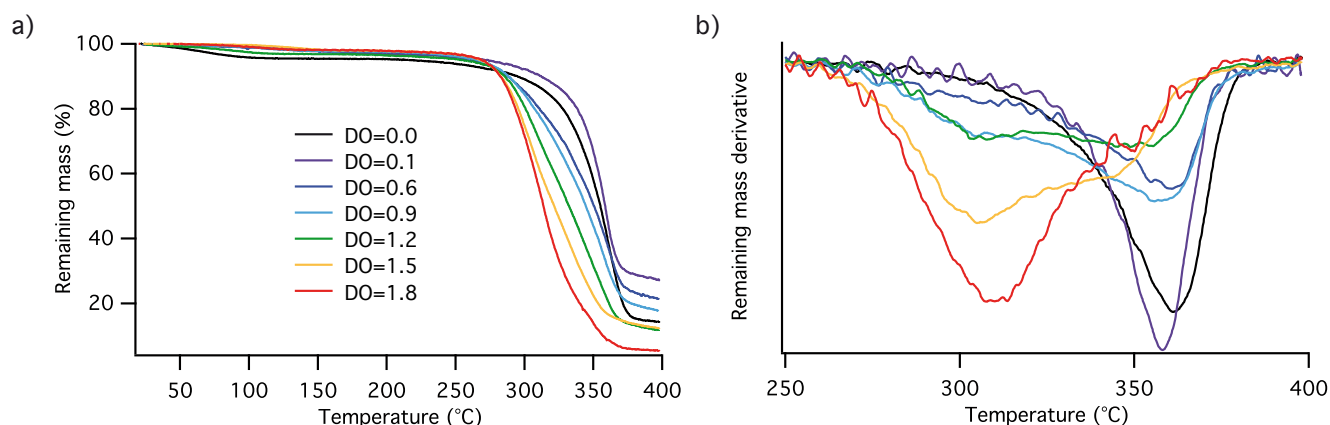


Figure 38: TGA thermogram (a) and TGA thermogram derivatives (b) for rPOC samples of variable DO.

Differential scanning calorimetry experiments were performed on the same series of samples investigated by  $^{13}\text{C}$  CP-MAS NMR and XRD. The different thermograms shown in Figure 39 display a change in the heat capacity for the most oxidized samples, most probably corresponding to the glass transition of an amorphous compound. Interestingly, the amplitude of this heat capacity difference increases with the degree of oxidation, highlighting the progressive appearance of an amorphous phase within the sample. The first heating cycle with some water melted all crystals and the subsequent cooling in dry conditions probably quenched the amorphous state.

The  $T_g$  of these rPOC films taken as the inflexion points are listed in Table 1. Data show that from a DO of 0.6 and up, all the samples have a measurable  $T_g$  that decreases with increasing DO and seems to level off above a DO of 1.5 to 65-67°C, as highlighted in Figure 39 (Black circles).

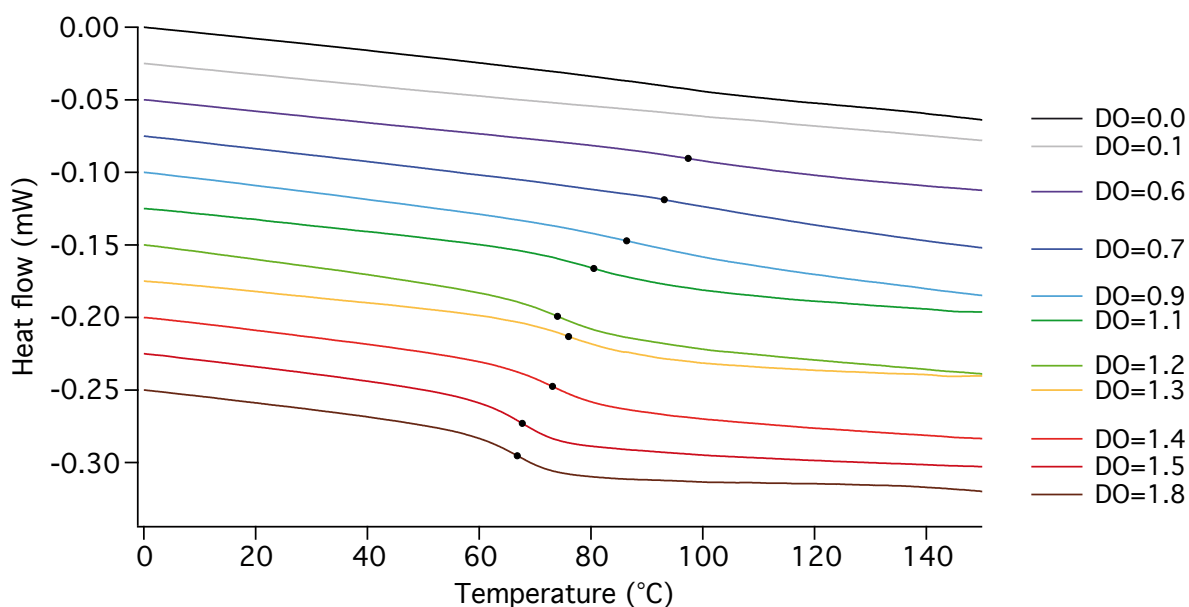


Figure 39: DSC heat flow on rPOC samples. Black dots show the glass transition temperature position.

Table 1. List of rPOC samples, DO of the parent POC samples, glass transition and degradation temperatures. \*Extrapolation based on Alfthan and de Ruvo's work.<sup>4</sup>

DO	T <sub>g</sub> (°C)	rPOC film degradation temperature (°C ± 5°C)
0.0	217*	362
0.1	n/a	358
0.6	97	358
0.7	98	ND
0.9	86	305
1.1	81	ND
1.2	74	305
1.3	76	ND
1.4	73	ND
1.5	68	305
1.8	67	310

### 3.3. Dynamic mechanical analysis

DMA can provide useful information on both the mechanical properties and relaxation processes of complex materials. Figures 40 and 41 display the storage modulus ( $E'$ ) and loss tangent ( $\tan \delta$ ) obtained on a series of rPOC samples with varying degrees of oxidation of the parent POC.

While native cellulose did not show any relaxation, with a storage modulus almost constant with temperature, the rPOC presented a wide variety of behaviors. For the lower DO (*i.e.*  $DO < 1$ ), the storage modulus started to decrease at temperatures well above 100 °C and remained at very high values in the GPa range, which corresponds to the stiffness of typical polymeric materials. For DO higher than 1.4, the modulus continuously decreased from an onset temperature at around 100 °C that seems to be more or less constant for all samples. In contrast to conventional thermoplastics that display sharp decrease of modulus at a mechanical relaxation temperature  $T_a$  associated to the glass transition, rPOC showed a rather continuous decrease with a slope of finite value. This behavior is reflected in the  $\tan \delta$  with broad peaks extending over a wide range of temperatures, with the exception of the highest degree of oxidation that exhibits a well-identified relaxation temperature. This complex behavior is likely related to the ultrastructural characteristics of different samples, but additional information regarding dynamics at the molecular level is needed before discussing the results.

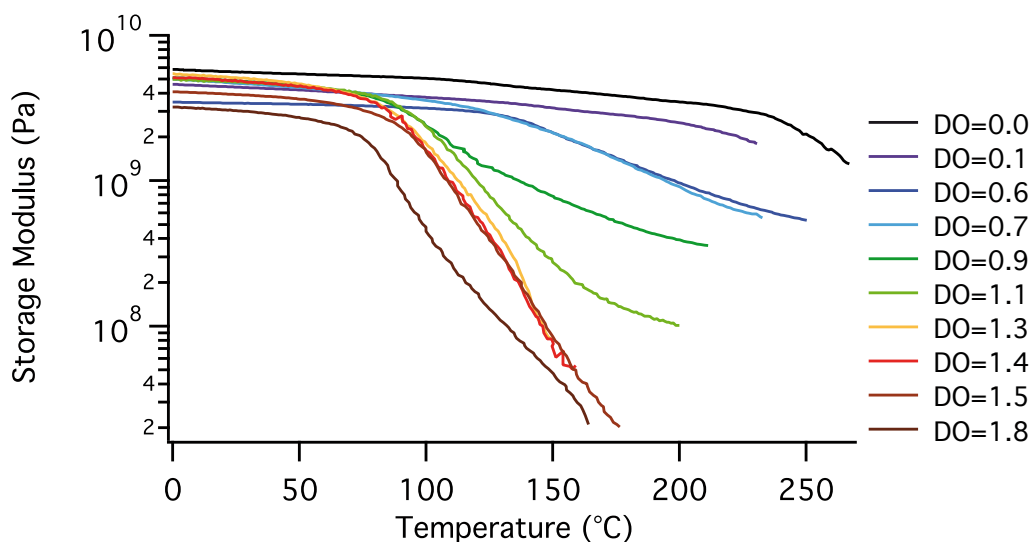


Figure 40. Storage modulus measured by DMA of rPOC films (the DO values are of the parent POC samples).

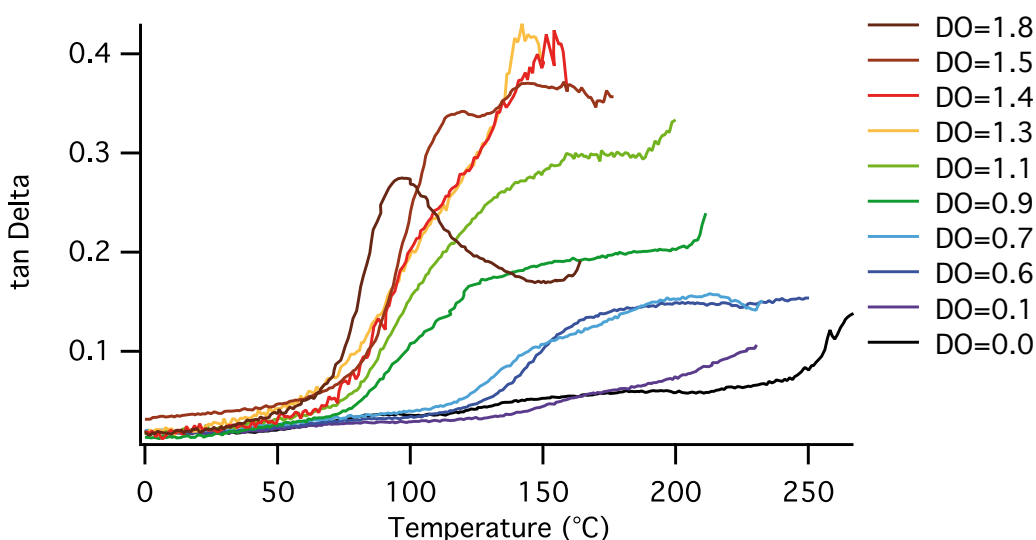


Figure 41. Tan  $\delta$  measured by DMA of rPOC films (the DO values are of the parent POC samples).

### 3.4. Wideline separation NMR (WISE)

The 2D WISE (Wideline SEparation) experiment is a 2D NMR technique that correlates the isotropic chemical shift in the  $^{13}\text{C}$  dimension obtained by conventional CP-MAS NMR with the proton line shape in the  $^1\text{H}$  dimension. The experiment gives information on the mobility of the surrounding protons for each given  $^{13}\text{C}$  site. The obtained spectra in the

proton dimension can be either narrow if the associated chemical moieties undergo rapid isotropic motion at a frequency greater than the strength of the dipolar coupling (20-30 kHz for conventional polymers) or broad if the motions are frozen either in the glassy state (under the glass transition temperature  $T_g$ ) or in the ordered phase for semi-crystalline polymer<sup>171</sup> (Supporting information Figure SC3-3). These experiments have been used to study the dynamics and organization of block copolymers and blends,<sup>172</sup> core shell particles<sup>173</sup> and even cellulose and polyvinyl alcohol blends.<sup>174</sup> In the case of structural heterogeneities with domains with distinct dynamical behaviors, two different components will coexist in the proton dimension corresponding to the two different regimes, either frozen or mobile. These signals were deconvoluted, and we were able to extract in the  $^{13}\text{C}$  dimension the rigid and mobile components from the two dimensional spectrum. Figure 42 displays the results of this deconvolution with the rigid and mobile parts, respectively, together with the overall CP-MAS NMR spectra for three rPOC films with different DOs. The WISE data for rPOC freeze-dried powders for the same DOs are presented in Figure SC-4. A difference compared to film samples can clearly be seen for the DO=1.8 product, where the spectral feature remains much more complex at 100 °C compared to the film samples, corroborating the low crystallinity observed with X-ray diffraction.

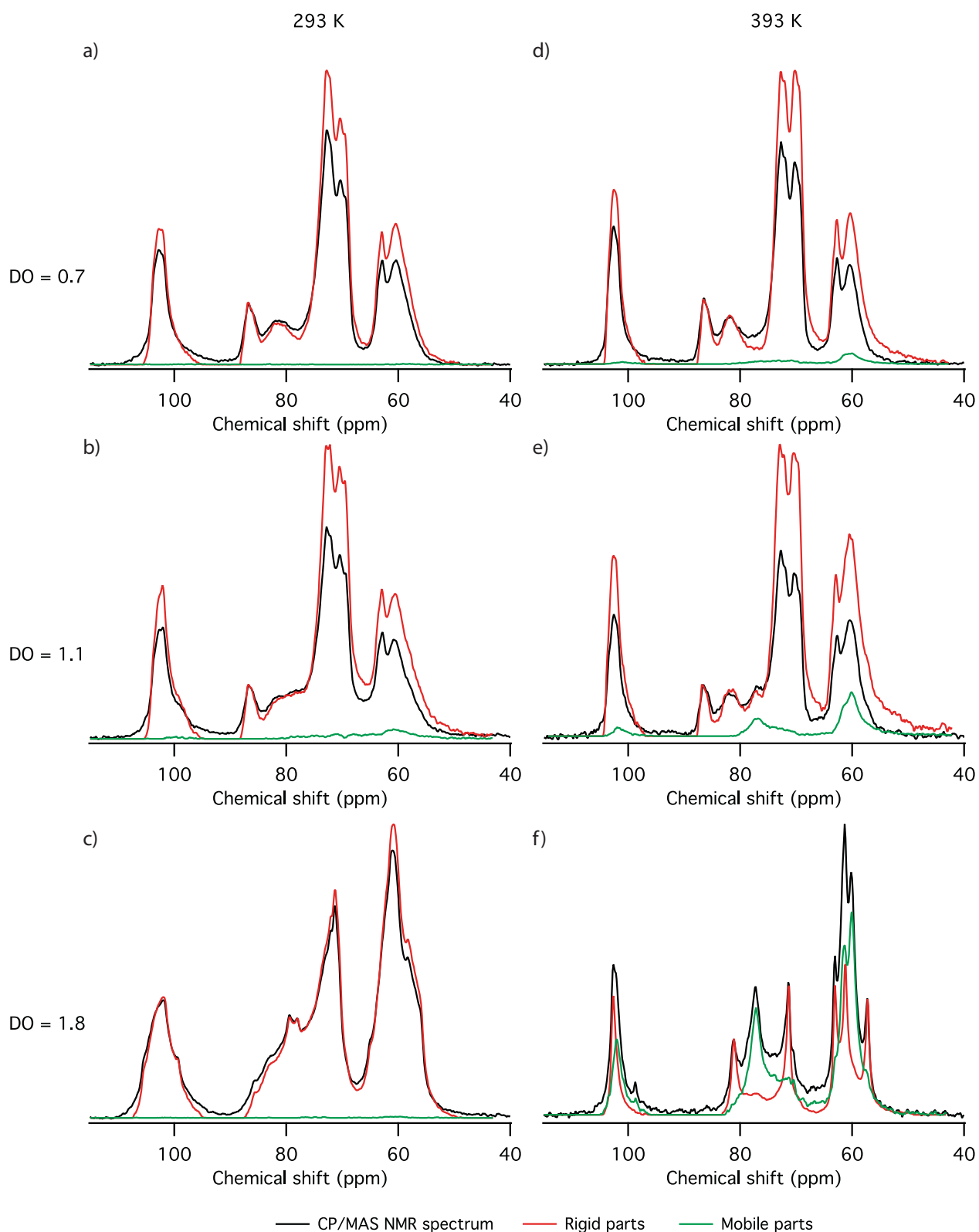


Figure 42.  $^{13}\text{C}$  NMR traces extracted from the 2D WISE experiments for mobile and rigid contributions and corresponding  $^{13}\text{C}$  CP-MAS NMR spectra for rPOC freestanding films with initial DO values of 0.7 (a), 1.1 (b) and 1.8 (c) at room temperature (293 K, before  $T_g$ ), and DO=0.7 (d), DO=1.1 (e) and DO=1.8 (f) at 393 K (after the  $T_g$ ).

For the three samples at room temperature (Figure 42 a, b, c), the deconvoluted spectra essentially show contributions from the rigid part, and almost nothing for the mobile contribution. This is perfectly in line with the fact that the three samples are well below their glass transition temperature (measured at 98, 81 and 67 °C respectively), hence in a frozen state. The situation is drastically different at higher temperature. The deconvolution procedure shows the appearance of a non-negligible mobile contribution. Even if a precise quantification of the ratio between mobile and rigid parts is difficult because they have different polarization efficiencies, the intensity of each signal reflects the amount of each phase.

A close observation of the different traces gives important information on the chemical nature of the two phases. For the lowest DO values (*i.e.* 0.7 and 1.1), the rigid part is very similar to a  $^{13}\text{C}$  CP-MAS spectrum of native cellulose, whereas the mobile part has clearly different chemical shifts, which correspond well to the ones of an amorphous dialcohol cellulose. This information strongly confirms the two-phase model of the intact native microfibrils surrounded by a shell of oxidized then reduced cellulose presented elsewhere.<sup>175</sup> At high temperature (393 K) the dialcohol cellulose phase is above its glass transition temperature and is highly mobile. The situation is a little bit more complex for the highest degree of oxidation (DO = 1.8). Even if the trace extracted from the mobile contribution is rather similar to the two preceding ones, the rigid contribution is drastically different. The native cellulose contribution has indeed almost vanished, which is quite logical considering the very high degree of oxidation (remaining cellulose represent only 10 mol% of the sample). Instead, new and well-defined contributions appeared for the rigid part of the sample, whose chemical shifts are compatible with the one of fully modified dialcohol cellulose and could most likely

correspond to the crystalline structure detected by XRD experiments. From these experiments, what could be qualitatively described is a two phases model of a crystal of native cellulose surrounded by an amorphous shell of dialcohol cellulose for samples with intermediate DOs, whereas a crystalline structure of dialcohol cellulose is likely to appear at the highest degree of oxidation.

### 3.5. Discussion

Gathering all the different experiments, a general description of these complex materials can be proposed. Concerning the thermal properties, the information coming from both DSC and DMA experiments can be analyzed and compared. Figure 43 reports the  $T_g$  or  $T_a$  values extracted from the inflexion point and onset of the storage modulus decrease, of the DSC and DMA experiments, respectively. The values obtained by Kasai *et al.* on homogeneously oxidized samples are also reported on the same plot.<sup>98</sup>

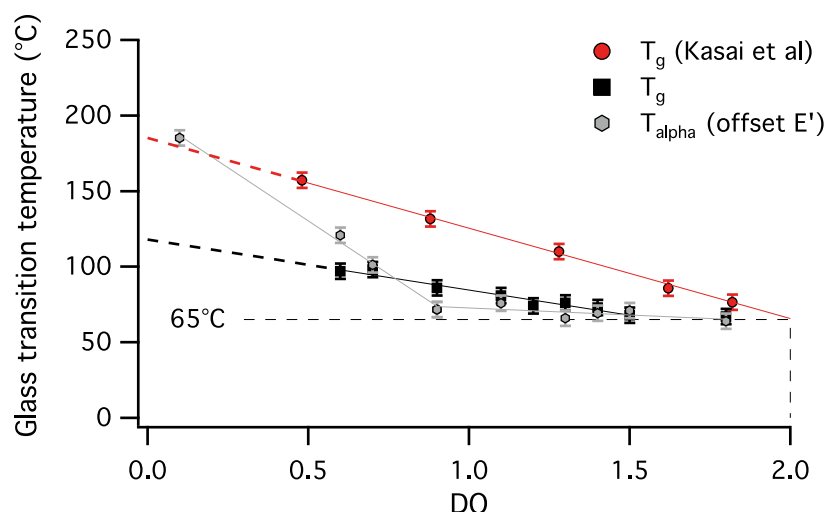


Figure 43.  $T_g$  of rPOC samples measured from DSC plotted as a function of the initial DO (black) compared to the  $T_g$  from Kasai *et al.*'s work<sup>98</sup> (red) and  $T_a$  from DMA (onset of storage modulus) (gray). The lines are guides for the eye.

The glass transition temperature as evaluated by DSC measurements exhibit a linear dependence with the DO, but strikingly with a much smaller slope than the one obtained by Kasai *et al.* on homogeneously modified samples.<sup>98</sup> For  $DO > 1.2$ , the evolution of the  $T_g$  is even imperceptible at the resolution of the experiments. Interestingly, the extrapolation of the homogeneous case to a degree of oxidation of zero, *i.e.* native cellulose, give values that are compatible with the estimated  $T_g$  value of pure amorphous cellulose, which is of course not the case of our own values.<sup>4</sup> Remembering that the difference in heat capacity ( $\Delta C_p$ ) is increasing with the degree of oxidation, these data can account for the proposed model of a two phase compound made of intact and fully modified cellulose, the amount of the latter increasing with increasing degree of oxidation at the expense of the first. The slight decrease in  $T_g$  with the DO can be explained by the decreasing constraints exerted on the amorphous chains by the remaining cellulose crystals for the lowest DO. The decrease of the  $T_a$  values is also in good agreement with this description. For the higher degree of oxidation ( $DO=1.8$ ), the material behaves as a thermoplastic, with a mechanical relaxation  $T_a$  that is related to the glass transition temperature. At lower degree of oxidation ( $DO < 1$ ), the values of  $T_a$  strongly depart from the  $T_a$  values seen for  $DO > 1$ , with a  $DT_a$  between the highest and lowest  $T_a$  greater than 50 °C. The onset value can be biased by the choice of the method used to determine it, but the general trend is also well supported by the shape of the  $\tan \delta$  curves. Indeed, as the DO decreases, the width of the relaxation strongly widens to lead to a very broad peak spreading over more than 100 °C for the lowest oxidation degrees, whereas a defined peak can be observed for the highest ones. This again is in line with the idea of a model of a shell of mobile amorphous dialcohol surrounding a rigid cellulose particle, with a gradient of the thermal properties of the amorphous part

from the surface to the most remote amorphous matrix. This phenomenon has already been evidenced in the situation where rigid particles are inserted in an amorphous matrix, as in the case of the reinforcement of elastomers. Indeed, in these materials, a shell of immobilized matrix has been identified and quantified by proton relaxation experiments, and their role on the mechanical properties quantitatively accounted for.<sup>176</sup> In these systems, a very high specific area of the particles ( $> 200 \text{ m}^2.\text{g}^{-1}$ ), a very good level of dispersion together with a high density of covalent bonds between the filler and the matrix is a prerequisite to observe this phenomenon. The rPOC system meets these requirements, at least as long as the cellulosic core is reasonably preserved (for  $\text{DO} < 1.5$ ). As described by the NMR, XRD, DSC and DMA experiments, the model of a core-shell particle is most likely the one that can account for the experimental results, describing also a gradient of mobility from the surface of native cellulose to the amorphous bulk of cellulose dialcohol. Then, intrinsically, this complex material exhibits all the characteristics of a charged elastomer, *i.e.* the high specific surface given by the native cellulose crystal dimensions, the level of dispersion that comes from the isolated character of the initial microfibril's dispersions and the strong interaction of dialcohol cellulose and native cellulose, as the modification occurred *in situ*.

Another way of investigating the properties of these materials is to try to quantify the change in the mechanical properties due to the presence of rigid cellulosic particles dispersed in an amorphous matrix. In order to evaluate this reinforcing effect, the storage modulus values at  $150 \text{ }^\circ\text{C}$  were plotted against the degree of oxidation, as shown in Figure 44a. As can be already visually seen from the initial DMA traces, a rather steep transition occurs between two different basic situations, either a completely percolated network of microfibrils, for  $\text{DO} < 0.8$ , or a flowing thermoplastic-like material for

DO>1.2. To be closer to the conventional representation of reinforcing effect with classical fillers, we converted the degree of oxidation to cellulose volume fraction by considering that the fraction that is not oxidized is pure cellulose, and that the fraction of amorphous matrix is the dialcohol cellulose part, based on our structural model. A density of 1.25 g/cm<sup>3</sup>, equivalent to polyvinyl alcohol, was tentatively attributed to the dialcohol cellulose fraction. The resulting curve shown in Figure 44b qualitatively displays the same behavior as the preceding representation, i.e. a rather sharp transition between two different situations of percolating and non-percolating particles.

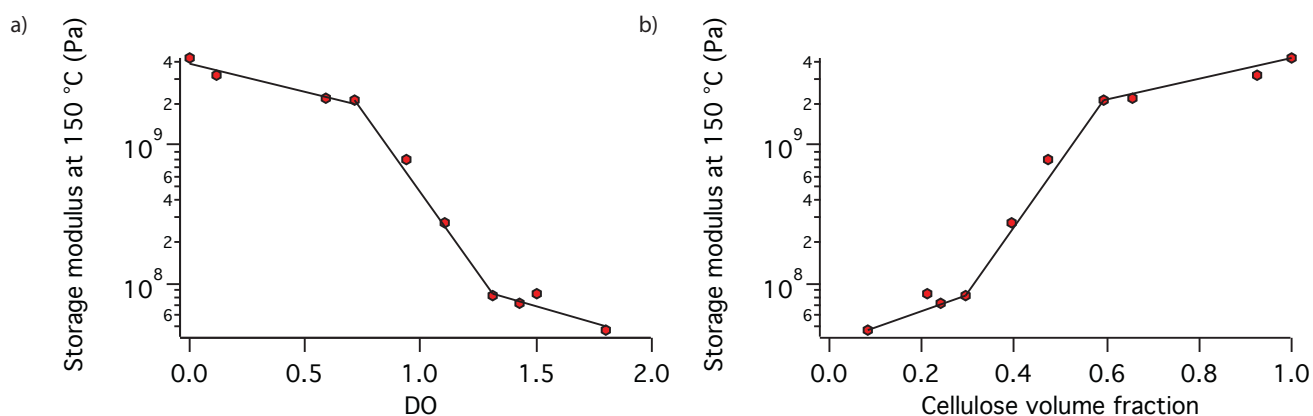


Figure 44. Storage modulus at 150 °C as a function of degree of oxidation (a) and cellulose volume fraction (b). The lines are guides to the eye.

The boundaries of this percolating / non-percolating transition in terms of cellulose volume fraction was between 0.35 to 0.55. This high percolation threshold is a situation very different from what is usually obtained by solvent casting, which leads to a percolating (and fragile) network of cellulose nanocrystals at low volume fraction, though the exact percolation threshold depends on the aspect ratio of the filler (nanocrystals). Here, we present a new type of material much closer to the concept of encapsulation, as the one used for obtaining high-k resistant materials, for which the contact between conducting particles has to be avoided.<sup>177-178</sup>

## 4. Conclusions

Cellulose microfibrils were heterogeneously modified successively by periodate oxidation and subsequent reduction by borohydride over a wide range of degree of oxidation. The ultrastructural studies by  $^{13}\text{C}$  CP-MAS NMR and X-ray diffraction clearly show the progressive erosion of native crystalline cellulose at the expense of newly formed cellulose dialcohol, in agreement with the core-shell structure model made of intact native crystalline cellulose embedded in a thermoplastic skin of dialcohol cellulose. The two-stage degradation behavior observed in thermogravimetric analysis also suggests the presence of two distinct phases in the material. Differential scanning calorimetry pictures however a slightly different situation: even if the glass transition temperature ( $T_g$ ) is not evolving linearly with the degree of modification, as in the homogeneous case, the  $T_g$  was higher at low oxidation degrees compared to the fully modified sample, indicating a confinement effect in this intimate mixture. The dynamic mechanical analysis showed two types of regimes depending on the degree of modification: (i) at low degree of oxidation, the material behaves almost like an entangled network of microfibrils, with a storage modulus that decreases with increasing oxidation degree whereas (ii) at high oxidation degree, the resulting materials are flowing but with a finite slope unusual in conventional thermoplastics, most probably due to the presence of the remaining crystalline cellulose particles. The  $T_a$  relaxation evaluated roughly as the onset of the storage modulus drop was much higher for the lowest DO than the  $T_g$  measured by DSC, revealing a huge confining effect (Figure 43), similar to the one obtained in highly charged elastomers. WISE experiments confirm the highly heterogeneous dynamics of the dialcohol cellulose chains, with the

coexistence of mobile and immobile segments. The rigidity of remaining cellulose was also confirmed.

All together, those observations lead to the following conclusions: the periodate oxidation followed by subsequent reduction leads to a material whose nature can be finely tuned over a wide range of properties, from the stiff film of microfibrils to the flowing thermoplastic. The adjustable parameter is the volume fraction of remaining cellulose, that define a sort of “percolation threshold” between indirectly interacting and non-interacting particles regimes that differentiate the two sorts of materials. These materials are different from the conventional cellulose nanocomposites obtained from dispersions for which the particles are directly interacting through hydrogen bonding and van der Waals forces, in the sense that these materials are able to flow and hence to be shaped. A first consequence is the apparent level of filler content that can be tuned over a wide range of volume fraction, especially including high volume fraction that is not conceivable in the conventional process. The high filler ratios give rise to self-reinforcing materials with a high degree of confinement. Even if more efforts are needed to fully characterize these materials, they already exhibit astonishing properties comparable to the core-shell latexes obtained with block copolymers with distinct mechanical properties, but with an anisometric shape that gives rise to unusual percolating properties.

# Chapter 3: Supporting information

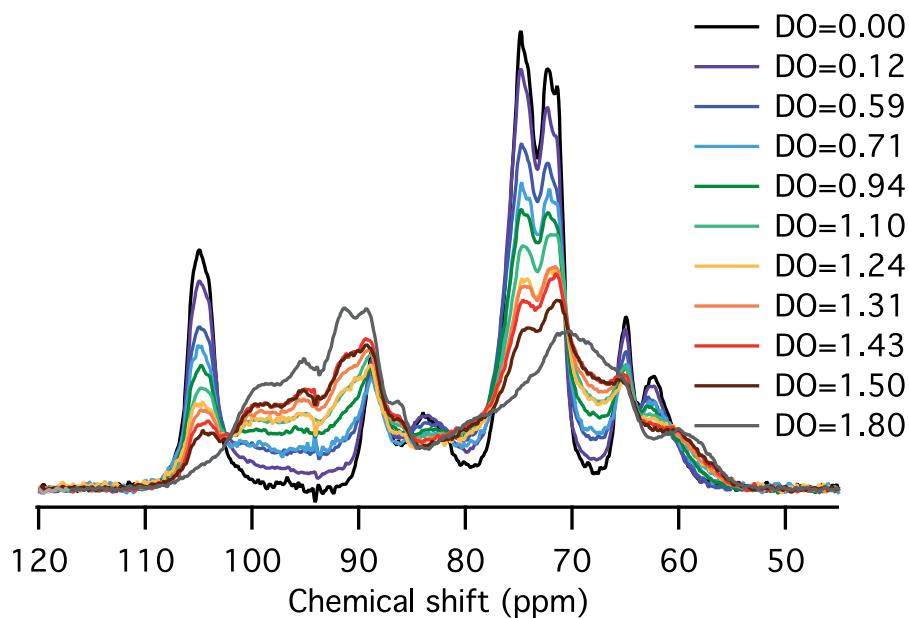


Figure SC3-1: NMR of POC samples.

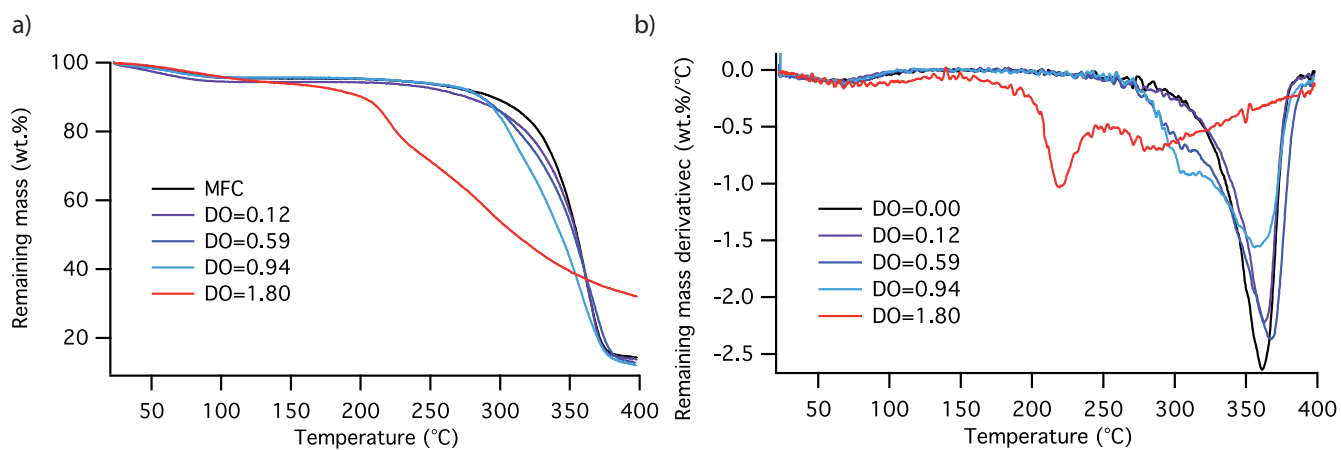


Figure SC3-2: TGA thermogram (a) and TGA thermogram derivatives (a) for rPOC samples of variable DO (freeze dried powder).

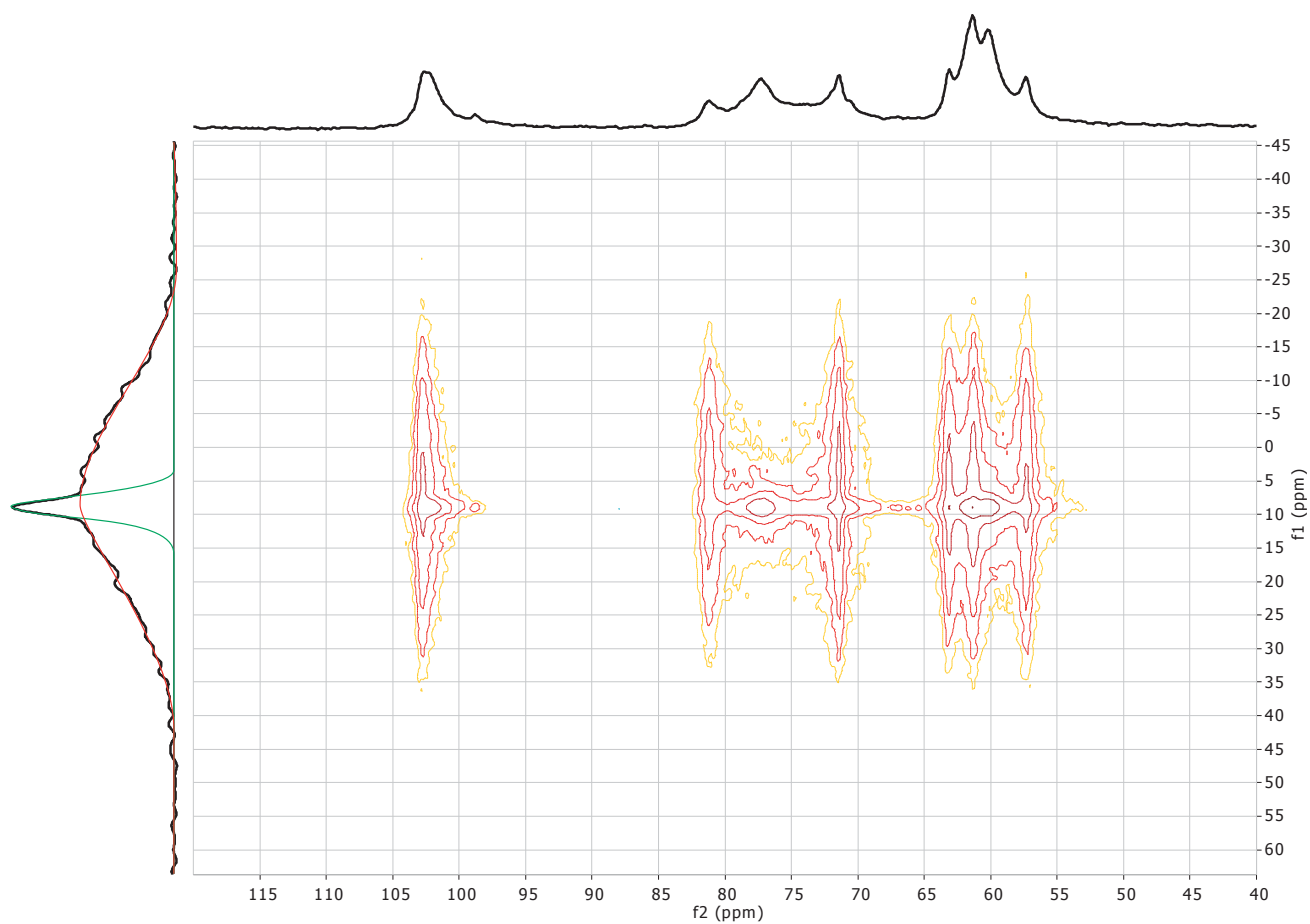


Figure SC3-3: 2D WISE example (sample DO=1.80 at 393 K). f1 corresponds to the proton chemical shifts, with on the left trace, the two deconvoluted parts: green mobile and red rigid. f2 corresponds to the carbon chemical shift with the CP-MAS NMR spectrum on the top trace.

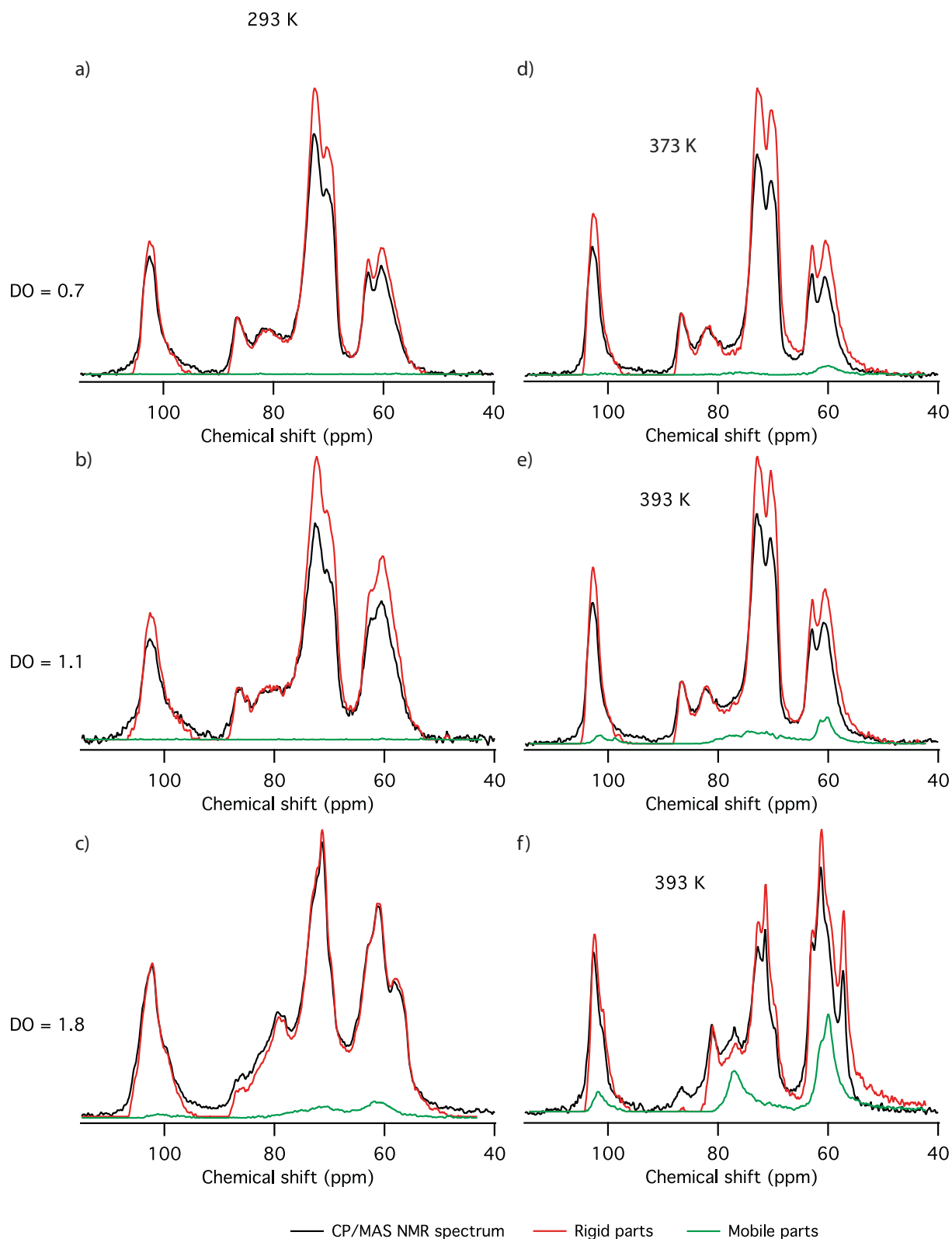


Figure SC3-4:  $^{13}\text{C}$  NMR traces extracted from the 2D WISE experiments for mobile and rigid contributions and corresponding  $^{13}\text{C}$  CP-MAS spectra for rPOC freeze-dried powders with initial DO values of 0.7 (a), 1.1 (b) and 1.8 (c) at room temperature (293 K), and DO=0.7 (d), DO=1.1 (e) and DO=1.8 (f) at 373, 393 and 393 K, respectively.



# **Chapter 4: Periodate oxidation followed by NaBH<sub>4</sub> reduction converts microfibrillated cellulose into sterically-stabilized neutral cellulose nanorod suspensions**

---

The nanocomposite-like materials studied in the previous chapter were synthesized from POC samples that were further reduced and cast into films. Remarkably, the rPOC suspensions before casting appear as stable colloidal suspensions, which were studied in this chapter using different structural characterization techniques.

## **1. Introduction**

Along with other rod-like nanoparticles such as carbon nanotubes, rod-like viruses, metallic oxide nanoparticles, imogolite, chitin nanocrystals or gold nanorods, cellulose nanocrystals (CNCs) have attracted increasing attention from both the academic and industrial communities for their unique properties. CNCs, which can be isolated using acid hydrolysis from many different cellulose sources, occur as slender rods with nanoscale dimensions ranging from 100 to 2000 nm in length and widths in the range of 2 to 50 nm.<sup>17, 179</sup> In addition to their renewable character, low density, recent industrial-

scale production and non-toxicity, their high mechanical properties (axial elastic modulus estimated between 110 and 220 GPa and tensile strength in the range of 7 GPa) make them particularly attractive for the materials community.<sup>13, 180-181</sup> These crystalline biosourced nanorods of tunable aspect ratio also exhibit unique colloidal properties since they can be used to stabilize emulsions<sup>182-183</sup> or be oriented by magnetic and electric fields,<sup>143-146, 184-186</sup> and spontaneously self-organize into liquid crystalline cholesteric phases,<sup>126, 140, 187</sup> leading to a host of exciting properties, in particular to spectacular iridescence.<sup>18, 142</sup> While several aqueous acid media can be used for the conversion of cellulose fibers into CNC suspensions,<sup>188</sup> sulfuric acid is most commonly used since it imparts the nanoparticles with negatively charged sulfate half ester groups on their surface, resulting in stable suspensions in aqueous media. However, the electrostatic nature of the colloidal stability hampers the use of CNCs in high ionic strength aqueous media, results in disordered gel-like structures when the concentration is increased and prevents a good dispersion in apolar solvents or matrices. Surface sulfate half-esters are also detrimental to the temperature stability of the CNCs since they cause an about 100 °C downshifting of the degradation temperature compared to pure cellulose, which prevents the use of CNCs in thermoplastic nanocomposites. These issues can be solved by replacing the electrostatic stabilization by a steric one following either the adsorption or surface grafting of polymer or surfactant layers.<sup>124</sup> The non-covalent physical adsorption has been successfully demonstrated using surfactants<sup>135-137</sup> or triblock copolymers,<sup>189</sup> leading to colloidal stability in organic solvents such as toluene or high level of dispersion in apolar matrices,<sup>190-191</sup> or using carboxymethylcellulose or xyloglucan to improve colloidal stability in aqueous medium.<sup>192-193</sup> The polymer covalent grafting strategy achieved by

different groups resulted in steric stabilization in high ionic strength aqueous media and organic solvents.<sup>39, 124, 130, 134, 194-197</sup>

Another route to produce CNCs was introduced by van de Ven and coworkers based on a controlled periodate oxidation reaction.<sup>106, 116-120, 198</sup> In this well described oxidation reaction mechanism, sodium metaperiodate breaks the glucosyl rings constituting the building blocks of cellulose at the C2-C3 bond to produce two aldehyde groups, leading to periodate oxidized cellulose (POC).<sup>87-88</sup> When applied to cellulose nanofibrils, van de Ven and coworkers<sup>106, 116-120, 198</sup> report that due to reduced ion diffusion in the crystalline regions, the oxidized chains are preferentially located in the amorphous regions and the outer layer of the crystalline segments. Upon solubilization of the oxidized moieties by heating in various solvents, or further oxidation by a chlorite treatment, amorphous regions would disintegrate to yield hairy cellulose nanocrystalloids constituted of a rod-like crystalline core and either POC or dicarboxylated cellulose chains (DCC) at the poles. The solubilization method leads to neutral sterically-stabilized particles,<sup>116, 119-120</sup> while with the derivatization to DCC an electrosteric stabilization is obtained.<sup>117-118</sup>

In the present work, cellulose microfibrils were reacted with periodate to yield POC samples with a controlled degree of oxidation, which were subsequently subjected to a reduction treatment. The reduction would convert the aldehyde moieties into alcohols to create acyclic stereoregular polyalcohol chains with polyoxyethylene-methylene alternating copolymer backbone. Each carbon on the backbone holds a methoxyl group. We expect this modified segment to have increased solubility and flexibility, especially in contrast to POC chains that can easily recombine through the formation of hemiacetal linkages.<sup>64, 168</sup> Core-shell-like particles of enhanced dispersibility are thus expected from

this strategy. The properties of the prepared suspensions were analyzed by dynamic light scattering, zeta potential, turbidity measurements, and small angle X ray scattering, while the individual components of the suspensions were visualized and their geometric dimensions measured by transmission electron microscopy (TEM).

## 2. Materials and methods

### 2.1. Materials

A batch of paste-like never dried microfibrillated cellulose (MFC) of spruce sulfite pulp, prepared by a mechano-enzymatic treatment,<sup>158-159</sup> was purchased from the Centre Technique du Papier (CTP), Grenoble, France. It had a consistency of about 2% and contained less than 4 wt % of hemicellulose on dry weight basis. Sodium metaperiodate (NaIO<sub>4</sub>) with purity ≥ 99.8% and sodium borohydride (NaBH<sub>4</sub>) with purity ≥ 96 % were acquired from Carl Roth and Sigma Aldrich (France) respectively.

### 2.2. MFC oxidations to POC

For a typical experiment, about 15 g on dry basis of a MFC suspension was inserted into a flask equipped with magnetic stirring. The right amount of periodate [from 0.8 to 1.3 equivalent of the total amount of anhydro glucose units (AGU)] was dissolved into 100 mL of deionized water and added to the MFC suspension. Another 1000 mL of deionized water was added to reach a cellulose concentration of around 8 g/L. The flask was wrapped with aluminum foils to avoid the UV-light degradation of the sodium metaperiodate<sup>61</sup> and the oxidation was carried out at room temperature from 45 to 123 h. The mixture was then dialyzed against deionized water with a 14 kDa cutoff membrane. The dialysis was stopped when the conductivity of the dialysis bath was

stable and close to the conductivity of deionized water (around 30  $\mu$ S). The products with a final consistency of about 5.5 g/L were kept at 4°C in a never dried condition. Aliquots were freeze-dried for analysis purposes. The yield of the reaction was given as the ratio of final and initial dry mass. Since the molecular weight of each AGU change from 162 to 160 g/mol by the oxidation, the theoretical yield is 98.8%.

### **2.3. POC reduction by NaBH<sub>4</sub> (rPOC)**

A typical experiment to synthesize rPOC consisted of reacting 10 g on dry basis of POC with 4.7 g of NaBH<sub>4</sub> (2 eq per total AGU). The reaction proceeded for about 48 h at room temperature (20-25°C) under magnetic stirring. The mixture was then dialyzed with a 14 kDa cutoff membrane against deionized water for several days until the dialysis bath reached a stable conductivity close to that of deionized water i.e. less than 30  $\mu$ S. After dialysis, the samples in batches of 200 mL were sonicated with a Branson Digital Sonifier operated at 50 % of its full power for 4  $\times$  2 min. The samples were then filtered first through a 5  $\mu$ m filter and then a 1  $\mu$ m one, using a Sartorius air-pressured-type filter. They were kept never dried at 4°C for storage before use at a consistency of about 4.3 g/L. The yield of the reaction was calculated from the ratio of dried mass from recovered rPOC over the initial mass of POC since the molecular weight of an oxidized/reduced AGU is only changing from 160 to 164 g/mol compared to an oxidized AGU.

### **2.4. <sup>13</sup>C CP-MAS solid-state NMR**

The NMR measurements were made on freeze-dried POC or rPOC samples. Solid-state <sup>13</sup>C NMR spectra were acquired using a Bruker Avance III DSX 400 MHz spectrometer operated at 100.6 MHz for <sup>13</sup>C, using the combination of the cross-polarization, high-power proton decoupling and magic angle spinning (CP-MAS) method. The spinning

speed was set at 12,000 Hz. The <sup>1</sup>H radio-frequency field strength was set to give a 90° pulse duration of 2.5 μs. The <sup>13</sup>C radio-frequency field strength was obtained by matching the Hartman-Hahn conditions at 60 kHz. At least 2,000 scans were integrated with a contact time of 2 ms using a ramp CP protocol and a recycle delay of 2 s. The acquisition time was 35 ms and the sweep width set at 29,400 Hz. The chemical shifts were calibrated with respect to the carbonyl peak of glycine (176.03 ppm).

### 2.5. Carbonyl group content: degree of oxidation (DO)

The carbonyl content of each sample was determined using the previously described <sup>13</sup>C-CP-MAS NMR method.<sup>168</sup> It is expressed as a degree of oxidation (DO) representing the average number of carbonyl groups introduced per AGU. In this expression, a fully oxidized sample had a DO of 2 since the oxidation of one glycosyl ring leads to 2 aldehyde groups at the C2 and C3 position of the AGU.

Briefly, the NMR spectra of the oxidized sample (S) and the initial cellulose (S0) were superimposed and normalized against the height of the C1 signal of cellulose at 105 ppm (the C1 signal is believed to keep its shape and chemical shift, independent of the increasing DO). Once normalized, the integral of the spectra S0 represents the contribution of unoxidized cellulose in the spectra S and the ratio of integrals  $\int S0 / \int S$  gives the ratio of unoxidized units over the total number of units in the sample S. The DO is then deduced from the following formula:

$$DO_{NMR} = 2\left(1 - \frac{\int S0}{\int S}\right)$$

### 2.6. Dynamic light scattering (DLS)

DLS measurements were performed with a Malvern NanoZS instrument operated with a 2 mW HeNe laser at a wavelength of 632.8 nm and detection at an angle of 173°. All

measurements were performed in a temperature-controlled chamber at 20 °C ( $\pm$  0.05 °C). Three measurements of 10 runs each were usually averaged. The intensity size distribution was obtained from the analysis of the correlation function using the multiple narrow mode algorithm of the Malvern DTS software. The samples had a concentration between 0.5 and 0.6 wt %.

### 2.7. $\zeta$ -potential measurements

The electrophoretic mobility of the rPOC particles was measured with the Malvern NanoZS apparatus, set at 17°. The  $\zeta$ -potential values were determined by applying the Henry equation. The  $\zeta$ -potential values were averaged over at least three measurements with at least 30 runs per measurement. The samples had a concentration between 0.5 and 0.6 wt %.

### 2.8. Turbidimetry measurements

The turbidity measurements were made with 0.05-0.1 wt % suspensions using a quartz cuvette with a path length of 1 cm, using a Varian CARY 50 BIO UV-Visible spectrometer, scanning the samples between 200 and 800 nm. The average diameters of the particles were calculated following the Carr-Hermans theory with the assumption that the particles had a constant cross-section.<sup>199</sup> The particle diameters were calculated from:

$$\tau = \frac{88\pi^3nc}{15\lambda^3N} \left(\frac{dn}{dc}\right)^2 \mu$$

with:  $\mu = 9.85 \cdot 10^9 \cdot d^2 \text{ g.mol}^{-1}.\text{cm}^{-1}$ ,

and where

$\tau$  is the turbidity ( $\text{cm}^{-1}$ ),

$n$  is the refractive index of water (1.33),

$c$  is the suspension concentration ( $\text{g.mL}^{-1}$ , here either 0.5 or 1.0  $\text{g.mL}^{-1}$ ),

$\lambda$  is the wavelength (cm),

$N$  is the Avogadro's number ( $6.022 \cdot 10^{23} \text{ mol}^{-1}$ ),

$dn/dc$  is the specific refractive index increment ( $0.135 \text{ mL.g}^{-1}$ , calculated from the refractive index of cellulose, 1.55 being the refractive index of water and 1.33 that from the density of cellulose,  $1.63 \text{ g.mL}^{-1}$ ),<sup>200</sup>

$\mu$  is the mass-length ratio of the particles ( $\text{g.mol}^{-1}.\text{cm}^{-1}$ ),

and  $d$  is the average particle diameter (cm).

## 2.9. Transmission electron microscopy (TEM)

Drops of about 0.001 wt % suspensions were deposited onto carbon-coated TEM grids freshly glow-discharged in a PELCO easiGlow unit. After 2 min, the liquid in excess was absorbed with filter paper and a drop of aqueous 2 wt % uranyl acetate negative stain was deposited on the grids before complete drying. After 2 min, the stain in excess was blotted away and the remaining liquid film was allowed to dry. The specimens were observed using a Philips CM200 CRYO microscope operated at 80 kV. The images were recorded with a TVIPS F216 TemCam camera ( $2040 \times 2040$  pixels) and processed using the imageJ software.

## 2.10. Small-angle X-ray scattering (SAXS)

SAXS experiments were performed at the European Synchrotron Research Facility (ESRF, Grenoble, France), on the ID02 beamline with an X-ray energy of 12.46 keV and sample-detector distances of 31 m and 1.5 m. Two dimensional (2D) scattering patterns were recorded with a 0.08 s integration time and 10 frames were recorded per sample, yielding a total exposure time of 0.8 s. The 1D static scattering profiles  $I(Q)$  as a function of  $Q$  were obtained by azimuthal averaging of the measured 2D patterns after normalization by incident flux, sample transmission, detector response function and the

solid angle subtended by the pixels, where  $Q$  is the magnitude of the scattering vector given by  $Q = (4\pi/\lambda) \times \sin q/2$ ,  $\lambda$  being the incident X-ray wavelength (0.0996 nm) and  $q$  the scattering angle.

### 3. Results and discussion

#### 3.1. POC and rPOC synthesis

First, following the protocol presented in the experimental part and as previously described,<sup>175</sup> four POC samples were prepared by varying the oxidation time from 45 to 123 hours and the periodate concentration from 1.0 to 1.3 equiv./AGU. The corresponding <sup>13</sup>C CP-MAS NMR spectra are shown in Figure 45a. As well documented in the literature, the very reactive aldehyde groups resulting from the periodate oxidation readily recombine with neighboring hydroxyl groups to yield intra or inter hemiacetal/hemialdal entities.<sup>64, 110-111, 168</sup> The multiplicity of these recombined structures gives rise to a broad composite signal in the 90-100 ppm region, as observed in the spectra of the four POC samples (Figure 45a), and to the absence of a carbonyl signal in the 190-200 ppm region (not shown). The intensity of this broad signal increases with reaction time and periodate to AGU ratio. Using the <sup>13</sup>C CP-MAS NMR quantification method we have developed,<sup>168</sup> the degree of oxidation of these samples were calculated as ranging from 1.4 to 1.7 (Table 2), the DO increasing with reaction time and NaIO<sub>4</sub>/AGU ratio. The corresponding yields were between 75 and 84 wt % (Table 2).

Each sample was subsequently subjected to a sodium borohydride reduction using a NaBH<sub>4</sub>/AGU ratio equal to 2 for two days at room temperature, yielding reduced POC (rPOC) samples. The yield of the reduction reaction ranged from 85 to 94 wt % with respect to the POC samples, corresponding to an overall yield of 67 to 79 wt % with

respect to the initial cellulose microfibrils (Table 2). Compared to other reaction processes involving a different purification procedure, substantially high yield could be obtained using our protocol.<sup>119</sup>

Table 2. Periodate oxidation conditions used for the synthesis of the POC samples and corresponding DOs. Intermediate mass yields are given after the oxidation (\*) and reduction steps (\*\*).

Sample	Periodate oxidation				NaBH <sub>4</sub> reduction	
	NaIO <sub>4</sub> /AGU molar ratio	Reaction time (h)	Yield* (wt %)	DO	Yield** (wt %)	Total Yield (wt %)
a	1.0	123	84	<b>1.4</b>	94	79
b	1.2	45	82	<b>1.5</b>	89	73
c	1.1	123	84	<b>1.6</b>	92	77
d	1.3	123	79	<b>1.7</b>	85	67

The <sup>13</sup>C CP-MAS NMR spectra of periodate oxidized sample and subsequently reduced samples are shown in Figure 45a and b, respectively. After the NaBH<sub>4</sub> reduction step, the broad hemiacetal signal in the 90-100 ppm regions totally disappeared, indicating a quantitative reduction of all the aldehyde groups into primary alcohol moieties. Furthermore, the signals in the 55-65 region increased at the expense of the signals in the 70-80 region. This can be attributed to the shift of the C2 and C3 signals originally in the 70-80 ppm region to the 55-70 ppm region upon conversion into CH<sub>2</sub>-OH groups typically exhibiting a chemical shift in the latter region (similar to the C6 of native cellulose). The molecular composition of the rPOC thus corresponds to a mixture of intact native cellulose and dialcohol cellulose moieties (fully modified chains of reduced dialdehyde cellulose synthesized during the oxidation).

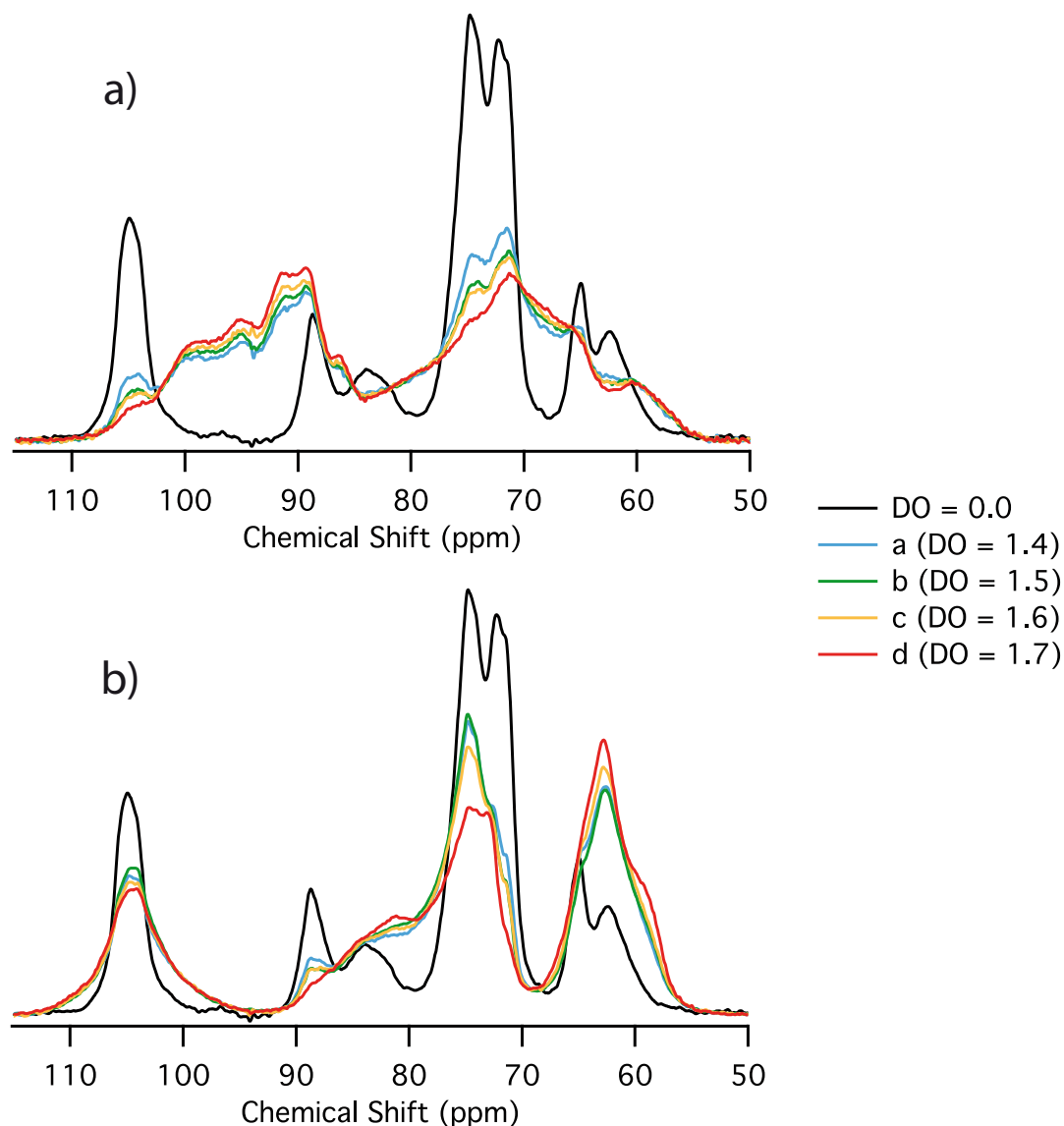


Figure 45.  $^{13}\text{C}$  CP-MAS NMR spectra of the intermediate POC (a) and the final rPOC (b) samples. For each spectrum, the total integrated area was normalized to 1.

### 3.2. Suspension stability and nanoparticles dimensions

Visual inspection of all POC samples showed that the oxidation reaction resulted in turbid suspensions prone to rapid sedimentation. No dispersion in water could be obtained even after intensive sonication. An example of such a POC suspension for  $\text{DO} = 1.6$  is shown in Figure 46a. This observation is not surprising and likely due to the cross-linking arising from the aforementioned hemiacetal linkages, which results in

stable connections between POC particles even for never-dried suspensions in water. After complete reduction with  $\text{NaBH}_4$  and purification, the rPOC samples were somewhat turbid and had a tendency to sediment (Figure 46b). However, a sonication treatment followed by filtration through 1  $\mu\text{m}$  membranes resulted in transparent stable suspensions without any sedimentation effect, whatever the initial DO. An example of such a stable rPOC suspension (initial DO = 1.6) is shown in Figure 46c. Over 90 wt % of the sample was recovered after the sonication/filtration steps, which indicates that this process is breaking aggregates rather than removing large particles. In contrast to the POC case where strong connections resulted in sedimenting aggregates, rPOC samples initially formed aggregates of weakly interacting particles that could easily be turned into stable suspensions of submicron-sized particles using a moderate sonication treatment.

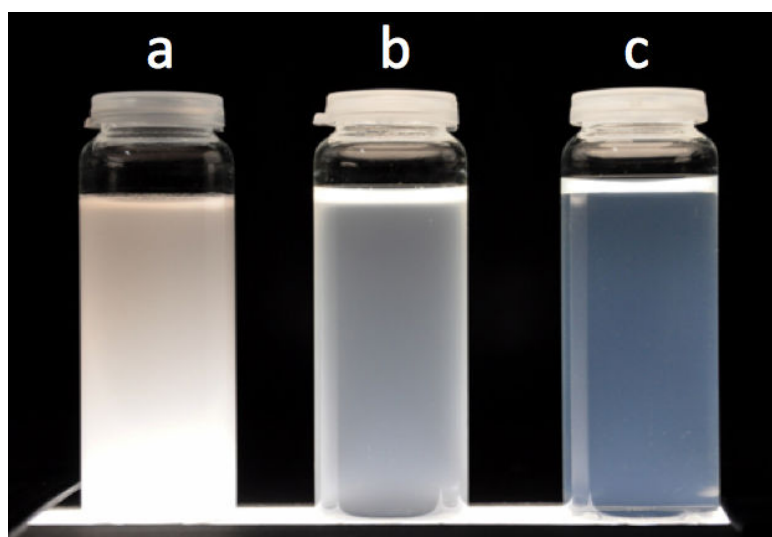


Figure 46. Aqueous POC suspension with a DO of 1.6 at a concentration of 0.4 wt % (a) and corresponding rPOC suspension before (b) and after a sonication-filtration process (c).

The dimensions and stability of rPOC particles were further investigated using DLS and turbidimetry. As shown in Figures 47, rPOC particles exhibited hydrodynamic diameter ( $D_H$ ) values in the 150-210 nm range with a moderate polydispersity, showing that individualized nanoparticles were obtained. The hydrodynamic diameter decreased with increasing DO of the initial POC samples (60 nm decrease in  $D_H$  when DO increases from 1.4 to 1.7). The hydrodynamic size of the particles did not change after 2-months storage at 4°C (figure SC4-1), proving the long-term colloidal stability of the rPOC suspensions.

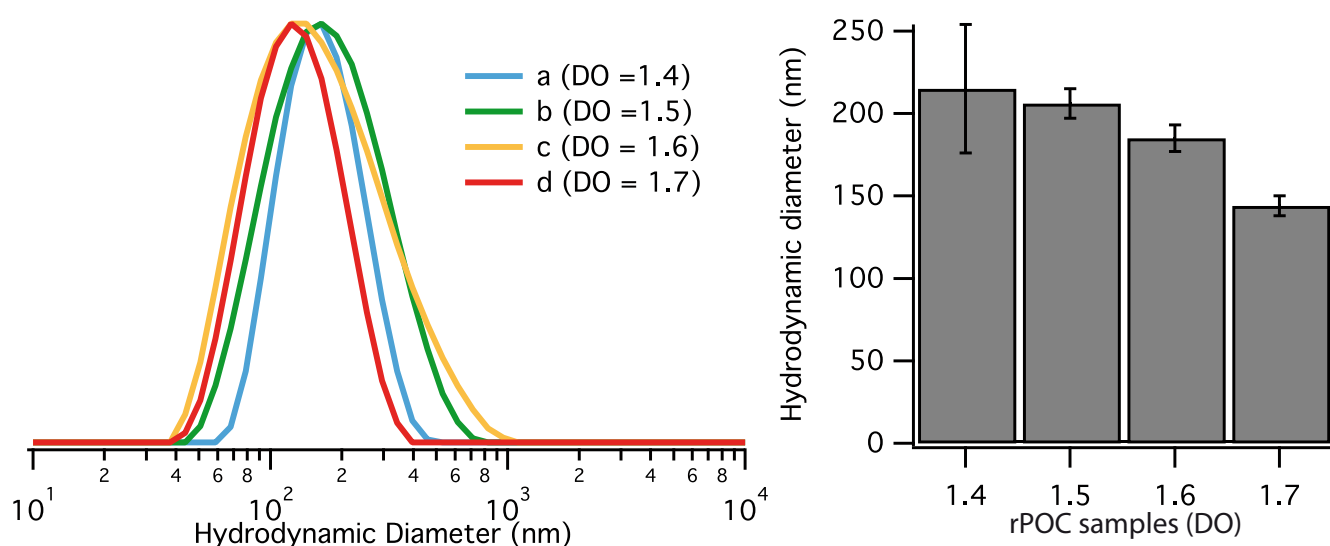


Figure 47. Hydrodynamic diameter distributions (left) and average values deduced from DLS measurements of rPOC samples at  $t_0$  (right).

The turbidity-derived average particle diameter also decreased with increasing DO (from 7 nm for DO = 1.4 to 3.8 nm for DO = 1.7) (Figure 48). Again, these values were relatively stable with time (Supporting information Figure SC4-2), confirming the colloidal stability of the samples for at least 2 months.

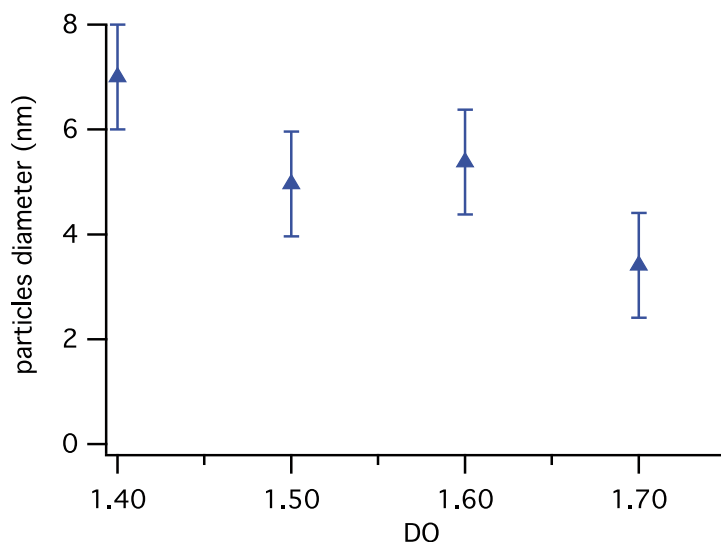


Figure 48. Turbidity-derived average particle diameter of the rPOC nanoparticles (suspension concentration = 1 g/L).

The difference between DLS data giving hydrodynamic diameters in the 150-210 nm range and turbidimetry data yielding cross-section dimensions in the 4-7 nm range can be explained by considering rPOC nanoparticles as elongated objects. To check this point and further characterize the dimensions of the rPOC nanoparticles, TEM micrographs of dried and negatively stained samples were recorded and are shown in Figure 49.

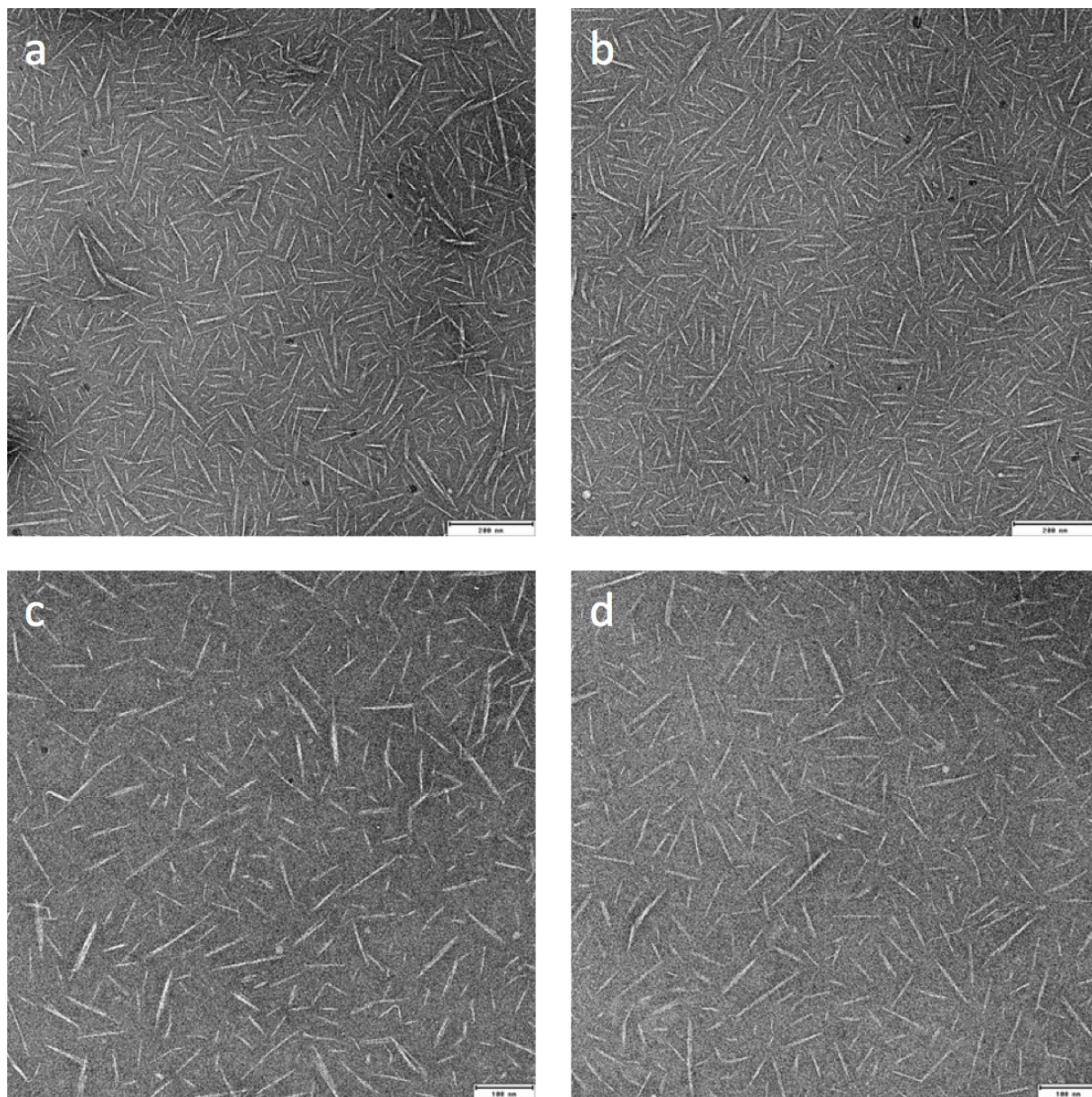


Figure 49. TEM micrographs from dried negatively stained rPOC suspensions for DOs equal to 1.4 (a), 1.5 (b) 1.6 (c) and 1.7 (d) (scale bar = 200 nm for a and b, 100 nm for c and d)

Table 3: Length and width and corresponding standard deviations of rPOC nanorods measured from TEM micrographs as a function of the DO of the parent POC samples.

DO	Average length (nm)	Length $\sigma$ (nm)	Average width (nm)	Width $\sigma$ (nm)
1.4	66	27	6.5	1.9
1.5	67	25	6.5	2.0
1.6	64	28	6.1	2.0
1.7	54	26	6.5	1.9

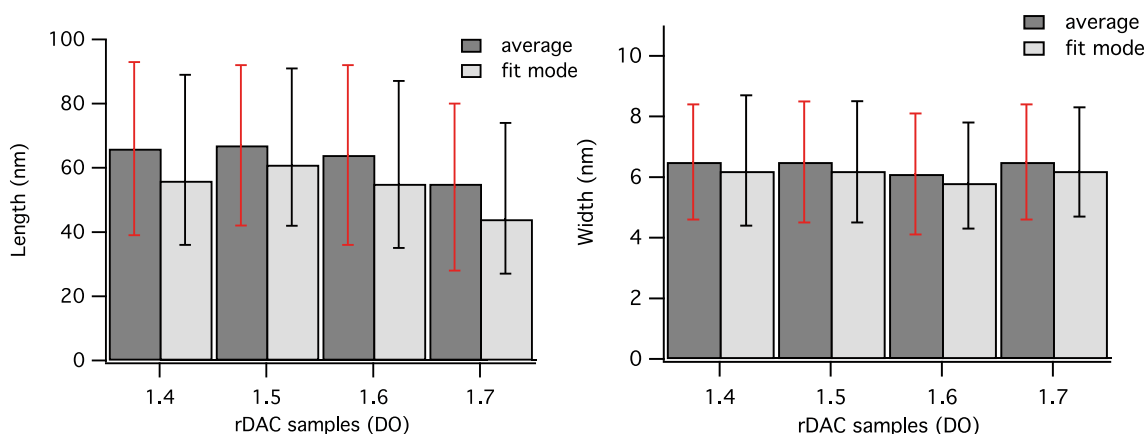


Figure 50. Plot of the average and maximum from fit data for length (left) and width (right) from size distributions measurements in the TEM images (see size distributions in Supporting Information Figure SC4-3 and SC4-4) against the degree of oxidation (DO) of the parent POC. (red error bars: standard deviation from TEM size distributions, black error bars: full width at half maximum of fit data from TEM size distributions).

Typical negatively stained transmission electron micrographs corresponding to the four different original DO values are shown in Figure 49. Each of the four micrographs displays very well separated rod-like particles, showing similarities with CNCs obtained with conventional HCl<sup>38, 129, 201</sup> or H<sub>2</sub>SO<sub>4</sub><sup>24, 127, 202</sup> acid hydrolysis. The length and width distribution histograms obtained from these micrographs are shown in the Supporting Information Figures SC4-3 and SC4-4, respectively. The lengths of these rPOC nanorods exhibit a substantial polydispersity with a skewed distribution, as some elements are no longer than 10 nm whereas a few reach over 200 nm. The widths also display a

pronounced polydispersity and an asymmetric distribution, as most elements have widths between 4 and 15 nm. Both size distributions could be fitted using a lognormal function as shown in Supporting Information Figures SC4-3 and SC4-4. The number averages lengths and widths are listed in Table 3 with their corresponding standard deviations. The number averages and the peak position of the fitted lognormal function are shown in Figure 50, together with the standard deviation or half width at half maximum of the peak function as error bars. The length slightly decreased with increasing DO (of the parent POC sample): from 66 nm to 54 nm (20% reduction) for DO increasing from 1.4 to 1.7 (50 % reduction of intact cellulose). The change in width was more subtle in the DO range investigated.

### 3.3. Core-shell structure

With all techniques employed, the nanoparticle size decreased with increasing DO. However, the extent of the decrease depended on the experimental technique and the probed dimension. Especially, it can be seen that there is a reduction by a factor of about 3 between the hydrodynamic diameters derived from DLS (about 200 nm) and the observed lengths by TEM (about 60 nm). This result has to be compared with what can be obtained for conventional acid hydrolyzed CNCs where DLS and TEM measurement fit one another (about 100 nm for both DLS and TEM).<sup>24,39</sup> This difference between DLS and TEM data suggests a drastic reduction of the diffusion coefficient due to the presence of swollen water soluble hydroxylated oligo or polymer appendages attached to solid crystalline native cellulose nanorods. Such a possibility is in full agreement with the solid-state <sup>13</sup>C NMR data showing the presence of both native cellulose signals and hydroxylated chains. Indeed, for nanoparticles of DO equal to 1.4, 1.5, 1.6 and 1.7, the molar ratio of solid intact cellulose versus potentially swollen cellulose dialcohol chains

is 0.43, 0.33, 0.25 and 0.18 respectively. Even if all the corona made of reduced chains is not completely unfolded in the surrounding media, the particles at this level of modification can be considered as a tiny solid core surrounded by a spongy swollen shell. To go further in this direction, one can compare turbidity and TEM results. The dimensions as probed by turbidity showed a significant decrease of the measured diameter with DO, whereas TEM did not point out real differences between the samples. As TEM micrographs have been obtained on dried samples, and the yield of the reduction is close to 100%, it is reasonable to expect a roughly constant diameter whatever the DO, the initial native cellulose being replaced by an approximately equivalent volume of dialcohol cellulose chains upon drying on the TEM grids. In the case of turbidity measurements performed in aqueous suspension, the dimension that are probed are the one of swollen particles. Indeed the 43% of native cellulose present in the particles of DO=1.4 should have an apparent diameter higher than the 18% found in the particles of DO=1.7, the swollen shell most probably contributing less than the core, further supporting the factor 3 difference between DLS and TEM data.

While TEM essentially focuses on the dimension of the compact object, turbidity and DLS brought informations on the swollen particles but in a rather indirect manner. Altogether, the colloidal stability and the non-touching particles observed in TEM combined with anomalous hydrodynamic behavior strongly suggest the presence of highly swollen surface layer. To validate this hypothesis, small-angle X-ray scattering experiments were carried out on dilute suspensions of rPOC (DO of the parent sample equal to 1.4, 1.6 and 1.7) and on a dilute suspension of sulfuric acid-derived wood cellulose nanocrystals produced by the Forest Products Laboratory (University of Maine, USA). The corresponding scattered intensity normalized by the sample concentration,

$I/C$ , versus the scattering vector,  $Q$ , spectra are shown in Figure 51. In the low  $Q$ -region, rPOC samples exhibit a close to  $Q^{-1}$  behavior, which is typical of rod-like objects. The same  $Q$ -dependence should be observed for the CNC sample but this behavior is not clearly seen here due the presence of a correlation peak at  $Q^* = 4.74 \times 10^{-2} \text{ nm}^{-1}$ , arising from long-range electrostatic repulsions between sulfated nanocrystals. For the series of three rPOC samples, the intensity scattered at low- $Q$  decreased when the DO of the parent POC increased. This is consistent with a decrease in the cross-section of the rod-like particles. This result is also in agreement with the tendencies indicated by DLS, turbidimetry and TEM results. A very remarkable difference can be observed between the rPOC suspensions and the CNC suspension in the high  $Q$ -region, where the interface between the nanoparticles surface and the solvent is probed. For the CNCs, the scattered intensity follows a  $Q^{-4}$  decay, which is typical of a sharp interface with a low roughness. Such a result is consistent with the crystalline CNC-water smooth interface. For the rPOC nanorods however, a  $Q^{-2}$  decay was observed whatever the DO of the parent POC at this local length scale. This strong deviation from the  $Q^{-4}$  power law is in agreement with the rPOC-water interface being composed of polymer chains in a theta solvent (Gaussian statistics). The SAXS data therefore confirm that the rPOC particles are hairy nanorods composed of native cellulose crystalline cores surrounded by a shell of neutral hydroxylated oligomers. The overall cross-section of these colloids decreases when the DO of the parent POC increases.

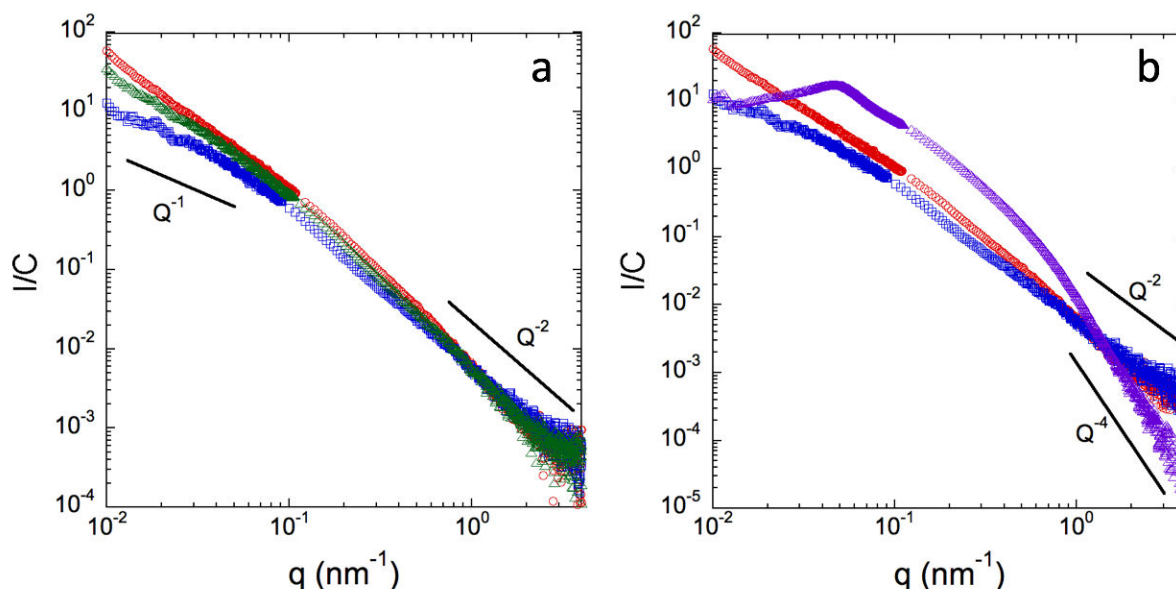


Figure 51. Small angle X-ray scattering spectra of dilute suspensions of (a) rPOC with DOs of the parent POC equal to 1.4 (red), 1.6 (green) and 1.7 (blue) and of (b) rPOC with DO equal to 1.4 (red) and 1.7 (blue) and of a suspension of sulfuric acid-derived wood cellulose nanocrystals from FPL (purple). The scattered intensity has been normalized to the concentration.

Table 4:  $\zeta$ -potential of conventional wood CNCs and rPOC particles (DO of the parent POC = 1.70).

Sample	$\zeta$ -potential (mV)	$\sigma$ (mV)
Wood CNCs	-41.4	$\pm 13.3$
rPOC	-2.7	$\pm 9.9$

The highly consistent set of data gathered in this study show that colloiddally stable suspensions of individualized rPOC core-shell nanorods were produced. Such nanoparticles can be schematically depicted as in Figure 52. The origin of their colloidal stability must be attributed to steric repulsion provided by the presence of soluble dialcohol cellulose chains at the surface of the rPOC nanoparticles. As shown in Table 4, the zeta potential of our rPOC nanorods is very close to zero, confirming the absence of

any charge and suggesting a purely steric stabilization. In contrast, CNCs obtained from sulfuric acid hydrolysis display a zeta potential value of about -40 mV due to the presence of surface sulfate half-esters that provide long-range electrostatic stabilization of the particles in aqueous media. The overall cross-section of the hairy rPOC nanorods decreases when the DO of the parent POC increases but the quantity of dangling chain in Gaussian conformation appears to be enough above a DO value of 1.4, to preserve the colloidal stability. The apparent reduced influence of the DO on the width of the nanoparticles shown by TEM data could be attributed to the tight adsorption of part of the dangling appendages on the crystalline core observed under dry conditions.



Figure 52. Schematic representation of the core-shell structure of rPOC nanorods. These hairy colloids are composed of a native cellulose crystalline core surrounded by a shell of neutral hydroxylated oligomers providing steric stabilization in aqueous medium.

## 4. Conclusions

In this work, we have applied periodate oxidation treatments of various intensities to microfibrillated cellulose, leading to a series of POC samples, which were characterized by their DO values. When subsequently reduced by  $\text{NaBH}_4$ , the initially oxidized samples of DOs comprised between 1.4 and 1.7 had lost their microfibrillar character after the reduction treatment to be chopped into slender crystalline cellulose nanorods. Remarkably these nanoparticles showing lengths of the order of 55 to 67 nm and widths

of no more than 6.5 nm, could easily be dispersed homogeneously, leading to aqueous non-flocculated suspensions of permanent stability. This stability was not due to any electrostatic repulsion - as these nanoparticles proved to be un-charged - but to a steric repulsion mechanism resulting from the presence of dangling dialcohol cellulose chains anchored at the surface of the crystalline nanorods, in a typical core-shell type organization.

We think that the results presented here are important since they show that a controlled periodate oxidation of native cellulose followed by a NaBH<sub>4</sub> reduction step is an attractive alternative route to the standard acid hydrolysis protocol systematically used so far for the preparation of crystalline cellulose nanorod batches.

## Chapter 4: Supporting information

The Supporting Information contains additional DLS and turbidimetry data showing the dimensional stability of the rPOC particles in time, in addition with length and width histogram derived from TEM observations.

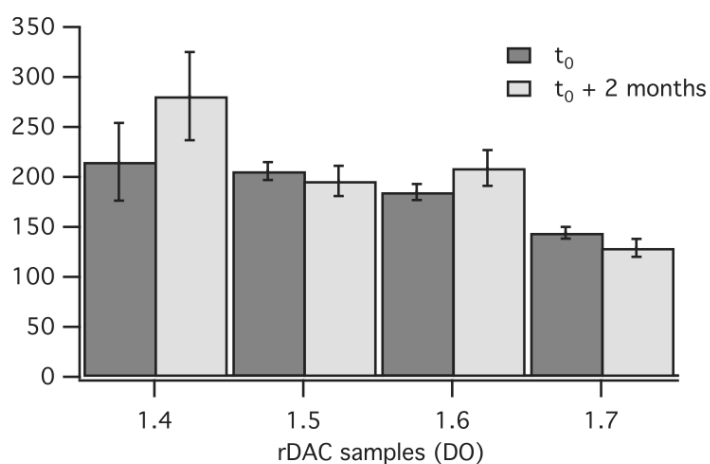


Figure SC4-1. Average hydrodynamic diameter of rPOC suspensions at  $t_0$  and  $t_0+2$  months extracted from DLS measurements.

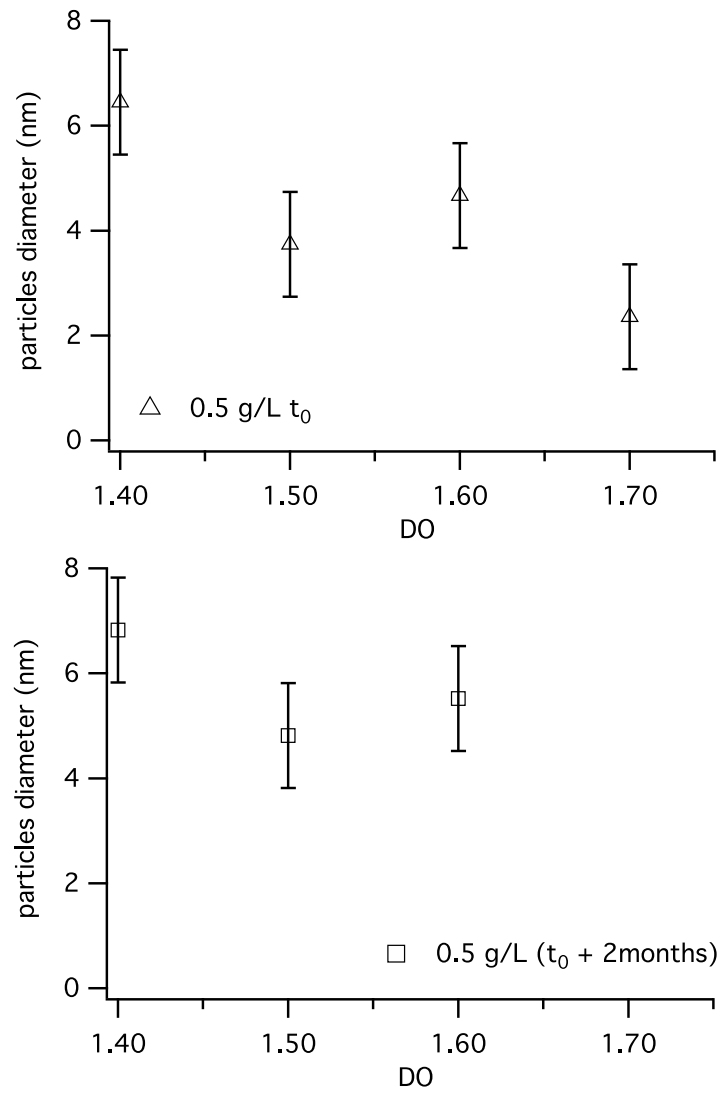


Figure SC4-2. Turbidity measurements of rPOC suspensions at  $t_0$  and  $t_0+2$ months at 0.5g/L

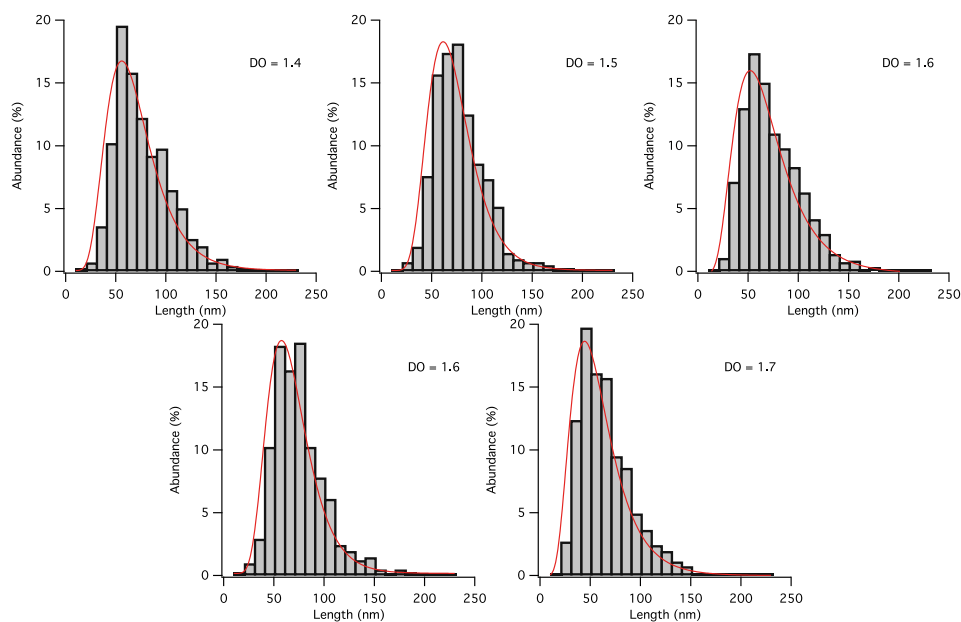


Figure SC4-3. Length histograms from TEM images of rPOC samples as a function of the DO of the parent POC with their log-normal fit.

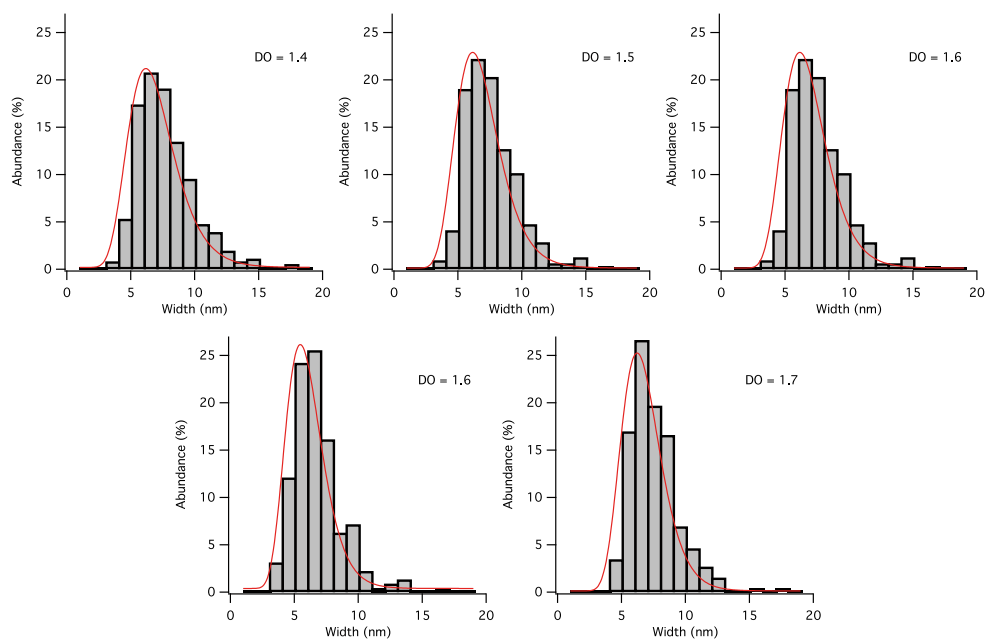


Figure SC4-4. Width histograms from TEM images of rPOC samples as a function of the DO of the parent POC with their log-normal fit.



# Chapter 5: Cellulose-based thermoplastics through periodate cleavage and amine grafting

## Foreword

The aim of the chapter is to graft side groups on the freshly formed aldehyde groups of POC samples in order to maximize the free volume around the polymer chains, based on the hypothesis that it would further plasticize the polymer. Since the aldehyde groups are highly reactive towards amines, a reductive amination reaction was chosen. This reaction presented in Figure 53 follows a two-step mechanism: first the primary amine condenses on the aldehyde group forming an imine bond ( $-C=N-$ ), as seen in Figure 53a, then the cyanoborohydride can selectively reduce the imine into a secondary amine (Figure 53b). This is due to the fact that at pH range of 6-7 hydrides of  $\text{NaBH}_3\text{CN}$  can quickly reduce  $C=N$  bonds, while the kinetics of reduction of aldehyde groups to alcohol is very slow.<sup>203</sup>

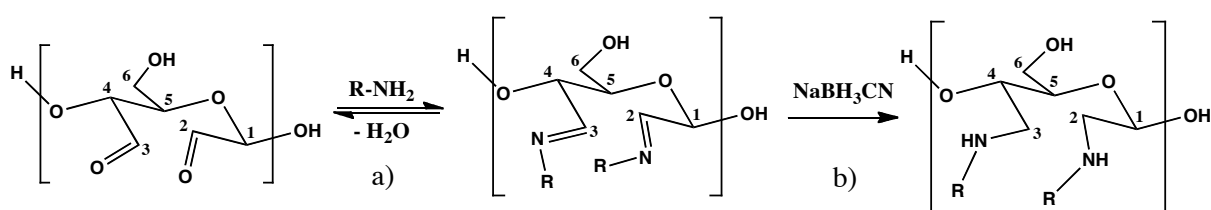


Figure 53. Grafting of POC by reductive amination: imination (a) followed by reduction (here with  $\text{NaBH}_3\text{CN}$ ).

Different reaction media from the literature were first tested with the aim to identify the best conditions to achieve a successful amination with a reasonable yield.

The reductive amination with phosphate buffer of pH 6<sup>111</sup> was compared with simple amination in toluene.<sup>62</sup> Both protocols exhibited a brown coloration during the reaction. We suspect this browning to be due to reactions collectively called Maillard reactions between amine and carbonyl groups that are accelerated in basic conditions due to the increased nucleophilicity of amines.<sup>204-205</sup> The final products are volatile compounds and brown aromatic molecules called melanoidins,<sup>206</sup> hence the coloring of the solutions. This process usually occurs at high temperature<sup>207</sup> but could be accelerated by the high density of aldehydes after periodate oxidation. Chimpibul *et al.*<sup>204</sup> reported for oxidized dextran with a DO around 0.8, a molecular weight decrease from 70 kDa to less than 15 kDa when mixed with a 5% amine solution for less than one hour, proving the degradation power of the Maillard reaction on polysaccharides.

The reductive amination carried out in water without any buffer, with 2 eq amine (propylamine and ethanolamine) and 4 eq of NaBH<sub>3</sub>CN for 24 h exhibited a pH value around 10 and the mixture became brown after only a couple a minutes. This was reasonable as the quantity of phosphate in the system was, in fact, not sufficient enough to counteract the amount of amine and reductive agent. Furthermore, whatever the purification conditions (dialysis, ultrafiltration, precipitation in various solvents...) the yields were extremely low (less than 15%) and the analysis of the recovered product showed that it was only constituted of unmodified cellulose as seen in Figure 54. Our hypothesis is that the oxidized part was degraded due to the Maillard reaction leaving only the core of unmodified cellulose. This reaction will happen if the pH is too high: we experience the browning reactions at pH around 9-10.

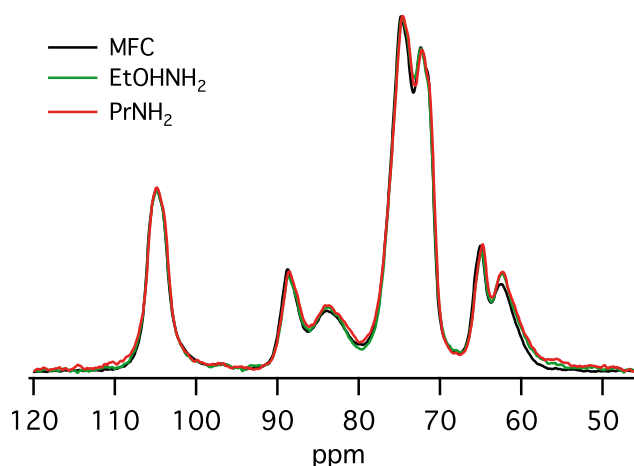


Figure 54.  $^{13}\text{C}$  CP-MAS of products after reductive amination on DAC at pH 10 with ethanolamine and propylamine compared to the spectrum of the initial MFCs

One way to avoid the Maillard side reaction is to control the pH during the reaction, for example using a buffer at pH 4.4 and diluted conditions (1 g/L).<sup>85</sup> The pH can be also controlled by addition of strong acids such as HCl<sup>76-77</sup> since no report of any browning was ever made using those reductive aminations conditions.

According to these tests and literature data, we finally decided to use the latter protocol with amines or with hydrochloride salts of amines. These salts would have the same effect as adding HCl, and was more convenient for handling. Only a small amount of HCl was needed to compensate the basicity of  $\text{NaBH}_3\text{CN}$ .

Butylamine, ethanolamine and benzylamine were grafted on oxidized MFC with a wide range of starting DOs: from 0.8 to about 1.8. After reaction and purification by dialysis, the samples were solvent cast. The degree of substitution (DS), defined as the average number of amine introduced per AGU ( $0 \leq \text{DS} \leq \text{DO} \leq 2$ ), was measured by  $^{13}\text{C}$  CP-MAS NMR and the thermo-mechanical properties of all the prepared materials were tested by TGA, DSC, or DMA and reported in the following chapter.

## 1. Introduction

Transforming cellulose, the most abundant organic resource, into thermoplastics in an energy efficient way to replace petroleum-based polymers is one of the main challenges towards the development of sustainable materials. Despite the numerous merits of cellulose, including natural abundance, renewability, stability and remarkable mechanical properties,<sup>13</sup> cellulose or its derivatives still cannot replace commodity plastic materials due to difficulties in processing.<sup>4-5, 8</sup> Suspension filtration or dissolution and regeneration are among the many classic ways of shaping cellulose, but these processes require large amounts of solvent or water. Chemical modifications such as acetylation,<sup>26, 40</sup> often with addition of small molecule plasticizers, can bring the melting (softening) temperature down to the processing window,<sup>43</sup> but this implies addition of significant amount of exogenous carbon from fossil resource. For example, cellulose acetate with a degree of substitution of three implies the introduction of the same number of carbon atoms from the coal as from the biomass. The full acetylation is still not enough to render cellulose melt processable, and longer side chains such as propionates<sup>44, 46</sup> or/and a large amount of plasticizers are used in the industrial process.<sup>26</sup>

One of the reasons for the high glass-transition temperature ( $T_g$ ) of cellulose is considered to be due to the chain stiffness, as  $T_g$  is empirically a function of chain flexibility.<sup>6</sup> Indeed Gibbs and DiMarzio<sup>7</sup> relate the  $T_g$  to the configurational entropy, and thus the flexibility of the molecule. Thus, one way to decrease the  $T_g$  would be to introduce flexibility to the backbone.<sup>96</sup> The rigidity of the cellulose backbone arises from the intrinsic rigidity of the constituting glucose rings. The glycosidic linkage between

glucose residues also has limited freedom of rotation due to the steric hindrance related to the rigid and bulky nature of glucose residues.<sup>20</sup> By cleaving one bond of the glucose ring, the polymer would be released from the rigidity of both monomer and the inter-monomer linkages. This can be achieved by selective oxidation of vicinal alcohol groups by periodate. Indeed Kasai *et al.*<sup>98</sup> carried out periodate oxidation in a solvent in homogeneous conditions followed by reduction of aldehyde groups into alcohols, to produce from cellulose a water-soluble polymer with a glass transition temperature below 200 °C. However, when oxidized in a conventional aqueous system, it was shown that the so-called periodate oxidized cellulose (POC) is a biphasic system which, after reduction, transform into a self-reinforced nanocomposite made of intact native cellulose in the form of nanorods<sup>175</sup> surrounded by thermoplastic dialcohol cellulose.<sup>208</sup> Similarly, in a heterogeneous fibrous system, Larsson *et al.*<sup>99-100</sup> prepared a direct composite of dialcohol cellulose and intact cellulose that is plasticized by moisture. In this we further pursue the possibility of making thermoplastics out of cellulose by grafting limited amounts of side groups on the reactive aldehyde groups generated by periodate oxidation. We grafted ethanolamine, butylamine and benzylamine as typical examples of linear hydrophilic, linear hydrophobic and bulky hydrophobic groups, respectively.

## 2. Materials and methods

### 2.1. Materials

A batch of paste-like never dried microfibrillated cellulose (MFC) prepared by a mechano-enzymatic treatment<sup>158-159</sup> of spruce sulfite pulp, with a consistency of about 2 wt %, was purchased from the Centre Technique du Papier (CTP), Grenoble, France.

Sodium metaperiodate ( $\text{NaIO}_4$ ) with purity  $\geq 99.8\%$  was acquired from Carl Roth (France). Sodium cyanoborohydride ( $\text{NaBH}_3\text{CN}$ ) with purity  $\geq 95\%$ , benzylamine ( $\text{BnNH}_2$ ) (99%), ethanolamine hydrochloride ( $\text{EtOHNH}_2\text{-HCl}$ ) ( $\geq 99\%$ ) and butylamine ( $\text{BuNH}_2$ ) (99.5%) were purchased from Sigma Aldrich.

## 2.2. MFC oxidations to POC

In a typical experiment, about 50 g of the 2% MFC suspension (equivalent to 1 g of dry cellulose) was put in a flask equipped with a magnetic stirrer. The periodate - from 0.2 to 1.3 eq of the total amount of anhydroglucose unit (AGU) - was dissolved in 40 mL of deionized water and added to the MFC suspension. About 50 mL of deionized water was further added to adjust the cellulose concentration to 7.2 g/L. The flask was covered with aluminum foils to avoid the UV-light degradation of the sodium metaperiodate.<sup>61</sup> The oxidation was carried out at room temperature for 24 to 65 h. At the end of the reaction, the mixture was dialyzed with a 14 kDa membrane, until reaching a conductivity below 30  $\mu\text{S}$ . The sample was decanted overnight at 4 °C. Then, a large part of the supernatant was removed in order to increase the concentration of the POC to about 20 to 50 g/L. Free standing films for mechanical analysis were prepared by casting in polystyrene petri dishes.

## 2.3. POC grafting via reductive amination

In a typical experiment 1 g (dry basis) of never dried POC was put in a beaker. In a second beaker, the aqueous solution of the considered amine (5 eq per AGU) and  $\text{NaBH}_3\text{CN}$  (5 eq per AGU) was set to pH 6 by adding 3 M HCl. The amine solution was then mixed with the wet POC to start the reaction. The concentration of POC during the reaction was around 20 g/L. The reaction was carried out at constant pH of 6 for 2 to 3

days. The samples were then dialyzed against deionized water with a 1 kDa dialysis membrane until a conductivity below 30  $\mu\text{S}$  was reached.

#### **2.4. $^{13}\text{C}$ CP-MAS solid-state NMR**

Solid-state  $^{13}\text{C}$  NMR spectra were measured using a Bruker Avance III DSX 400 MHz spectrometer operating at 100.6 MHz for  $^{13}\text{C}$ , using the combination of cross-polarization, high-power proton decoupling and magic angle spinning (CP-MAS). The spinning speed was set at 12 kHz. The  $^1\text{H}$  radio-frequency field strength was set to give a  $90^\circ$  pulse duration of 2.5  $\mu\text{s}$ . The  $^{13}\text{C}$  radio-frequency field strength was obtained by matching the Hartman-Hahn conditions at 60 kHz. At least 2,000 scans were integrated with a contact time of 2 ms using a ramp CP protocol and a recycle delay of 2 s. The acquisition time was 35 ms and the sweep width set at 29,400 Hz. The chemical shifts were calibrated using the carbonyl peak of glycine (176.03 ppm).

#### **2.5. Two-dimensional wide-line separation nuclear magnetic resonance (WISE NMR)**

The 2D wideline separation (WISE) experiment is a 2D technique that correlates the isotropic chemical shift in the  $^{13}\text{C}$  dimension obtained by conventional CP-MAS with the proton line shape in the  $^1\text{H}$  dimension, which gives information on the mobility of the surrounding protons. The obtained spectra in the proton dimension can be either narrow if the associated chemical moieties undergo rapid isotropic motion at a frequency greater than the strength of the dipolar coupling (20-30 kHz for conventional polymers) or broad if the motion are frozen either in the glassy state (under the glass transition temperature  $T_g$ ) or in the ordered phase for semi-crystalline polymer.<sup>171</sup> These experiments have been used to study the dynamics and organization of block

copolymers and blends,<sup>172</sup> core shell particles<sup>173</sup> and even cellulose and polyvinyl alcohol blends.<sup>174</sup>

For the 2D experiments, a short CP contact time of 300  $\mu\text{s}$  was used in order to minimize spin diffusion transfer that would lead to the same proton line shape for all carbons. For each increment, a typical number of 4800 scans were acquired using the same decoupling conditions as the 1D CP-MAS spectra. The size of the data matrix was 128 in the t1 dimension ( $^1\text{H}$ ) and 2048 in the t2 dimension ( $^{13}\text{C}$ ). The dwell time were 5  $\mu\text{s}$  in t1 and 25  $\mu\text{s}$  in t2, leading to spectral width of 200 kHz and 20 kHz in the proton and carbon dimensions, respectively.

### 2.6. Carbonyl group content: degree of oxidation (DO)

The carbonyl content of each sample was determined using a  $^{13}\text{C}$ -CP-MAS NMR technique previously described.<sup>168</sup> It is expressed as a degree of oxidation (DO) representing the average number of carbonyl groups introduced per anhydroglucose unit. The theoretical maximum DO is 2.

### 2.7. Degree of substitution (DS)

The DS is defined as the average number of amines grafted per AGU (the DS will be between 0 and DO) and measured by  $^{13}\text{C}$  CP-MAS NMR, by deconvolution of the C1 signal of unmodified AGU at 105 ppm and the C1' signal of grafted AGU at 98 ppm, with the formula:

$$DS = 2 \left( \frac{\int_{98\text{ppm}}}{\int_{98\text{ppm}} + \int_{105\text{ppm}}} \right),$$

where  $\int_{98\text{ppm}}$  is the integration of the deconvoluted NMR peak centered at 98 ppm corresponding to the C1' of the grafted AGU and  $\int_{105\text{ppm}}$  is the integration of the deconvoluted NMR peak centered at 105 ppm corresponding to the C1 of remaining unmodified AGU.

### 2.8. Thermogravimetric analysis (TGA)

About 20 mg of sample was heated from 20 to 400 °C at a 5 °C/min rate under nitrogen flow using a STA 6000 apparatus from Perkin Elmer.

### 2.9. Differential Scanning calorimetry (DSC)

The Q200 apparatus from TA instruments was used. The samples were put in a 40 µL pan with a perforation in the lid and heated at 5 °C/min to 200 °C to erase the thermal history of the sample and to evaporate the adsorbed water. The samples were then cooled down to -80 °C at -10 °C/min and heated again to 200 °C at 5 °C/min. The heat flows during the second heating ramp are presented as results. All the analyses were carried out under a 50 mL/min nitrogen flow.

### 2.10. Dynamic mechanical analysis (DMA)

The DMA analyses were performed with a DMA50 apparatus from Metravib. The sample dimensions were approximately 15 (H) × 15-20 (W) × 0.04-0.15 (T) mm<sup>3</sup> (the span was 6 mm). The samples are mounted on the DMA apparatus and then fully dried *in situ* by heating to 100 °C at 5 °C/min. A static tensile load was applied on the sample and monitored for the viscoelasticity measurements during the drying by using a 1 N static tensile load and a 3 µm dynamic deformation from the equilibrium position. Immediately after the drying process, the DMA measurement was performed with a 2 N static tensile load and a 5 µm dynamic displacement. The temperature was decreased from 100 to -125 °C at -5 °C/min with a 15 min plateau at -125 °C. Then the temperature was raised at 3 °C/min to 270 °C (usually the sample breaks before reaching that temperature). The drying and measurements were done under nitrogen flow.

### 3. Results and Discussion

#### 3.1. POC synthesis and amine grafting

A series of POC samples were synthesized by periodate oxidation of MFC by varying the reaction time and the periodate to AGU molar ratio (Table 5). As explained elsewhere,<sup>168</sup> the <sup>13</sup>C CP-MAS NMR spectra of POC (Figure 55) did not exhibit any carbonyl signal in the 180-200 ppm region (not shown) but rather multiple hemiacetal signals in the 90-100 ppm regions due to the recombination of the aldehyde with surrounding alcohol groups. As the extent of the periodate oxidation increases, the hemiacetal signal increases.<sup>111, 168</sup> However, the hemiacetal signals do not overlap with the C1 signal of unmodified cellulose, which can be used to deduce a DO.<sup>168</sup> Hence, DO ranging from 0.8 to 1.76 were calculated from the <sup>13</sup>C solid-state CP-MAS NMR spectra (Figure 55).

Table 5. Reaction conditions and DO values extracted from NMR measurements of the synthesized POC samples.

DO	NaIO <sub>4</sub> (eq/AGU)	Time (h)
0.80	1.0	24
0.96	0.8	65
1.01	1.4	24
1.10	1.3	24
1.22	0.8	65
1.59	1.1	65
1.65	1.3	65
1.76	1.3	65

After the periodate oxidation, butylamine, ethanolamine and butylamine were grafted on the freshly formed aldehyde groups of the oxidized MFC with DO ranging from 0.80 to 1.76 (Figure 56).

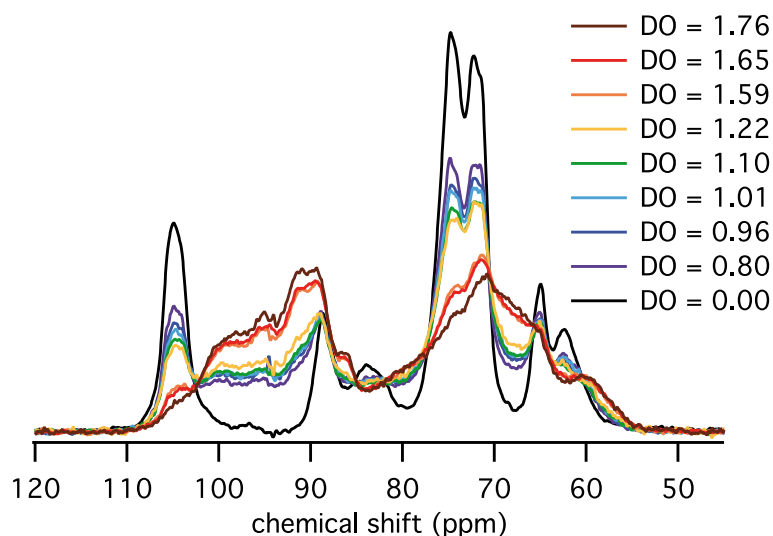


Figure 55.  $^{13}\text{C}$  CP-MAS NMR spectra of the POC samples.

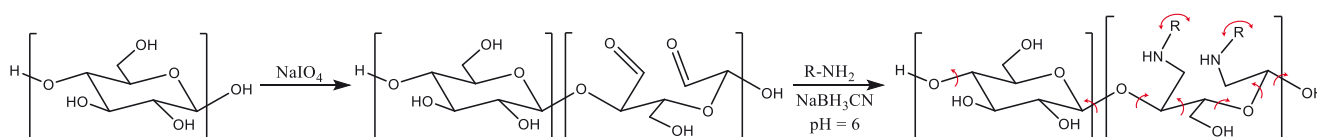


Figure 56. Reaction scheme of periodate oxidation of MFC followed by reductive amination with an amine ( $\text{R-NH}_2$ ). Red arrows illustrate the difference in mobility between intact glucosyl rings and grafted oxidized rings as monomers.

In the  $^{13}\text{C}$  NMR spectra of the grafted samples new signals corresponding to the aliphatic carbons of butylamine in the 10-35 ppm region (Figure 57a) or the phenyl carbons of benzylamine in the 115-150 ppm region (Figure 57b) are detected, proving the presence of the grafts. Additionally, the appearance of resonances between 40 and 68 ppm arising mainly from carbons 6, 6', 2', 3' 7' depicted in Figure 57 of each product that increase with the initial carbonyl content were common to the three types of grafting, due to the newly formed  $\text{CH}_2$  groups next to the nitrogen atoms (carbons, 2', 3' 7' of each product, Figure 57) and initial hydroxymethyl groups of cellulose (6 and 6'). The massive presence of peaks assigned to the newly formed secondary amines is a clear proof of the covalency and the quantitative character of the reaction. However, the superimpositions of different resonances make the calculation of a DS from the integration of the

convoluted peaks rather difficult. Indeed, the presence of very different chemical moieties in the case of butylamine and benzylamine should help to evaluate a DS, but in the case of ethanolamine, all carbon signals from the grafted moieties overlap with the cellulosic backbone. In this case the DS can be estimated from the signals of C1 (105 ppm) and C1' (98 ppm) that were attributed to unmodified and grafted glucosyl rings, respectively. Hence for comparison purposes, all the DS values were calculated from the integration of the C1 and C1' signals.

Table 6. Initial DO, DS, mass yields and glass transition temperatures of grafted samples.

Initial DO	Butylamine (Bu)					Benzylamine (Bn)				Ethanolamine (Et)				
	Name	DS	Yield (%)	T <sub>g</sub> (°C)	T <sub>α</sub> (°C)	Name	DS	Yield (%)	T <sub>g</sub> (°C)	Name	DS	Yield (%)	T <sub>g</sub> (°C)	T <sub>α</sub> (°C)
0.80	-	-	-	-	-	Bn0.80	0.49	87.0	122	-	-	-	-	-
0.96	-	-	-	-	-	Bn0.96	0.58	n/a	111	-	-	-	-	-
1.01	Bu1.01	0.46	68.1	114	128	-	-	-	-	Et1.01	0.53	45.5	103	150
1.10	Bu1.10	0.58	68.8	102	-	Bn1.10	0.64	90.1	101	Et1.10	0.59	n/a	93	123
1.22	Bu1.22	0.87	66.8	98	105	-	-	-	-	Et1.22	0.80	43.4	96	137
1.59	Bu1.59	1.17	50.2	84	-	Bn1.59	1.06	58.0	103	Et1.59	1.20	46.2	90	151
1.65	-	-	-	-	-	Bn1.65	1.23	76.1	91	-	-	-	-	-
1.76	Bu1.76	1.22	38.2	73	-	-	-	-	-	Et1.76	1.22	20.8	69	-

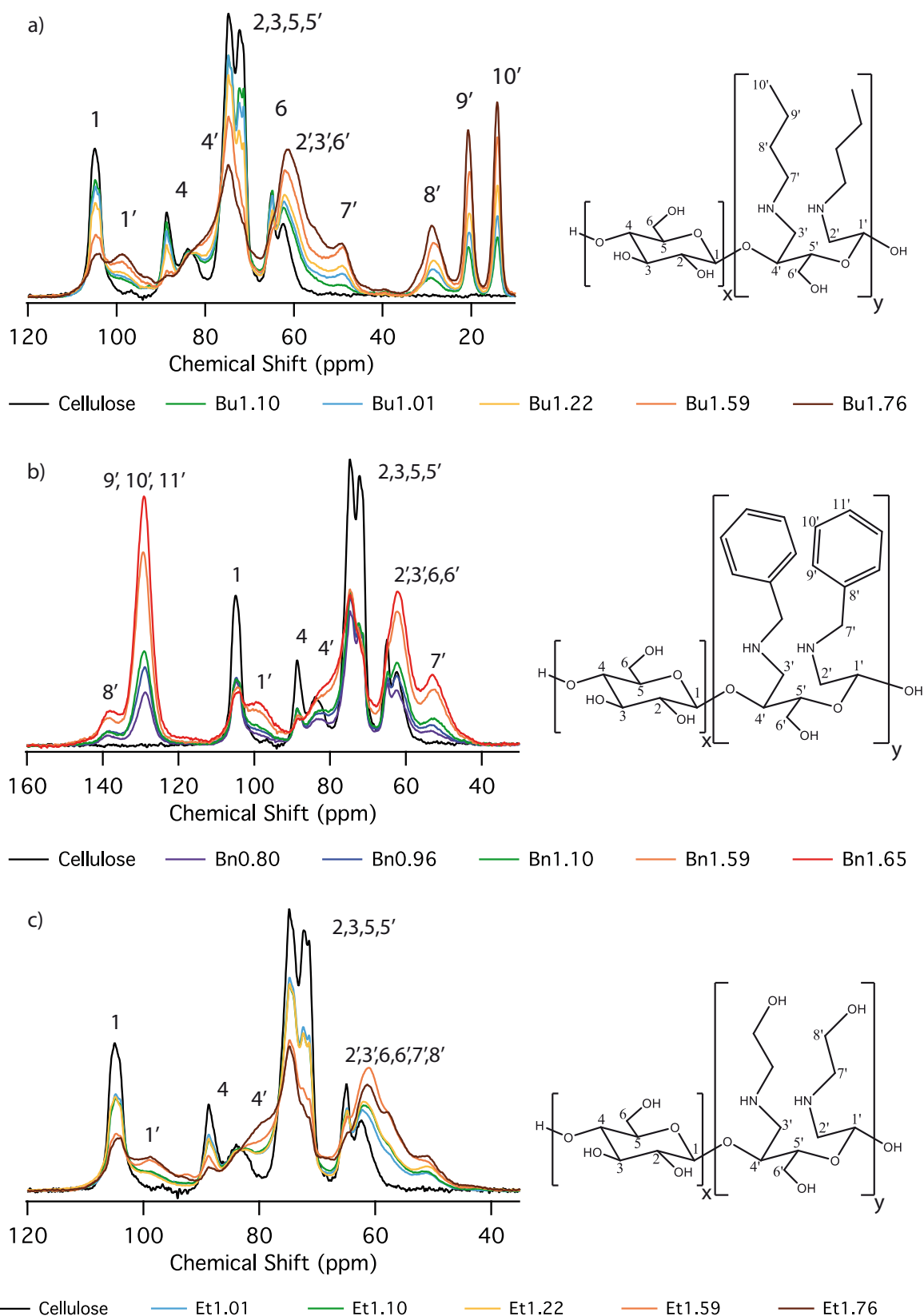


Figure 57.  $^{13}\text{C}$  CP-MAS NMR spectra with C1+C1' normalized area (90 to 115 ppm) with carbons attributions and the corresponding molecule after butylamine (A), benzylamine (B) and ethanolamine (C) graftings (with  $x = \left(1 - \frac{DS}{2}\right)$  and  $y = \frac{DS}{2}$ ).

The resulting DS reported in Table 6 confirm that the higher the starting DO, the higher the DS, and the trends were similar for the three types of amines examined. The evolution of the measured DS with the DO for the three types of amines in Figure 58 shows a systematic difference between the initial DO and the measured DS of the reaction for all the products. Remarkably, the DS values are significantly below the 1:1 slope in the plot, whereas NMR spectra (Figure 57) do not show any trace of remaining hemiacetals at 91 ppm.<sup>64, 111</sup> This absence of characteristic signals of ungrafted POC thus rather indicates a complete reaction.

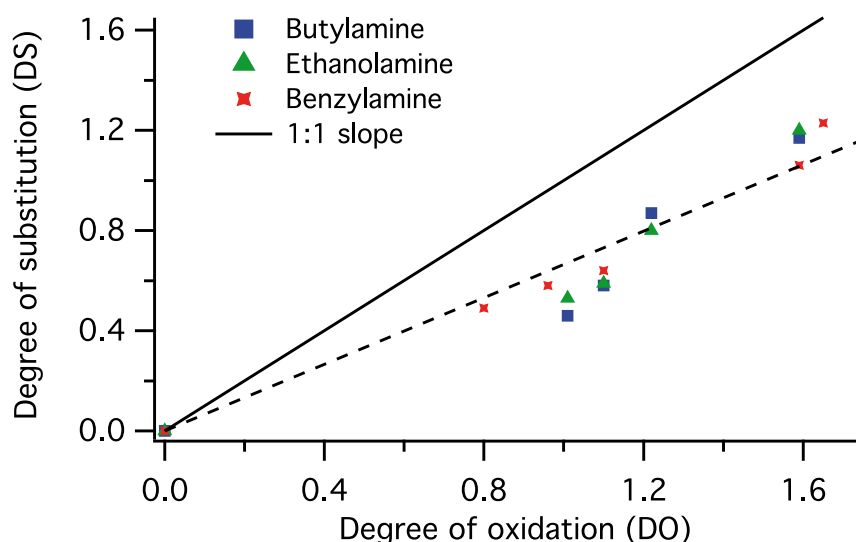


Figure 58. Degree of substitution (DS) obtained on the amine-grafted products as a function of the initial degree of oxidation (DO).

Since we did not recover 100 % of the material, the difference between the DO and the DS can be explained if highly oxidized short-chain oligomers were lost after grafting during the purification procedure, as in the initial periodate oxidation step.<sup>168</sup> Part of the short chains that were formed during the oxidation probably remained in the POC sample due to the hemiacetal linkages that keep all the chains attached together. Once these chains are modified into amine-grafted products, they can be easily eliminated in

the purification step after grafting. Interestingly, all the prepared samples roughly exhibited measured DS approximately equal to two third of the expected ones (slope of 0.66 in Figure 58), indicating that the origin of the phenomenon is more likely of ultrastructural origin rather than related to the chemistry of the grafts. Figure 59 schematically summarizes this scenario taking as an example the case of butylamine grafting on a POC of initial DO=1.76.

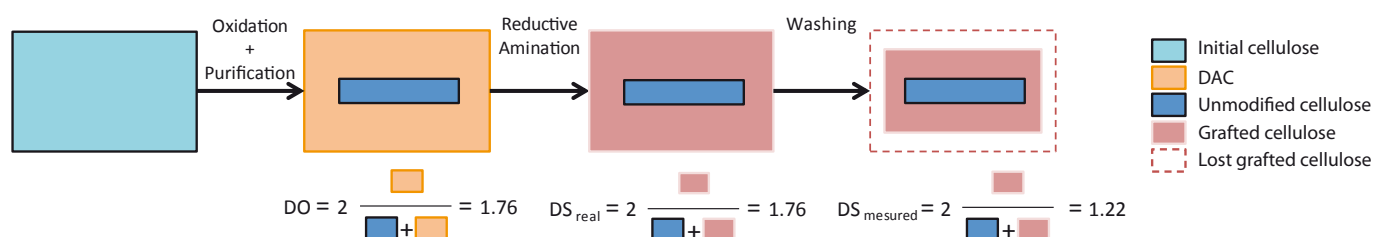


Figure 59. Scheme of oxidation and grafting for butyl-aminated sample with DO=1.76 and final DS=1.22 (Bu1.76).

### 3.2. Characterization of thermal properties

Thermogravimetric curves of the three samples exhibiting the highest degree of grafting for each amine are shown in Figure 60. The first weight loss completed below 150 °C is attributed to water evaporation. The temperature of the offset of mass loss follows the hydrophilicity of the grafted moiety, *i.e.* benzylamine < butylamine < ethanolamine. The pyrolysis starts at around 200 °C, with peaks of weight loss at 250 °C for butylamine, 275 °C for ethanolamine and 300 °C for benzylamine.

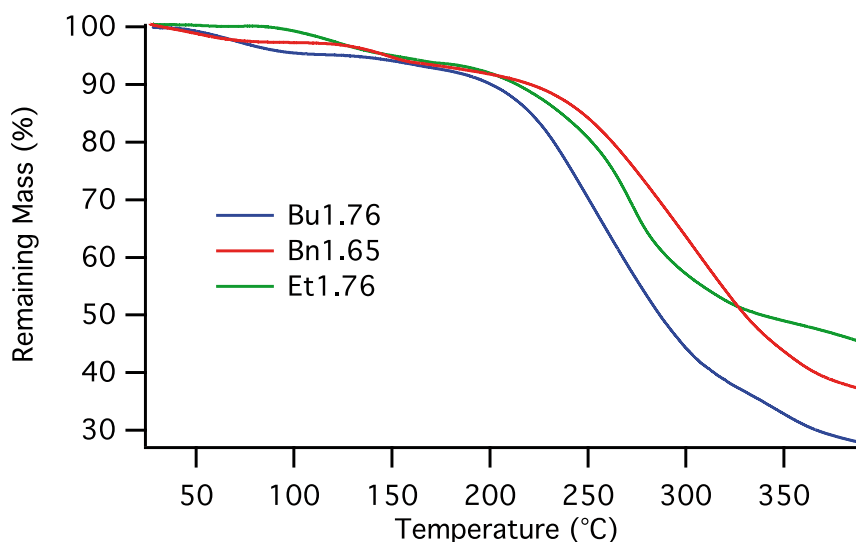


Figure 60. TGA analysis of the grafted samples with the highest DS for each amine.

The heat flow curves extracted from the differential scanning calorimetry (DSC) experiments are shown in Figure 61. All the grafted products showed a discontinuity in their heat capacity indicative of a glass transition. The glass transition temperature values are summarized in Table 6. Little differences between the three amines are observed, as shown in Figure 62, indicating that the predominant mechanism that governs the decrease of  $T_g$  is mostly the opening of the ring, as already observed in the heterogeneous reduction of periodate oxidized cellulose.<sup>208</sup> Nevertheless, these data most importantly indicate that thermoplastic materials are formed. In fact,  $T_g$ s slightly higher than 100 °C are reached with DS as low as 0.5 (meaning that only 25 % of the AGUs are modified), and for each amine, the  $T_g$  decreased with increasing DS to reach values around 70 or 75 °C for DS of 1.2, while having degradation temperatures above 200 °C. These results show that not only were thermoplastics formed but the materials exhibit sufficiently low  $T_g$  values and high degradation temperatures to be potentially thermoprocessable.

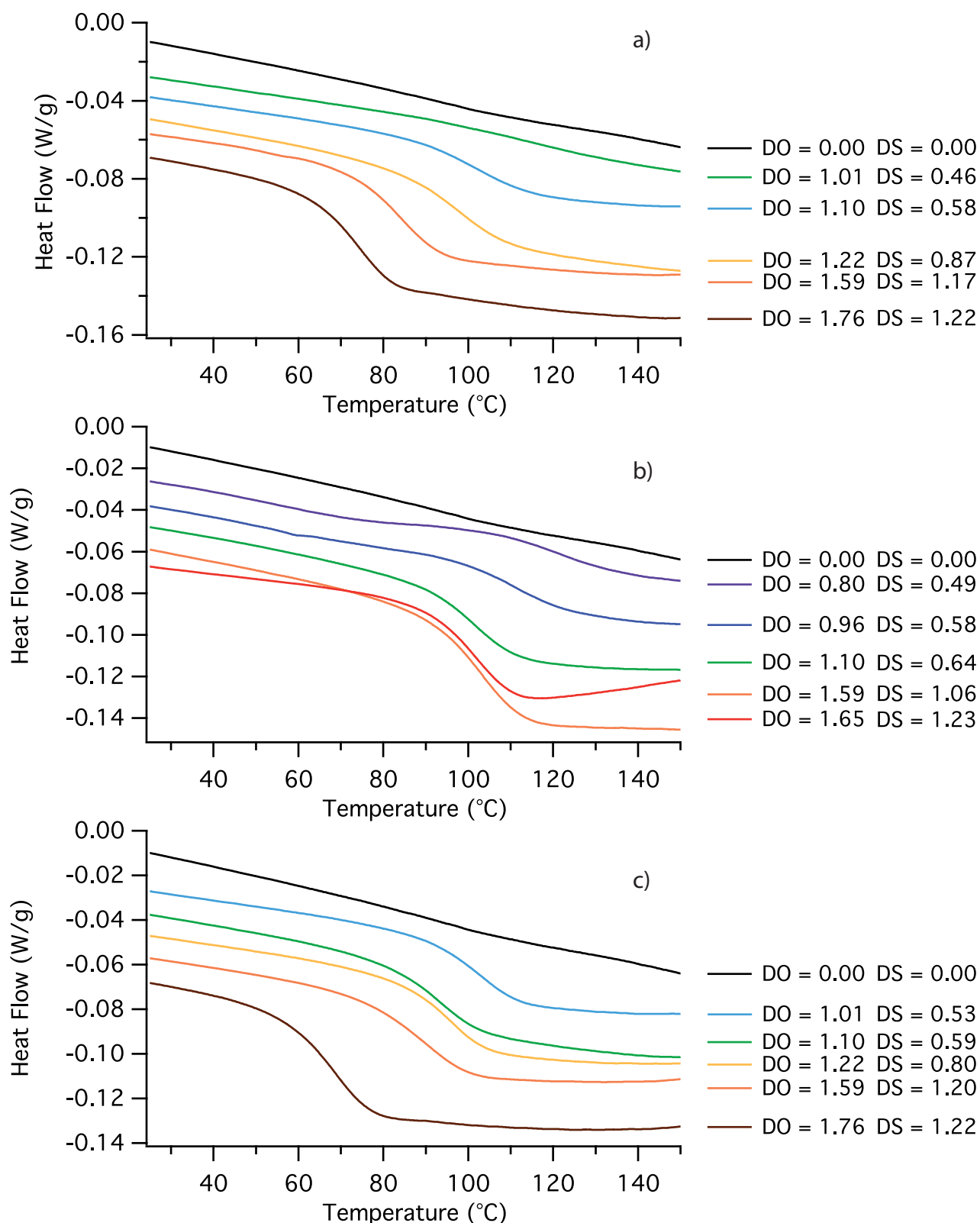


Figure 61: DSC thermograms of butylamine- (a), benzylamine- (b) and ethanolamine- (c) grafted products with variable initial DO and corresponding DS. Heat flow curves were vertically shifted for clarity.

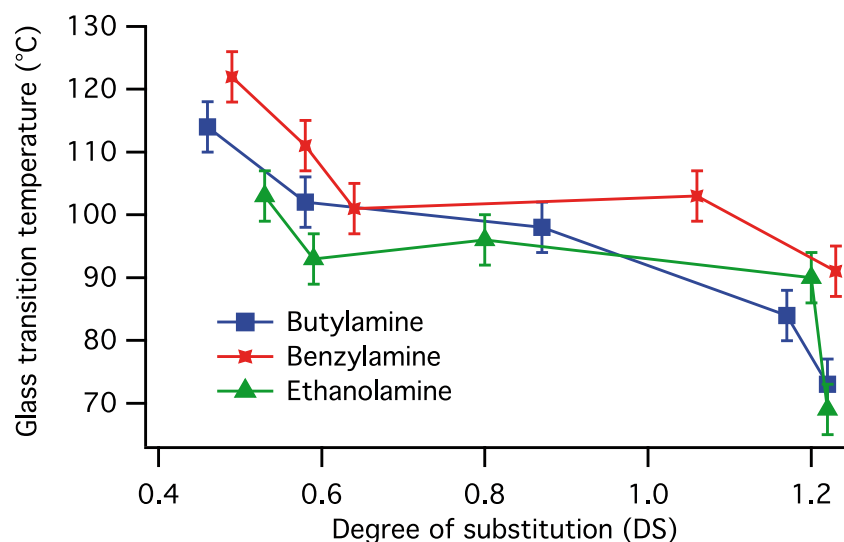


Figure 62. Evolution of the glass transition temperature of the amine-grafted products as a function of their DS.

### 3.3. Mechanical properties of amine-grafted samples films

Amine-grafted samples were used to prepare solid films by casting from water dispersions. Even if their  $T_g$  values in the dry state were very similar, their behavior regarding the presence of water was different, owing to the different hydrophilicity/hydrophobicity. Films made from ethanolamine or even butylamine were sufficiently plasticized by water to allow a correct film-formation during the last stages of the casting, whereas films made from benzylamine-grafted compounds were too brittle to be analyzed using standard mechanical testing. In the case of ethanolamine- and butylamine-grafted samples, the storage modulus and tangent delta obtained by DMA are displayed in Figure 63 and 64, respectively. All the samples displayed a glassy plateau for the storage modulus at low temperature followed by a rapid drop, most probably associated with a mechanical relaxation,  $T_\alpha$ , around 150 °C. For the ethanolamine grafted sample with DS=0.53 (Et 1.01)  $T_\alpha$  was even higher, at 174 °C, followed by a rubbery plateau.

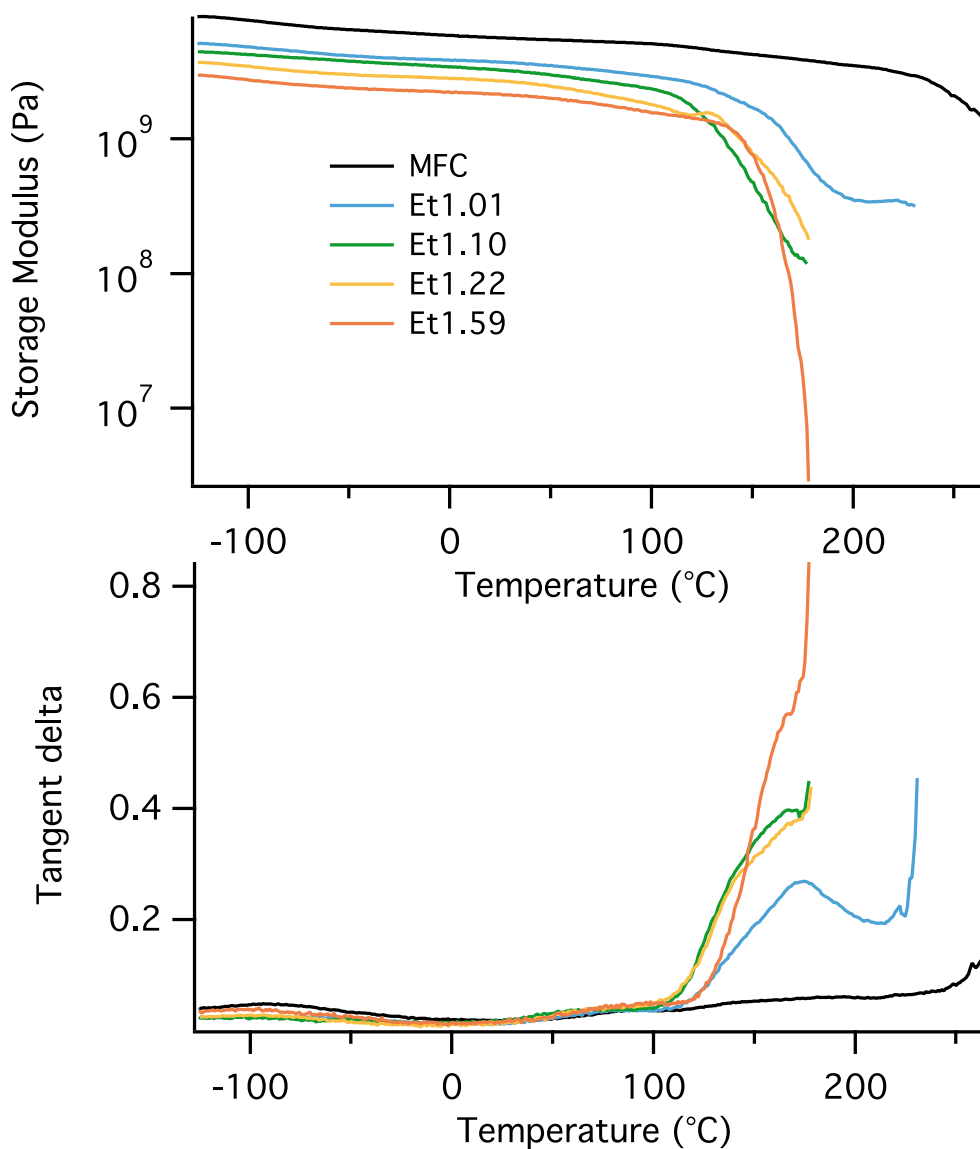


Figure 63. Storage modulus (top) and tangent delta (bottom) from DMA measurements on ethanolamine-grafted samples.

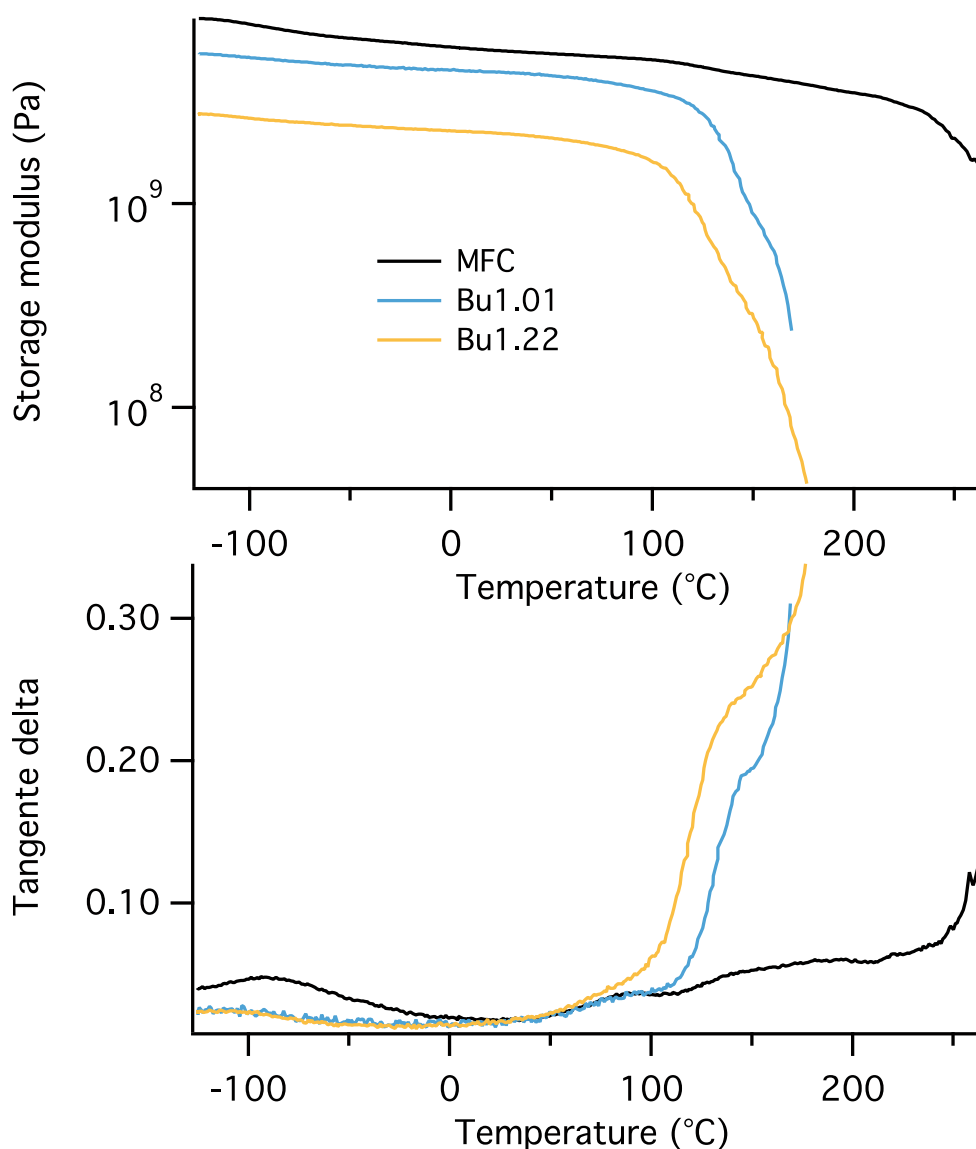


Figure 64. Storage modulus (top) and tangent delta (bottom) from DMA measurements on butylamine-grafted samples.

Only 2 samples from butylamination could be tested due to the brittleness of the films for the highest (and hence most hydrophobic) DS. Contrary to the ethanolamine-grafted equivalent, the rubbery plateau is not visible with  $DS=1.01$  obtained from the same POC and with the same final DS (light blue results in Figures 63 and 64). Another difference is the lower modulus of the butylaminated samples in the glassy state as compared to the ethanolaminated equivalents. One possible explanation for the differences in mechanical properties between the ethanolamine and the butylamine grafted POC could

be the difference in hydrogen bonding density, which should be higher with ethanolaminated than with butylaminated samples. This difference leads to a higher modulus in the glassy state and a higher cohesion at high temperature, making the rubbery plateau visible for the ethanolamine version. In both cases the  $T_a$  corresponding to a mechanical relaxation, even if not clearly observed, is well above the  $T_g$  that can be measured from DSC traces.

The general behavior of these two grafted polymers, including differences between  $T_a$  and  $T_g$ , is very close to what has been observed for materials obtained after reduction of periodate oxidized cellulose (or rPOC) for which two very different behaviors have been clearly observed: one at high DO, for which a flow is clearly evidenced, whereas at lower DO a plateau with a very high storage modulus appeared, as in the case of the less substituted ethanolaminated sample.<sup>208</sup> In that case, the differences between the two temperatures were related to the nano-confinement of the thermoplastic modified chains resulting from the ultrastructure of the materials. Possible crystallization phenomena (as observed for the rPOC at the highest DO) could also play a role but have not been investigated here. Interestingly, the most polar polymer (grafted with ethanolamine) has higher moduli compared to the more hydrophobic compound (grafted with butylamine).

### 3.4. Mobile versus rigid components from 2D WISE NMR

2D NMR experiments have been performed on butylaminated and ethanolaminated samples in order to investigate the dynamics of the different chemical moieties. From the 2D WISE data, rigid (broad peak in H dimension) and mobile (sharp peak in H dimension) parts of the CP-MAS NMR spectrum (Figure SC5-1) were extracted

separately in the case of two butylaminated samples and two ethanolaminated samples (Figure 65 and 66).

At room temperature, only the C9' and C10' carbons of butylamine-modified POC show some mobility, probably because of their position as carbons in side chains far from the backbone. Indeed, their positions correspond to the 6<sup>th</sup> and 7<sup>th</sup> carbon away from the C1' and C4' carbons of the backbone main chain, respectively.

At 120 °C, signals including some of the backbone carbons among C2, C3, C5, C4' C5' appear as mobile, whereas C1, C4 (105 and 88 ppm, respectively) from intact native cellulose remain essentially rigid and C1' experiments fewer mobility. The separation between mobile and rigid components depicts a two-phases system made of rigid cellulose embedded in a thermoplastic matrix of mobile modified polymer.

The situation is similar for the ethanolamine-modified samples for which a mobile subspectra can be clearly evidenced at 120 °C (Figure 66), giving indications on the chemical shifts corresponding to the ethanolamine-modified thermoplastic chains (which originally superimposed with the cellulosic backbone chemical shifts in CP-MAS NMR data).

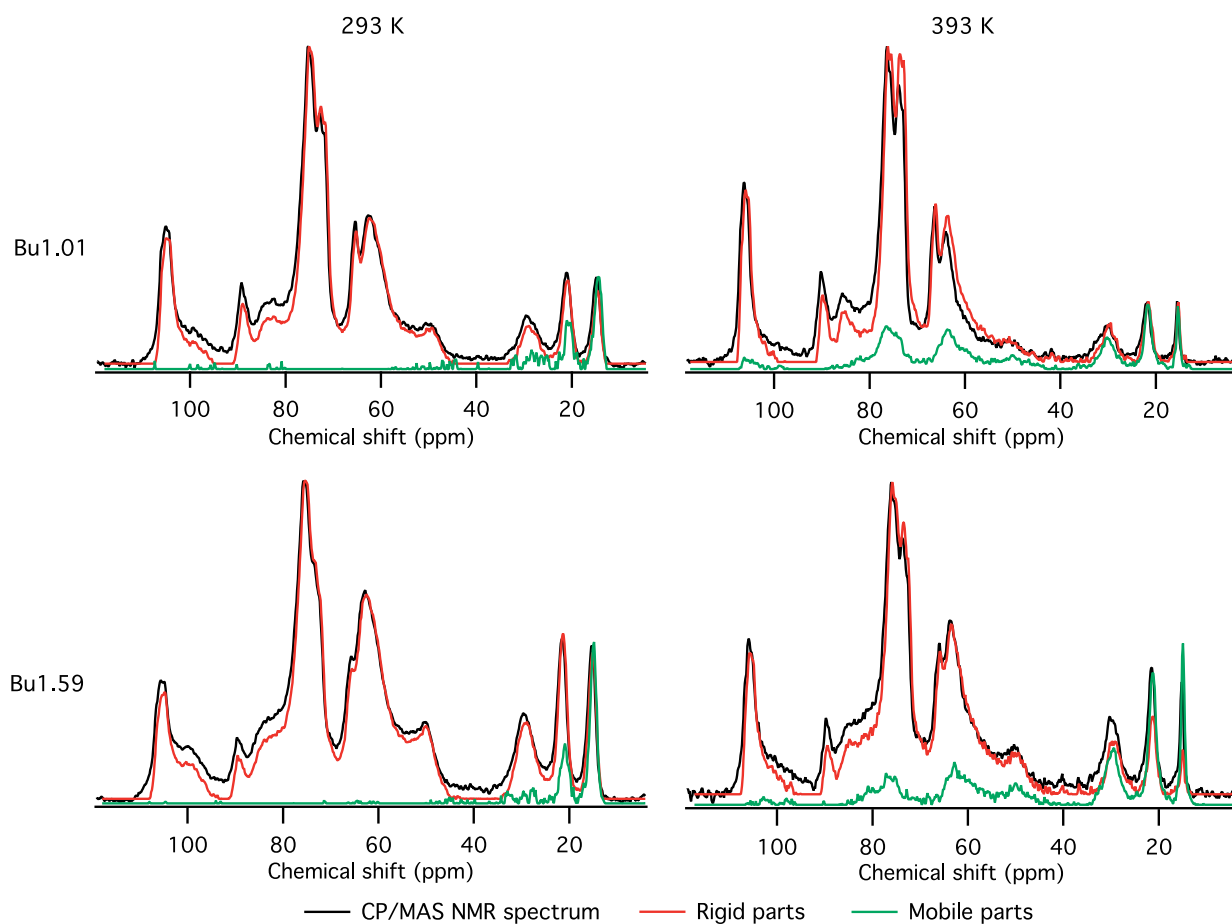


Figure 65. CP-MAS NMR spectra and WISE NMR extracted rigid and mobile spectra of butylamine-modified samples with DS=0.46 (top) and DS=1.17 (bottom) at 293 (left) and 393 K (right).

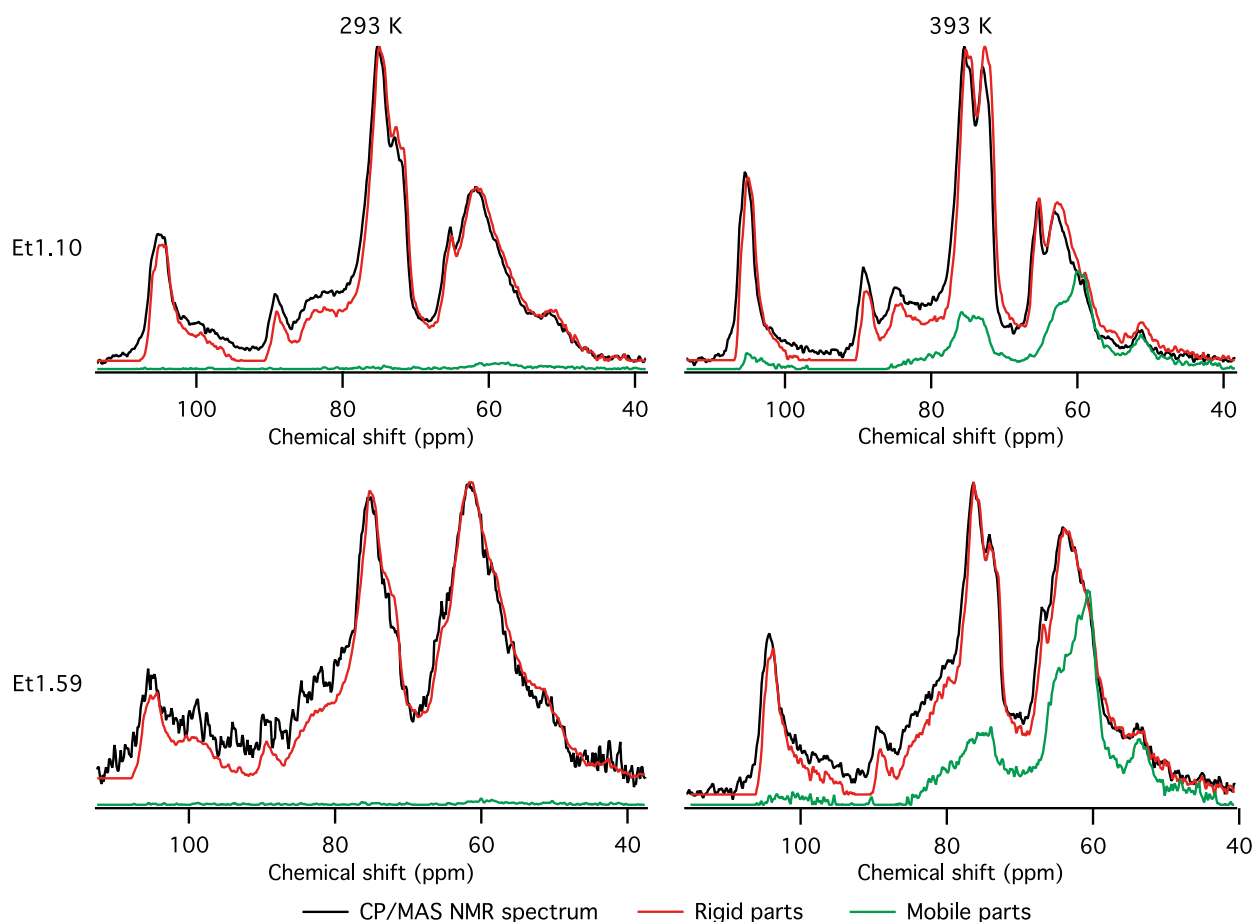


Figure 66. CP-MAS NMR spectra and WISE NMR extracted rigid and mobile spectra of ethanolamine-modified samples with DS=0.59 (top) and DS=1.2 (bottom) at 293 (left) and 393K (right).

## 4. Conclusions

POC was successfully grafted with different amines using HCl to control the pH during the reductive amination. All three types of modifications led to materials with thermoplastic behavior both in DSC and in DMA and the  $T_g$  of these polymers decreased with increasing degree of substitution, leading to materials with  $T_g$  in the processable region (low  $T_g$  and high degradation temperatures). The combination of experiments led to the description of materials made of intact native cellulose surrounded by a thermoplastic shell of an aminated version of dialcohol cellulose, with a low  $T_g$  mainly due to the opening of the sugar rings occurring during the periodate oxidation. Thus

grafting amine on periodate oxidized cellulose is a versatile route to introduce plasticity and diverse functionality to cellulose, which proved to be much more efficient than the classical esterification or etherification of cellulose: pure cellulose acetate (without plasticizers) with a DS of 1.2 leads to a  $T_g$  around  $218\text{ }^\circ\text{C}$ <sup>47</sup> while the grafted POC samples with the same DS of 1.2 showed  $T_g$ s between  $70$  and  $90\text{ }^\circ\text{C}$ .

There was however significant yield loss probably of full substituted and low-molecular weight component, most probably due to a somehow substantial decrease of molar mass decrease occurring during the periodate oxidation. The goal of the present study was not to optimize the reaction mass yield and minimize the use of reactant, and further improvement is needed. However, based on the properties of the products, a proof of concept of the potential of periodate oxidation followed by reductive amination modification as a way to produce bio-based plastics was achieved. With degrees of substitution as low as 0.5, and thus low amount of exogenous carbon compared to cellulose, the material undergoes softening (glass transition) more than  $50\text{ }^\circ\text{C}$  below the thermal degradation temperature. This process confers plasticity to cellulose with much better atom efficiency compared to other cellulose derivatives such as cellulose acetate, which furthermore require the addition of external plasticizers.



---

# Conclusions and perspectives

---

## Conclusions

In this PhD work we have studied a new pathway for cellulose plasticization using periodate oxidation, leading to periodate oxidized cellulose (POC), based on the working hypothesis that the opening of the sugar cycle will bring some flexibility to the rather stiff polysaccharidic backbone. The extent of the periodate oxidation was characterized by its degree of oxidation (DO) and measured on the recovered solid POC. The DO being a key parameter for the understanding of the structure-property relationship of materials synthesized from POC, it was important to rely on an accurate DO quantification. Thus, different DO measurement methodologies from the literature, namely oxime titration and periodate consumption, were compared with another method developed in the lab based on  $^{13}\text{C}$  CP-MAS solid-state NMR (SSNMR). We have shown that since the NMR resonances corresponding to the oxidized part do not overlap with the resonance of the C1 from unoxidized AGU, the C1 signal could be used to quantify the amount of residual cellulose and hence to deduce a DO. The limitations of DO measurement methods in the literature based on chemical reactions were clarified and the suitable conditions for accurate measurements were identified. In short, at low pH (pH 3) the oxime titration suffered from unreliable values mostly due to acid hydrolysis of the POC substrate. At pH around 5, the hydrolysis was limited and led to results 90% identical to the NMR values. Thus, both oxime titration method at controlled pH and SSNMR methods are reasonably accurate to quantify the degree of oxidation, the

latter providing interesting ultrastructural information on the integrity of the initial substrate.

In the case where the unreacted periodate was quantified by UV absorbance to calculate the degree of oxidation of the product, the values were systematically overestimated, compared to the NMR results. This difference between the two methods could be accounted for by taking into account the chains that were solubilized, assuming a higher oxidation level for the soluble discarded material. Indeed, the quantity of periodate consumption indicates the extent of the oxidation reaction that has taken place in the system, but the solid material recovered had systematically a lower degree of oxidation due to the heterogeneous reaction and partial solubilization of fully oxidized chains.

NaBH<sub>4</sub>-reduced POC samples were casted into thin films, and were analyzed and characterized by SSNMR and X-ray diffraction to give information on their ultrastructure and by DSC, TGA and DMA to investigate their thermo-mechanical behavior. Both NMR and XRD showed a progressive transformation of the native cellulose into a first biphasic then almost pure crystalline dialcohol cellulose. The core-shell structure of the rPOC films was evidenced by the persistence of native cellulose until a DO of 1.8, where only a few chains remains untouched, which is in very good agreement with the observation of solid colloidal nanorods. Both DSC and TGA results confirm the heterogeneous character of the reaction and the coexistence of two different phases, attested by the presence of two distinct degradation peaks in TGA. Concerning the T<sub>g</sub> as measured by DSC, their values only slightly varies with the DO: from 98 to 65 °C for DO varying from 0.6 to 1.8, compared to the more-than-100 °C variation observed in homogeneous derivatization of cellulose from earlier works. This difference could be attributed to constraints exerted by the cellulose crystals onto the surrounding amorphous dialcohol cellulose phase, due to the intimate mixture at nanometric length

scale and the resulting confinement effect. The DMA experiments interestingly showed two different typologies of thermo-mechanical properties: a first set of sample at high degree of oxidation exhibited a thermoplastic-like behavior, with a slow decrease of the modulus after the main relaxation  $T_a$ , in contrast to conventional thermoplastics that usually exhibit a steeper decrease, most probably due to a large quantity of solid cellulose inclusions in the partially oxidized samples. A second set of materials for the lower oxidation degrees kept high storage moduli in the GPa range above 200 °C.  $T_a$  as measured from the onset of the decrease of the moduli showed a sharp increase above a critical DO value around 1.0 revealing the consequences of the confinement of the cellulose dialcohol chains. 2D-WISE NMR experiments, that probe the local mobility in heterogeneous material also showed the differences in dynamics depending on the degree of oxidation and temperature. The extended motions were localized in the amorphous dialcohol cellulose phase, which crystallizes for the highest degree of oxidation. The general picture of these rPOCs is a two-phase material made of fused core-shell like nanorods, that percolate at high volume fraction of remaining intact cellulose, displaying a wide family of self-reinforced nanocomposite materials with tunable properties.

When POC suspensions of various DOs were submitted to substantial reduction, the never-dried suspensions showed a stable colloidal suspension behavior. It appears that during the periodate oxidation, the defects / amorphous regions are preferably attacked and cleaved leading to the formation of nanorods with mass yields between 60 to 71 % after oxidation, reduction, sonication and filtration, which is comparable to what is obtained by sulfuric acid hydrolysis of cellulose to produce CNCs, in the best cases. The various structural investigation techniques used to evaluate the particle sizes, namely DLS, TEM, SAXS and turbidity, all led to the conclusion that the size of the particles

decreases with increasing DO (length and section) but were in average 60 nm long and 7 nm wide. Furthermore, DLS and zeta-potential measurements showed that the particles were uncharged yet stable over a period of 2 months. Additionally, the combination of TEM, DLS and SAXS data allowed us to show that the nanorods have a core-shell structure. To conclude, we could show that the stable rPOC nanorods are composed of a crystalline cellulose core surrounded by a shell of dangling dialcohol cellulose chains providing a steric stabilization. These neutral sterically-stabilized cellulosic nanorods can be an alternative to the classical sulfate half ester grafted CNCs that tend to flocculate in high ionic strength conditions or form gel-like phases when the concentration is increased, and which also exhibit poor thermal stability.

POC were then further grafted with amines by reductive amination reactions. Three types of amines were tested: butylamine, ethanolamine and benzylamine. It was noticed that a precise control of the pH during the reaction is mandatory to avoid side reactions such as Maillard's reaction and the total peeling of the modified shell surrounding the unmodified cellulose crystals. The measured DS values are systematically lower than the DO even though the graftings are fully efficient since no hemiacetals are visible in NMR spectra after grafting. The difference between DO and DS is related to the low yields (as low as 20 %), which are far lower than the 90 % yields obtained when preparing rPOC derivatives. The lost fraction most probably has a higher DO and thus a higher DS, since no residual aldehyde groups were detected in the recovered products. Amine-grafted POC films showed thermoplastic behaviors with a  $T_g$  decreasing with increasing DS. Among the three types tested, the type of amine did not have any significant impact on the measured  $T_g$ . The same potential core-shell structure as in the case of rPOC is at the origin of the mechanical properties.

Furthermore, both rPOC and grafted films showed the same increased mobility at high temperature in WISE NMR experiments, especially for the grafted moieties, in agreement with what is expected to happen in thermoplastics when heated above their  $T_g$ , whereas no mobile part was visible at room temperature, except the butylamine end  $-\text{CH}_2-\text{CH}_3$  groups.

The glass transition temperatures of both rPOC and grafted samples show the same evolution with the DO (or DS) as seen in Figure 67. So, depending on the targeted application and depending on their behavior in extrusion for example, going to the grafted samples is probably not necessary as the rPOC samples can perform as good as the grafted ones.

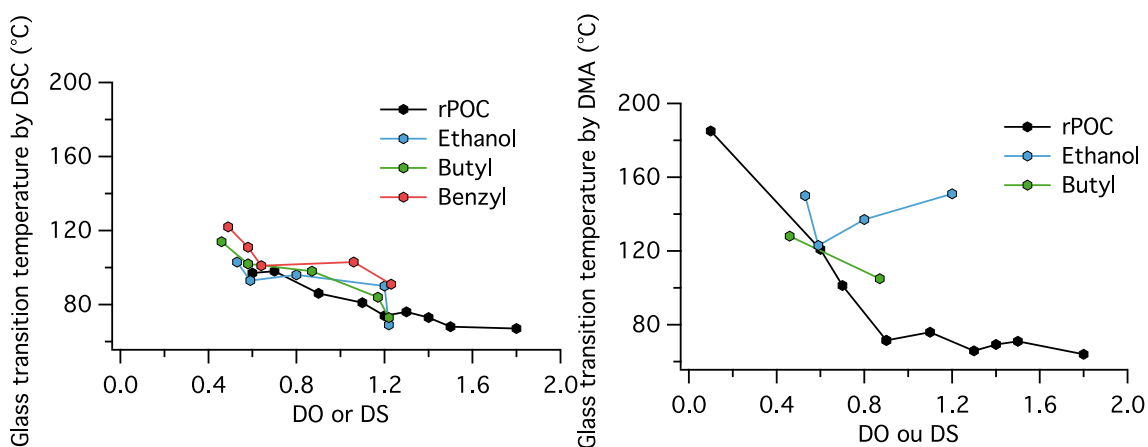


Figure 67. Glass transition temperature as function of the DO for the rPOC samples and as function of the DS for the grafted samples measured by DSC (left) or by DMA (right)

## Perspectives

The high potential of the periodate oxidation reaction to design biosourced materials described in Chapter I was further evidenced in this work, which provides proof of concept of the preparation of new “hairy” colloids and design of solid internally-plasticized materials with DO-tunable original properties. While a broad variety of

experimental techniques were combined in this project to extract the most detailed information possible at different length scales, from the molecular level to the macroscopic level, some fundamental as well as application-targeted issues still need to be addressed.

At the molecular length scale, it would be interesting to measure the evolution of the **degree of polymerization (DP)** of the cellulosic substrates after periodate oxidation and after further modification, since this parameter can greatly influence the behavior of the corresponding material. Especially, the influence of pH, the oxidation time and amount of periodate, which are potentially the most influential parameters on the DP, should be evaluated. Such a study would require the solubilization of the cellulose without degradation, that is to say the use of specific solvents such as DMAc / LiCl and compatible chromatography columns.

At the colloidal length scale, all techniques used here converge towards the identification of rPOC samples as being composed of an intact rod-like crystalline cellulose core surrounded by a covalently-linked shell of soluble dialcohol cellulose chains. In contrast, van de Ven and coworkers report on nanocrystalline cellulosic rods prepared from a POC treatment and subsequent heating/solubilization process, which are steric stabilized by dangling chains positioned *only* at the extremities of the crystals. **Further structural investigations** using either small-angle X-ray or neutron scattering would allow us to get more insight into the particles' morphology prepared using one or the other protocol. Experiments should include the investigation of a wide range of DO as well as different solvent conditions (good vs poor solvent). Analysis of such experiments using adequate data fitting should give, for example, the size and conformation of the polymer chains stabilizing the particles.

In line with the detailed investigation of their morphology, a fascinating question concerns the **assembling properties of the rPOC nanorods**. One might especially wonder if such colloids are able to self-organize into liquid crystalline nematic or cholesteric phases. Preliminary studies on concentrated suspensions revealed that most of the samples tend to form gels / highly viscous suspensions. However, some of these concentrated suspensions seem to be organized in a nematic liquid crystalline phase revealed by a Schlieren texture when observed by polarized light optical microscopy. A systematic investigation is required to elucidate this point and properly map the phase diagrams.

Beyond these rather fundamental questions, the internally-plasticized solid films would deserve further study in order to meet the needs for green preparation processes and to enhance their properties and application potential. First, an **optimization of the reaction protocols** towards the use of a reagents to AGU ratio closer to stoichiometry should be carried out to make the process more atom efficient, since in the current study a large excess amount of reagents (5 equivalents of amine and 5 equivalents of reductive agent per AGU) based on literature protocols was used. Secondly, an important step towards the scale-up of the aminated samples production would be to **increase the final yields**, which were limited in some cases (only 20 % for ethanolamine but up to 70 % for butylamine). The improvements in yields should be partially related to a better control of the DP that might be reached through the aforementioned DP study. Working at high concentrations during reductive aminations would also potentially prevent partial solubilization of fully modified oligomers and hence improve the final yields. Furthermore, working in more stoichiometric conditions as previously suggested, would participate in reaching higher yields by limiting the extent of the purifications.

The enhancement of the thermo-mechanical properties of the aminated materials could be envisaged by **varying the types of grafted amine groups**. For example, longer aliphatic amines or bulkier ones such as phthalates, currently used as plasticizers in cellulose acetate formulations could be tested. The application potential of the internally-plasticized materials should also be investigated by **extrusion tests**. A preliminary experiment performed by the Solvay company on a 40 g rPOC batch displaying a DO of 1.8 using a twin screw extrusion revealed that below 180 °C the processability was hampered by a high viscosity and above this temperature the viscosity dropped suddenly leading to long residence time inside the extruder provoking the degradation of the product. More positive results would be expected from the other types of thermoplastic materials produced and/or based on the suggested process improvements. Additionally, the strategy we followed could be applied to a **variety of starting cellulosic substrates** such as cellulose acetate, amorphous cellulose or regenerated cellulose to target a broad range of properties including enhanced extrusion ability, transparency or production of fibrous materials.

# Résumé étendu en français

---

Ce travail de thèse avait pour objectif de s'appuyer sur la réaction d'oxydation périodate pour concevoir de nouveaux matériaux cellulosiques et en particulier aboutir à des dérivés auto-plastifiés. Il entre dans le projet collaboratif PLACELMAT (PLAsticized CELLulose MATerials) financé par l'ANR qui regroupe trois laboratoires académiques, l'INSA et l'IRCE à Lyon et le CERMAV à Grenoble, ainsi que la société SOLVAY.

## **Contexte :**

Une grande partie des matériaux dit de commodités utilisés dans la vie de tous les jours sont des polymères thermoplastiques pétrosourcés possédant une température, nommée température de transition vitreuse ou  $T_g$ , au-delà de laquelle ils se ramollissent. Les industriels utilisent cette propriété pour mettre en forme ces matériaux grâce à des procédés de thermoformage. Le principe est de chauffer le polymère à  $T_g + 50$  °C pour atteindre des viscosités suffisamment basses pour que le matériau puisse être, par exemple, aisément injecté dans des moules. Une fois refroidis, ces thermoplastiques ont la capacité de retrouver leurs propriétés mécaniques initiales tout en conservant la forme qui vient de leur être donnée.

La cellulose, polymère biosourcé, abondant et renouvelable, se présente comme une source de matière première idéale pour remplacer les matériaux pétrosourcés. Malheureusement, bien qu'étant un polymère linéaire semi-cristallin, qui pourrait être considéré comme thermoplastique, la cellulose ne peut être utilisée dans les procédés classiques de mise en forme. Cela est dû à une température de fusion supérieure à celle

de dégradation. Ainsi la cellulose doit nécessairement être chimiquement modifiée pour être thermoformée. L'un des dérivés cellulosiques le plus utilisé est l'acétate de cellulose. Ce matériau possède des températures de transition vitreuse et de fusion inférieures à sa température de dégradation. En revanche, les écarts entre transition vitreuse / fusion et dégradation sont encore trop faibles et l'acétate de cellulose, comme un certain nombre de thermoplastiques pétrosourcés, nécessite l'ajout de molécules de faible poids moléculaire, appelés plastifiants externes, pour faciliter sa mise en forme. Ces plastifiants externes servent de lubrifiants entre les chaînes de polymères, ce qui a pour conséquence de diminuer la température de transition vitreuse (et la température de fusion pour les polymères semi-cristallins) et d'atteindre une plage de température où le thermoformage est possible. De plus, ces additifs améliorent les propriétés mécaniques des matériaux en général comme la ductilité, la ténacité ou la résilience.

Cependant, au cours de la vie du matériau, les plastifiants migrent de la matrice polymère vers la surface et sont expulsés : ce phénomène est appelé exsudation. Cela provoque une diminution de la quantité de plastifiants dans le matériau, conduisant à une dégradation des propriétés et pouvant entraîner des problèmes sanitaires et environnementaux si les plastifiants utilisés sont des molécules toxiques, cancérigènes, mutagènes ou reprotoxiques, par exemple.

Dans ce contexte, ce projet consiste à modifier chimiquement la cellulose afin d'obtenir une plastification interne. Celle-ci est différente de la plastification externe dans le sens où le plastifiant est lié de manière covalente au polymère, évitant ainsi tout risque d'exsudation. Cette méthode n'est généralement pas employée industriellement car relativement onéreuse en coûts de R&D et de fabrication, suite à la nécessité d'introduire des étapes de synthèse supplémentaires.

Les propriétés thermiques de la cellulose découlent de la structure de sa chaîne : un enchainement de monomères cycliques de  $\beta$ -D-glucose très rigides qui ne possèdent que très peu de degrés de liberté rotationnelle. La stratégie retenue a donc consisté à augmenter la flexibilité des chaînes et à ajouter du volume libre grâce à des modifications chimiques contrôlées. Dans ce contexte, l'oxydation au périodate de sodium, s'est imposée comme une option prometteuse car cette réaction permet de cliver l'unité de répétition entre les carbones C2 et C3 et d'introduire des groupes aldéhydes réactifs à la place des deux alcools secondaires initialement portés par ces carbones. Dans cette optique le clivage apporterait la flexibilité et le greffage de molécules sur les aldéhydes l'augmentation du volume libre. Par ailleurs, l'oxydation au périodate de sodium est devenue ces dernières années une voie particulièrement attractive pour obtenir des dérivés cellulosiques fonctionnels tels que des aérogels. En effet lorsque la cellulose oxydée périodate (POC) est post-modifiée, elle donne lieu à une large variété de propriétés en fonction de la modification réalisée. Ainsi, des POC réduites et introduites dans des formulations de papiers donne une meilleure ductilité à ceux-ci ainsi que de meilleures propriétés barrières à l'oxygène, laissant envisager de nouveaux type d'emballages par exemple. Cette même POC réduite a également démontré ces propriétés thermoplastiques si elle est synthétisée par un procédé d'oxydation en solution. A l'inverse, les POC peuvent être post-oxydées en acides carboxyliques pour donner des matériaux hautement chargés, ce qui peut être utilisé comme charge de colonnes de chromatographies échangeuses d'ions. Enfin les POC peuvent également être greffées par des amines. Ces matériaux greffés montrent des propriétés très diverses en fonction des amines. Ainsi des films transparents avec des propriétés de filtre UV ont été synthétisés par exemple. En modifiant des nanocristaux de cellulose (CNC) en POC d'une part et avec des hydrazines d'autre part, des aérogels

avec des propriétés super-absorbantes peuvent être obtenus via réticulation entre les 2 types de CNCs. Ce projet de thèse a donc consisté à explorer plus avant le potentiel de l'oxydation périodate et les moyens de contrôler cette réaction pour le design de matériaux cellulosiques innovants et en particulier de dérivés thermoplastiques.

Le manuscrit est divisé comme suit :

- le premier chapitre est consacré à une étude de l'état de l'art sur les réactions chimiques envisagées ainsi que sur les propriétés et fonctionnalités des matériaux cellulosiques qui découlent de ces modifications,
- le second chapitre traite de l'oxydation périodate de la cellulose et des moyens de déterminer précisément le degré d'oxydation (DO),
- le troisième chapitre s'intéresse à l'ultrastructure et aux propriétés thermomécaniques de films « tout cellulose » obtenus par séchage/évaporation de suspensions de cellulose oxydée ayant subi une réaction de réduction,
- le quatrième chapitre explore les propriétés de ces suspensions en termes de stabilité colloïdale et de structures et dimensions des nanoparticules obtenues,
- enfin, l'effet du greffage d'amines par amination réductrice sur des échantillons de cellulose oxydée par le périodate est examiné et les propriétés thermomécaniques des films préparés à partir de ces produits sont caractérisées.

Pour simplifier la lecture, différents acronymes seront utilisés dans ce manuscrit. POC désigne la cellulose oxydée périodate (periodate oxidized cellulose en anglais), comprenant une partie non oxydée de cellulose et des chaînes complètement oxydées due à l'hétérogénéité de la réaction d'oxydation. Ces chaînes 100 % oxydées seront alors désignées comme DAC pour dialdéhyde cellulose et leur degré d'oxydation est égal à 2. Avec la même analogie, les produits oxydés puis réduits seront nommés cellulose

oxydée périodate réduite (rPOC) et les chaînes complètement modifiées seront nommées DALC (dialcool cellulose).

**Chapitre 2 :** Oxydation périodate de la cellulose et moyens de caractérisation précis et fiables du degré d'oxydation.

Des microfibrilles de cellulose ont été soumises à différentes conditions d'oxydation en faisant varier la quantité de périodate et le temps de réaction, ainsi que, dans une moindre mesure, la température. Grâce au suivi de plusieurs cinétiques d'oxydation, une cartographie des degrés d'oxydation en fonction du temps d'oxydation et de la quantité de périodate a été réalisée. Cette étude a permis de connaître quelles conditions opératoires utiliser pour obtenir un niveau d'oxydation spécifique. Lors de cette étude s'est également posé le problème de la mesure précise du DO. En effet le DO reflète le taux de modification de la cellulose et donc sera un point clé dans la compréhension des relations structures-propriété des matériaux issus des POC. Une nouvelle méthode initiée préalablement à ce projet au laboratoire à partir de données de spectroscopie de résonance magnétique nucléaire du solide (RMN) a été développée et étendue. Elle est basée sur la non-superposition du signal du C1 de la cellulose cristalline à 105 ppm avec les signaux de la partie oxydée et fournit des données quantitatives fiables sur le DO. Cette méthode a été comparée à deux méthodes usuellement utilisées dans la littérature : (i) la quantification de la consommation de périodate par absorbance UV, et (ii) le dosage d'acide chlorhydrique après réaction des groupements aldéhydes avec l'hydroxylamine pour former des oximes. Ces comparaisons ont permis de démontrer que la méthode UV surestime le DO alors que la méthode d'oximation peut donner des

résultats correspondants à 90% du DO obtenu par RMN à condition de réaliser le dosage à pH 5 et non à pH 3. En effet, dans ce dernier cas la réaction est lente ce qui conduit à une sous-estimation du DO si le temps de réaction avec l'hydroxylamine est trop court. Si le temps de réaction hydroxylamine/aldéhyde est augmenté, cela entraîne une hydrolyse acide de la DAC qui conduit à une surestimation du DO. Les valeurs de DO par RMN et par absorbance UV peuvent être réconciliées si l'on considère que la POC qui n'est pas récupérée (les rendements sont inférieurs à 100 %) est complètement oxydée. La méthode d'absorbance UV est donc utile pour suivre rapidement et facilement l'avancement de la réaction mais il faut obligatoirement utiliser la RMN ou le dosage à l'oxime à pH 5 pour une valeur fiable du DO de la POC solide récupérée. La RMN fournit également des données utiles sur la structure des matériaux en démontrant que la POC est formée de 2 composés, probablement avec une structure du type cœur-écorce du fait de la nature hétérogène de la réaction d'oxydation périodate sur la cellulose.

### **Chapitre 3 :** Synthèse et caractérisation de matériaux thermoplastiques tout cellulose (rPOC)

Des échantillons de POC en suspension aqueuse avec des DO allant de 0,1 à 1,8 ont été réduits en présence de NaBH<sub>4</sub> puis séchés pour obtenir des films. La caractérisation par RMN et analyse thermogravimétrique (ATG) ont confirmé que ces films sont constitués de 2 composants, la cellulose non oxydée ainsi que des chaînes de DALC complètement modifiées. Ce résultat provient vraisemblablement d'une structure de type cœur-écorce : un cœur de cellulose cristalline non modifiée recouvert de DALC. La RMN ainsi que la diffraction des rayons X (DRX) ont permis de montrer que l'échantillon de

DO=1,80 cristallise, prouvant la régularité de la chaîne de DALC. La combinaison de la calorimétrie différentielle à balayage (DSC) et de l'analyse mécanique dynamique (DMA) a montré que ces échantillons étaient des thermoplastiques avec une  $T_g$  qui diminue linéairement quand le DO augmente, en variant de 100 à 65 °C sur la gamme de DO considérée. Cette décroissance linéaire peut être attribuée à la composante cristalline, dont le volume diminue avec le DO, qui joue le rôle de charge et provoque un effet de confinement de la matrice DALC. Un gradient de mobilité est alors présent entre l'extrémité des chaînes de DALC fixée aux parties cristallines et donc complètement figée jusqu'à l'autre extrémité des chaînes de DALC complètement libre de mouvement et donc avec la  $T_g$  la plus faible mesurable pour ces matériaux, soit 65 °C. La présence de la composante cristalline est également perceptible en DMA. L'échantillon de DO=1,8 se comporte comme un thermoplastique classique. Cependant, lorsque le DO diminue, la fraction volumique de cellulose augmente, conduisant à une élévation du module élastique au delà de la transition vitreuse. Pour des DO encore plus faibles la cellulose retrouve son caractère fibrillaire et dans ce cas le renforcement est encore plus important, et les valeurs de tangente  $\delta$  s'étendent sur plus d'une centaine de degrés au delà de la  $T_\alpha$ . Des analyses de RMN en deux dimensions de type WISE (wideline separation) ont montré que les parties mobiles de ces films étaient les chaînes de DALC alors que la cellulose cristalline restante est complètement immobile.

## **Chapitre 4 :** Suspensions colloïdales de nanobâtonnets cellulosiques neutres stabilisés stériquement obtenues après réduction $\text{NaBH}_4$ de POC.

Les suspensions aqueuses de rPOC de DO initial compris entre 1,4 et 1,8 présentent macroscopiquement un comportement de suspension colloïdale stable. Une combinaison de techniques d'analyse structurale a permis de montrer que les traitements chimiques imposés (oxydation puis réduction) transforment les microfibrilles de départ en nanobâtonnets. Cette déstructuration est attribuée à une action préférentielle de l'oxydation periodate dans les zones de défauts / régions amorphes conduisant à un clivage longitudinal des objets fibreux initiaux. La production des ces nanobâtonnets se fait avec des rendements massiques compris entre 60 et 71%, comparables à ceux obtenus par hydrolyse acide dans les meilleurs cas. La diffusion dynamique de la lumière (DLS), la microscopie électronique en transmission (MET) et la turbidité ont été utilisées pour accéder aux dimensions des nanobâtonnets et révèlent une longueur comprise entre 55 et 67 nm et une largeur aux alentours de 6.5 nm. De plus, les mesures de DLS et de potentiel zêta ont montré que les particules étaient non chargées mais stables sur une période d'au moins 2 mois. Par ailleurs, la combinaison des données de MET et DLS avec des mesures de diffusion des rayons X aux petits angles a permis de montrer que les nanobâtonnets de rPOC présentent une structure cœur-écorce constituée d'un noyau de cellulose cristalline entouré d'une enveloppe de chaînes de DALC solubles gonflées assurant une stabilisation stérique. Ce résultat est en plein accord avec les mesures de RMN du solide. La stabilité colloïdale n'est pas observée avant réduction sur les POC car les groupements aldéhydes des chaînes DAC entraînent

une réticulation à travers des liaisons hémiacétales, ce qui provoque une agglomération des particules et leur floculation.

**Chapitre 5 :** Synthèse et caractérisation de thermoplastiques par oxydation périodate de cellulose suivie de greffages d'amines.

Des POC de DO variable ont été modifiées via amination réductrice. Cette méthode a permis le greffage de trois types d'amines, l'éthanolamine, la butylamine et la benzylamine permettant d'obtenir des POC avec comme chaînes latérales respectivement des groupements linéaires hydrophiles, linéaires hydrophobes ou aromatiques. Ces matériaux ont montré à la fois en DSC et en DMA des comportements de matériaux thermoplastiques avec des  $T_g$  comprises en 100 et 70 °C. Aucune réelle différence n'a pu être observée entre les amines qui contribuent de la même façon à une décroissance linéaire de la  $T_g$  des matériaux avec l'augmentation du degré de substitution (DS) mesuré par RMN du solide. Même si les rendements massiques de préparation de ces produits sont plus faibles en comparaison de ce qui a pu être obtenu pour les matériaux rPOC, cette stratégie permet d'obtenir des matériaux thermoplastiques avec de nouvelles fonctionnalités. De plus, en comparaison de l'acétate de cellulose, ces matériaux offrent des  $T_g$  bien plus basses pour des taux de modifications bien plus faibles et donc pour un apport en carbone d'origine pétrosourcée bien inférieur.

## **Conclusion :**

Le fort potentiel de la réaction d'oxydation au periodate appliquée à la cellulose pour concevoir des matériaux biosourcés a été démontré dans ce travail qui fournit des preuves de concept de la préparation de nouveaux colloïdes chevelus et de matériaux solides auto-plastifiés et auto-renforcés avec des propriétés originales accordables avec le niveau initial d'oxydation. De nombreuses techniques expérimentales ont été combinées pour extraire des informations détaillées à différentes échelles de longueur, du niveau moléculaire au niveau macroscopique, et mettre en lumière les relations structure-propriétés.

Les perspectives à cette étude incluent une description encore plus fine de certains phénomènes à l'échelle moléculaire comme la variation du degré de polymérisation des chaînes avec les traitements chimiques appliqués. Une étude structurale détaillée des nanobâtonnets cœur-écorce pourrait également être entreprise et servir de base à l'investigation des propriétés d'organisation et d'assemblage de ces nouveaux colloïdes biosourcés. Enfin, du point de vue matériau, une production d'échantillons à une échelle supérieure grâce à l'optimisation des rendements et avec une meilleure économie d'atomes permettrait de réaliser des tests de thermoformage. Les modifications chimiques réalisées ici et les méthodes de caractérisation mises au point pourraient également être transposées à d'autres substrats cellulosiques.

---

# References

---

1. McDonald, J. N., Thermoforming. In *Encyclopedia of Polymer Science and Engineering*, Mark, H. F.; Bikales, N. M.; Overberger, C. G.; Menges, G.; Kroschwitz, J. I., Eds. John Wiley and Sons: 1989; Vol. 16, pp 807 - 832.
2. Thermoplastic polymer. In *Encyclopedia of Polymer Science and Engineering*, Mark, H. F.; Bikales, N. M.; Overberger, C. G.; Menges, G.; Kroschwitz, J. I., Eds. John Wiley and Sons: 1989; Vol. 16, p 833.
3. Kihlman, M.; Wallberg, O.; Stigsson, L.; Germgård, U., Dissolution of dissolving pulp in alkaline solvents after steam explosion pretreatments. *Holzforschung* **2011**, *65* (4), 613 - 617.
4. Alfthan, E.; de Ruvo, A.; Brown, W., Glass transition temperature of oligosaccharides. *Polymer* **1973**, *14* (7), 329 - 330.
5. Szcześniak, L.; Rachocki, A.; Tritt-Goc, J., Glass transition temperature and thermal decomposition of cellulose powder. *Cellulose* **2008**, *15* (3), 445 - 451.
6. Chee, K. K., Dependence of glass transition temperature on chain flexibility and intermolecular interactions in polymers. *Journal of Applied Polymer Science* **1991**, *43* (6), 1205 - 1208.
7. Gibbs, J. H.; DiMarzio, E. A., Nature of the glass transition and the glassy state. *The Journal of Chemical Physics* **1958**, *28* (3), 373 - 383.
8. Nordin, S. B.; Nyren, J. O.; Back, E. L., Note on molten cellulose produced by a laser beam. *Svensk Papperstidning* **1973**, *76* (-), 609 - 610.

9. Pear, J. R.; Kawagoe, Y.; Schreckengost, W. E.; Delmer, D. P., Higher plants contain homologs of the bacterial *celA* genes encoding the catalytic subunit of cellulose synthase. *Proceedings of the National Academy of Sciences* **1996**, *93* (22), 12637 - 12642.
10. Menon, V.; Rao, M., Trends in bioconversion of lignocellulose: biofuels, platform chemicals and biorefinery concept. *Progress in Energy and Combustion Science* **2012**, *38* (4), 522 - 550.
11. Siqueira, G.; Bras, J.; Dufresne, A., Cellulosic Bionanocomposites: a review of preparation, properties and applications. *Polymers* **2010**, *2* (4), 728 - 765.
12. Kaushik, M.; Fraschini, C.; Chauve, G.; Putaux, J.-L.; Moores, A., Transmission electron microscopy for the characterization of cellulose nanocrystals. In *The transmission Electron Microscopy*, Maaz, K., Ed. Intech: 2015.
13. Sakurada, I.; Nukushina, Y.; Ito, T., Experimental determination of the elastic modulus of crystalline regions in oriented polymers. *Journal of Polymer Science* **1962**, *57* (165), 651 - 660.
14. Favier, V.; Chanzy, H.; Cavaille, J. Y., Polymer nanocomposites reinforced by cellulose whiskers. *Macromolecules* **1995**, *28* (18), 6365 - 6367.
15. Dufresne, A., Polysaccharide nanocrystal reinforced nanocomposites. *Canadian Journal of Chemistry* **2008**, *86* (6), 484 - 494.
16. Dufresne, A., Processing of polymer nanocomposites reinforced with polysaccharide nanocrystals. *Molecules* **2010**, *15* (6), 4111 - 4128.
17. Habibi, Y.; Lucia, L. A.; Rojas, O. J., Cellulose nanocrystals: chemistry, self-assembly, and applications. *Chemical Reviews* **2010**, *110* (6), 3479 - 3500.
18. Gray, D. G., Recent advances in chiral nematic structure and iridescent color of cellulose nanocrystal films. *nanomaterials* **2016**, *6* (11), 213 - 221.

19. De France, K. J.; Hoare, T.; Cranston, E. D., Review of hydrogels and aerogels containing nanocellulose. *Chemistry of Materials* **2017**, *29* (11), 4609 - 4631.
20. French, A. D.; Johnson, G.; Kelterer, A.-M.; Csonka, G., Fluorinated cellobiose and maltose as stand-ins for energy surface calculations. *Tetrahedron: Asymmetry* **2005**, *16* (2), 577 - 586.
21. Nishiyama, Y.; Langan, P.; Chanzy, H., Crystal structure and hydrogen-bonding system in cellulose I $\beta$  from synchrotron X-ray and neutron fiber diffraction. *Journal of the American Chemical Society* **2002**, *124* (31), 9074 - 9082.
22. Rånby, B. G., Aqueous colloidal solutions of cellulose micelles. *Acta Chemica Scandinavica* **1949**, *3* (-), 649 - 650.
23. Svedberg, T., Structure and polymolecularity of cellulose. *Svensk Papperstidning* **1949**, *52* (-), 157 - 164.
24. Elazzouzi-Hafraoui, S.; Nishiyama, Y.; Putaux, J.-L.; Heux, L.; Dubreuil, F.; Rochas, C., The shape and size distribution of crystalline nanoparticles prepared by acid hydrolysis of native cellulose. *Biomacromolecules* **2008**, *9* (1), 57 - 65.
25. Kamide, K.; Saito, M., Thermal analysis of cellulose acetate solids with total degrees of substitution of 0.49, 1.75, 2.46, and 2.92. *Polymer Journal* **1985**, *17* (8), 919 - 928.
26. Bao, C. Cellulose acetate / plasticizer systems : structure, morphology and dynamics. 2015.
27. Heinze, T.; Röttig, K., Synthesis of 2,3-O-carboxymethylcellulose. *Macromolecular Rapid Communications* **1994**, *15* (4), 311 - 317.
28. Landoll, L., Nonionic polymer surfactants. *Journal of Polymer Science* **1982**, *20* (2), 443 - 455.
29. Heinze, T.; Liebert, T., Unconventional methods in cellulose functionalization. *Progress in Polymer Science* **2001**, *26* (9), 1689 - 1762.

30. McGee, P. A.; Fowler, W. F. J.; Unruh, C. C.; Kenyon, W. O., Investigation of the properties of cellulose oxidized by nitrogen dioxide. VI The effect of alkali on the celluronic acids. *Journal of the American Chemical Society* **1948**, *70* (8), 2700 - 2705.
31. de Nooy, A. E. J.; Besemer, A. C.; van Bekkum, H., Highly selective TEMPO mediated oxidation of primary alcohol groups in polysaccharides. *Recueil des Travaux Chimiques des Pays-Bas* **1994**, *113* (3), 165 - 166.
32. Isogai, A.; Kato, Y., Preparation of polyuronic acid from cellulose by TEMPO-mediated oxidation. *Cellulose* **1998**, *5* (3), 153 - 164.
33. de Nooy, A. E. J.; Besemer, A. C.; van Bekkum, H.; van Dijk, J. A. P. P.; Smit, J. A. M., Tempo-mediated oxidation of pullulan and influence of ionic strength and linear charge density on the dimensions of the obtained polyelectrolyte chains. *Macromolecules* **1996**, *29* (20), 6541 - 6547.
34. Fujisawa, S.; Isogai, T.; Isogai, A., Temperature and pH stability of cellouronic acid. *Cellulose* **2010**, *17* (3), 607 - 615.
35. Isogai, A.; Saito, T.; Fukuzumi, H., TEMPO-oxidized cellulose nanofibers. *Nanoscale* **2011**, *3* (1), 71 - 85.
36. Isogai, A., Structural characterization and modifications of surface-oxidized cellulose nanofiber. *Journal of the Japan Petroleum Institute* **2015**, *58* (6), 365 - 375.
37. Saito, T.; Nishiyama, Y.; Putaux, J.-L.; Vignon, M.; Isogai, A., Homogeneous suspensions of individualized microfibrils from TEMPO-catalyzed oxidation of native cellulose. *Biomacromolecules* **2006**, *7* (6), 1687 - 1691.
38. Araki, J.; Wada, M.; Kuga, S., Steric stabilization of a cellulose microcrystal suspension by poly(ethylene glycol) grafting. *Langmuir* **2001**, *17* (1), 21 - 27.

39. Azzam, F.; Heux, L.; Putaux, J. L.; Jean, B., Preparation by grafting onto, characterization, and properties of thermally responsive polymer-decorated cellulose nanocrystals. *Biomacromolecules* **2010**, *11* (12), 3652 - 3659.
40. Schützenberger, P., Action de l'acide acétique anhydre sur la cellulose, l'amidon, les sucres, la mannite et ses congénères, les glucosides et certaines matières colorantes végétales. *Comptes Rendus Hebdomadaire de l'académie des Sciences* **1865**, *61*, 485 - 486.
41. Abel; Imray Manufacture of cellulose ester silk. 1928.
42. Drefus, C. Perfectionnements aux produits obtenus en partant des dérivés organiques de la cellulose. 1928.
43. Fordyce, C. R.; Meyer, I. W. A., Plasticizers for cellulose acetate and cellulose acetate butyrate. *Industrial and Engineering Chemistry* **1940**, *32* (8), 1053 - 1060.
44. Sand, I. D., The dependence of properties of cellulose acetate propionate on molecular weight and the level of plasticizer. *Journal of Applied Polymer Science* **1990**, *40* (5 - 6), 943 - 952.
45. Kano, H., Thermo-plasticization of cellulose and application for fiber manufacturing by melt spinning process. *Kobunshi Ronbunshu* **2011**, *68* (8), 570 - 578.
46. Buchanan, C. M.; Gedon, S. C.; White, A. W.; Wood, M. D., Cellulose acetate propionate and poly(tetramethylene glutarate) blends. *Macromolecules* **1993**, *26* (11), 2963 - 2967.
47. Glasser, W. G.; Samaranayake, G.; Dumay, M.; Davé, V., Novel cellulose derivatives. III. Thermal analysis of mixed esters with butyric and hexanoic acid. *Journal of Polymer Science: part B* **1995**, *33* (14), 2045 - 2054.
48. Ohno, T.; Nishio, Y., Cellulose alkyl ester/vinyl polymer blends: effects of butyryl substitution and intramolecular copolymer composition on the miscibility. *Cellulose* **2006**, *13* (3), 245 - 259.

49. Kosaka, P. M.; Kawano, Y.; Petri, H. M.; Fantini, M. C. A.; Petri, D. F. S., Structure and properties of composites of polyethylene or maleated polyethylene and cellulose or cellulose esters. *Journal of Applied Polymer Science* **2007**, *103* (1), 402 - 411.
50. Ohno, T.; Nishio, Y., Estimation of miscibility and interaction for cellulose acetate and butyrate blends with N-vinylpyrrolidone copolymers. *Macromolecular Chemistry and Physics* **2007**, *208* (6), 622 - 634.
51. Cao, Y.; Li, H.; Zhang, J., Homogeneous synthesis and characterization of cellulose acetate butyrate (CAB) in 1-allyl-3-methylimidazolium chloride (AmimCl) ionic liquid. *Industrial and Engineering Chemistry Research* **2011**, *50* (13), 7808 - 7814.
52. Teramoto, Y., Functional thermoplastic materials from derivatives of cellulose and related structural polysaccharides. *Molecules* **2015**, *20* (4), 5487 - 5527.
53. Sears, J. K.; Touchette, N. W., PLasticizers. In *Encyclopedia of Polymer Science and Engineering*, Mark, H. F.; Bikales, N. M.; Overberger, C. G.; Menges, G.; Kroschwitz, J. I., Eds. John Wiley and Sons: 1989; Vol. Supplement Volume, pp 568 - 647.
54. Macht, M. L.; Fletcher, D. A. Cellulose acetate molding compositions. 1937.
55. Kluwe, W. M.; Haseman, J. K.; Huff, J. E., The carcinogenicity of d1(2 - ethylhexyl) phthalate (dehp) in perspective. *Journal of Toxicology and Environmental Health* **1983**, *12* (1), 159 - 169.
56. Konduracka, E.; Krzemieniecki, K.; Gajos, G., Relationship between everyday use cosmetics and female breast cancer. *Polish Archives of Internal Medicine* **2014**, *124* (5), 264 - 269.
57. European Chemicals Agency List of REACH restricted chemicals. <https://echa.europa.eu/substances-restricted-under-reach>.
58. Directive 95/2/CE du parlement européen et du conseil du 20 février 1995 concernant les additifs alimentaires autres que les colorants et les édulcorants. Journal Officiel, 1995.

59. Perlin, A. S., Glycol-cleavage oxidation. In *Advances in Carbohydrate Chemistry and Biochemistry*, Vol 60, Horton, D., Ed. Elsevier Academic Press Inc: San Diego, 2006; Vol. 60, pp 183 - 250.
60. Head, F. S. H., Effect of light on the reaction between periodates and alpha-glycols. *Nature* **1950**, 165 (4189), 236 - 237.
61. Symons, M. C. R., Evidence for formation of free-radical intermediates in some reactions involving periodate. *Journal of the Chemical Society* **1955**, (0), 2794 - 2796.
62. Sabzalian, Z.; Alam, M. N.; van de Ven, T. G. M., Hydrophobization and characterization of internally crosslink-reinforced cellulose fibers. *Cellulose* **2014**, 21 (3), 1381 - 1393.
63. Maekawa, E.; Kosaki, T.; Koshijima, T., Periodate oxidation of mercerized cellulose and regenerated cellulose. *Wood Research* **1986**, 73 (0), 44 - 49.
64. Kim, U.-J.; Kuga, S.; Wada, M.; Okano, T.; Kondo, T., Periodate oxidation of crystalline cellulose. *Biomacromolecules* **2000**, 1 (3), 488 - 492.
65. Goldstein, I. J.; Hay, G. W.; Lewis, B. A.; Smith, F., Controlled degradation of polysaccharides by periodate oxidation, reduction, and hydrolysis. In *Methods in Carbohydrate Chemistry*, Whistler, R. L.; BeMiller, J. N.; Wolfrom, M. L., Eds. Academic Press: 1965; Vol. 5, pp 361 - 370.
66. Hay, G. W.; Lewis, B. A.; Smith, F., Periodate oxidation of polysaccharides: General procedures. In *Methods in Carbohydrate Chemistry*, Whistler, R. L.; BeMiller, J. N.; Wolfrom, M. L., Eds. Academic Press: 1965; Vol. 5, pp 357 - 361.
67. Hay, G. W.; Lewis, B. A.; Smith, F., Determination of the average chain length of polysaccharides. In *Methods in Carbohydrate Chemistry*, Whistler, R. L.; BeMiller, J. N.; Wolfrom, M. L., Eds. Academic Press: 1965; Vol. 5, pp 377 - 380.

68. Lindh, J.; Ruan, C.; Strømme, M.; Mihranyan, A., Preparation of porous cellulose beads via introduction of diamine spacers. *Langmuir* **2016**, *32* (22), 5600 - 5607.
69. Ruan, C.; Strømme, M.; Lindh, J., A green and simple method for preparation of an efficient palladium adsorbent based on cysteine functionalized 2,3-dialdehyde cellulose. *Cellulose* **2016**, *23* (4), 2627 - 2638.
70. Kim, U.-J.; Wada, M.; Kuga, S., Solubilization of dialdehyde cellulose by hot water. *Carbohydr Polym* **2004**, *56* (1), 7 - 10.
71. Sirviö, J.; Hyvakko, U.; Liimatainen, H.; Niinimäki, J.; Hormi, O., Periodate oxidation of cellulose at elevated temperatures using metal salts as cellulose activators. *Carbohydr Polym* **2011**, *83* (3), 1293 - 1297.
72. Sirviö, J. A.; Kolehmainen, A.; Visanko, M.; Liimatainen, H.; Niinimäki, J.; Hormi, O. E. O., Strong, self-standing oxygen barrier films from nanocelluloses modified with Rregioselective oxidative treatments. *ACS applied materials and interfaces* **2014**, *6* (16), 14384 - 14390.
73. Sirviö, J. A.; Hasa, T.; Ahola, J.; Liimatainen, H.; Niinimäki, J.; Hormi, O., Phosphonated nanocelluloses from sequential oxidative-reductive treatment - Physicochemical characteristics and thermal properties. *Carbohydr Polym* **2015**, *133* (-), 524 - 532.
74. Laitinen, O.; Hartmann, R.; Sirviö, J. A.; Liimatainen, H.; Rudolph, M.; Ämmälä, A.; Illikainen, M., Alkyl aminated nanocelluloses in selective flotation of aluminium oxide and quartz. *Chemical Engineering Science* **2016**, *144* (-), 260 - 266.
75. Sirviö, J. A.; Visanko, M.; Heiskanen, J. P.; Liimatainen, H., UV-absorbing cellulose nanocrystals as functional reinforcing fillers in polymer nanocomposite films. *Journal of Materials Chemistry A* **2016**, *4* (17), 6368 - 6375.

76. Sirviö, J. A.; Visanko, M.; Laitinen, O.; Ämmälä, A.; Liimatainen, H., Amino-modified cellulose nanocrystals with adjustable hydrophobicity from combined regioselective oxidation and reductive amination. *Carbohydr Polym* **2016**, *136* (-), 581 - 587.
77. Suopajarvi, T.; Sirviö, J. A.; Liimatainen, H., Cationic nanocelluloses in dewatering of municipal activated sludge. *Journal of Environmental Chemical Engineering* **2017**, *5* (1), 86 - 92.
78. Varma, A. J.; Kulkarni, M. P., Oxidation of cellulose under controlled conditions. *Polymer Degradation and Stability* **2002**, *77* (1), 25 - 27.
79. Kim, U.-J.; Kuga, S., Ion-exchange chromatography by dicarboxyl cellulose gel. *Journal of Chromatography A* **2001**, *919* (1), 29 - 37.
80. Potthast, A.; Kostic, M.; Schiehser, S.; Kosma, P.; Rosenau, T., Studies on oxidative modifications of cellulose in the periodate system: Molecular weight distribution and carbonyl group profiles. *Holzforschung* **2007**, *61* (6), 662 - 667.
81. Potthast, A.; Schiehser, S.; Rosenau, T.; Kostic, M., Oxidative modifications of cellulose in the periodate system – Reduction and beta-elimination reactions 2nd ICC 2007, Tokyo, Japan, October 25–29, 2007. *Holzforschung* **2009**, *63* (1), 12 - 17.
82. Maekawa, E., Analysis of oxidized moiety of partially periodate-oxidized cellulose by NMR-spectroscopy. *Journal of Applied Polymer Science* **1991**, *43* (3), 417 - 422.
83. Maekawa, E.; Koshijima, T., Properties of 2,3-dicarboxy cellulose combined with various metallic ions. *Journal of Applied Polymer Science* **1984**, *29* (7), 2289 - 2297.
84. Maekawa, E.; Koshijima, T., Preparation and structural consideration of nitrogen-containing derivatives obtained from dialdehyde celluloses. *Journal of Applied Polymer Science* **1991**, *42* (1), 169 - 178.
85. Kim, U. J.; Kuga, S., Thermal decomposition of dialdehyde cellulose and its nitrogen-containing derivatives. *Thermochimica Acta* **2001**, *369* (1-2), 79 - 85.

86. Malaprade, M. L., Oxydation de quelques polyalcools par l'acide periodique. Applications. *Comptes Rendus Hebdomadaire de l'académie des Sciences* **1928**, 186 (-), 382 - 383.
87. Jackson, E. L.; Hudson, C. S., The structure of the products of the periodic acid oxidation of starch and cellulose. *Journal of the American Chemical Society* **1938**, 60 (5), 989 - 991.
88. Rutherford, H. A.; Minor, F. W.; Martin, A. R.; Harris, M., Oxidation of cellulose: The reaction of cellulose with periodic acid. *Journal of Research of the National Bureau of Standards* **1942**, 29 (2), 131 - 141.
89. Hough, L., Periodate oxidation of neutral polysaccharides: Oxidation to formaldehyde. In *Methods in Carbohydrate Chemistry Vol V General Polysaccharides*, Whistler, R. L.; Green, J. W.; BeMiller, J. N.; Wolfrom, M. L., Eds. Academic Press: 1965; Vol. 5, pp 370 - 377.
90. Hay, G. W.; Lewis, B. A.; Smith, F.; Unrau, A. M., Determination of reducing end-groups by periodate oxidation. In *Methods in Carbohydrate Chemistry*, Whistler, R. L.; BeMiller, J. N.; Wolfrom, M. L., Eds. Academic Press: 1965; Vol. 5, pp 251 - 253.
91. Hay, G. W.; Lewis, B. A.; Smith, F., Determination of sugar residues in partially oxidized polysaccharides. In *Methods in Carbohydrate Chemistry*, Whistler, R. L.; BeMiller, J. N.; Wolfrom, M. L., Eds. Academic Press: 1965; Vol. 5, pp 381 - 382.
92. O'Colla, P. S., The Barry degradation. In *Methods in Carbohydrate Chemistry*, Whistler, R. L.; BeMiller, J. N.; Wolfrom, M. L., Eds. Academic Press: 1965; Vol. 5, pp 382 - 392.
93. Codou, A.; Guigo, N.; Heux, L.; Sbirrazzuoli, N., Partial periodate oxidation and thermal cross-linking for the processing of thermoset all-cellulose composites. *Composites Science and technology* **2015**, 117 (-), 54 - 61.

94. Henschen, J.; Larsson, P. A.; Illergård, J.; Ek, M.; Wågberg, L., Bacterial adhesion to polyvinylamine-modified nanocellulose films. *Colloids and Surfaces B: Biointerfaces* **2017**, *151* (-), 224 - 231.
95. Hollertz, R.; López Durán, V.; Larsson, P. A.; Wågberg, L., Chemically modified cellulose micro- and nanofibrils as paper-strength additives. *Cellulose* **2017**, *24* (9), 3883 - 3899.
96. Casu, B.; Meille, V.; Naggi, A.; Su, P.; Torri, G.; Zoppetti, G.; Allegra, G., Structure and conformation of polyalcohols and polyacids obtained from periodate oxyamylose and oxycellulose. *Carbohydr Polym* **1982**, *2* (4), 283 - 287.
97. Casu, B.; Naggi, A.; Torri, G.; Allegra, G.; Meille, S. V.; Cosani, A.; Terbojevich, M., Stereoregular acyclic polyalcohols and polyacetates from cellulose and amylose. *Macromolecules* **1985**, *18* (12), 2762 - 2767.
98. Kasai, W.; Morooka, T.; Ek, M., Mechanical properties of films made from dialcohol cellulose prepared by homogeneous periodate oxidation. *Cellulose* **2014**, *21* (1), 769 - 776.
99. Larsson, P. A.; Berglund, L. A.; Wågberg, L., Ductile all-cellulose nanocomposite films fabricated from core-shell structured cellulose nanofibrils. *Biomacromolecules* **2014**, *15* (6), 2218 - 2223.
100. Larsson, P. A.; Berglund, L. A.; Wågberg, L., Highly ductile fibres and sheets by core-shell structuring of the cellulose nanofibrils. *Cellulose* **2014**, *21* (1), 323 - 333.
101. Rahn, K.; Heinze, T., New cellulosic polymers by subsequent modification of 2,3-dialdehyde cellulose. *Cellulose Chemistry and Technology* **1998**, *32* (3), 173 - 183.
102. López Durán, V.; Larsson, P. A.; Wågberg, L., On the relationship between fibre composition and material properties following periodate oxidation and borohydride reduction of lignocellulosic fibres. *Cellulose* **2016**, *23* (6), 3495 - 3510.

103. Larsson, P. A.; Wagberg, L., Towards natural-fibre-based thermoplastic films produced by conventional papermaking. *Green Chemistry* **2016**, *18* (11), 3324 - 3333.
104. Varma, A. J.; Chavan, V. B., A study of crystallinity changes in oxidised celluloses. *Polymer Degradation and Stability* **1995**, *49* (2), 245 - 250.
105. Varma, A. J.; Chavan, V. B.; Rajmohan, P. R.; Ganapathy, S., Some observations on the high-resolution solid-state CP-MAS <sup>13</sup>C-NMR spectra of periodate-oxidised cellulose. *Polymer Degradation and Stability* **1997**, *58* (3), 257 - 260.
106. Yang, H.; Alam, M. N.; van de Ven, T. G. M., Highly charged nanocrystalline cellulose and dicarboxylated cellulose from periodate and chlorite oxidized cellulose fibers. *Cellulose* **2013**, *20* (4), 1865 - 1875.
107. Sirviö, J. A.; Liimatainen, H.; Visanko, M.; Niinimäki, J., Optimization of dicarboxylic acid cellulose synthesis: reaction stoichiometry and role of hypochlorite scavengers. *Carbohydr Polym* **2014**, *114* (-), 73 - 77.
108. Plappert, S. F.; Nedelec, J.-M.; Rennhofer, H.; Lichtenegger, H. C.; Liebner, F. W., Strain hardening and pore size harmonization by uniaxial densification: a facile approach toward superinsulating aerogels from nematic nanofibrillated 2,3-dicarboxyl cellulose. *Chemistry of Materials* **2017**, *29* (16), 6630 - 6641.
109. López Durán, V.; Larsson, P. A.; Wågberg, L., Chemical modification of cellulose-rich fibers to clarify the influence of the chemical structure on the physical and mechanical properties of cellulose fibers and thereof made sheets. *Carbohydr Polym* **2018**, *182* (-), 1 - 7.
110. Azzam, F.; Galliot, M.; Putaux, J.-L.; Heux, L.; Jean, B., Surface peeling of cellulose nanocrystals resulting from periodate oxidation and reductive amination with water-soluble polymers. *Cellulose* **2015**, *22* (6), 3701 - 3714.

111. Guigo, N.; Mazeau, K.; Putaux, J.-L.; Heux, L., Surface modification of cellulose microfibrils by periodate oxidation and subsequent reductive amination with benzylamine: a topochemical study. *Cellulose* **2014**, *21* (6), 4119 - 4133.
112. Jin, L.; Li, W.; Xu, Q.; Sun, Q., Amino-functionalized nanocrystalline cellulose as an adsorbent for anionic dyes. *Cellulose* **2015**, *22* (4), 2443 - 2456.
113. Yang, X.; Bakaic, E.; Hoare, T.; Cranston, E. D., Injectable polysaccharide hydrogels reinforced with cellulose nanocrystals: morphology, rheology, degradation and cytotoxicity. *Biomacromolecules* **2013**, *14* (12), 4447 - 4455.
114. Yang, X.; Cranston, E. D., Chemically cross-linked cellulose nanocrystal aerogels with shape recovery and superabsorbent properties. *Chemistry of Materials* **2014**, *26* (20), 6016 - 6025.
115. Yang, X.; Shi, K.; Zhitomirsky, I.; Cranston, E. D., Cellulose nanocrystal aerogels as universal 3D lightweight substrated for supercapacitor materials. *Advanced Materials* **2015**, *27* (40), 6104 - 6109.
116. Conley, K.; Whitehead, M. A.; van de Ven, T. G. M., Chemically peeling layers of cellulose nanocrystals by periodate and chlorite oxidation. *Cellulose* **2016**, *23* (3), 1553 - 1563.
117. Yang, H.; Tejado, A.; Alam, N.; Antal, M.; van de Ven, T. G. M., Films prepared from electrosterically stabilized nanocrystalline cellulose. *Langmuir* **2012**, *28* (20), 7834 - 7842.
118. Yang, H.; van de Ven, T. G. M., Preparation of hairy cationic nanocrystalline cellulose. *Cellulose* **2016**, *23* (3), 1791 - 1801.
119. Chen, D.; van de Ven, T. G. M., Morphological changes of sterically stabilized nanocrystalline cellulose after periodate oxidation. *Cellulose* **2016**, *23* (2), 1051 - 1059.

120. Yang, H.; Chen, D.; van de Ven, T. G. M., Preparation and characterization of sterically stabilized nanocrystalline cellulose obtained by periodate oxidation of cellulose fibers. *Cellulose* **2015**, *22* (3), 1743 - 1752.
121. Fitch, R. M., Colloids. In *Encyclopedia of Polymer Science and ENgineering*, Mark, H. F.; Bikales, N. M.; Overberger, C. G.; Menges, G.; Kroschwitz, J. I., Eds. John Wiley and Sons: 1985; Vol. 3.
122. van Nieuwenhuyzen, W.; Szuhaj, B. F., Effects of lecithins and proteins on the stability of emulsions. *European Journal of Lipid Science and Technology* **1998**, *100* (7), 282 - 291.
123. Clogston, J. D.; Patri, A. K., Zeta Potential Measurement. In *Characterization of nanoparticles intended for drug delivery*, McNeil, S. E., Ed. Methods in Molecular Biology (Methods and Protocols) Humana Press: 2011; p 70.
124. Araki, J., Electrostatic or steric? - preparations and characterizations of well-dispersed systems containing rod-like nanowhiskers of crystalline polysaccharides. *Soft Matter* **2013**, *9* (16), 4125 - 4141.
125. Araki, J.; Wada, M.; Kuga, S.; Okano, T., Flow properties of microcrystalline cellulose suspension prepared by acid treatment of native cellulose. *Colloids and Surfaces A: Physicochemical and Engineering Aspects* **1998**, *142* (1), 75 - 82.
126. Marchessault, R. H.; Morehead, F. F.; Walter, N. M., Liquid crystal systems from fibrillar polysaccharides. *Nature* **1959**, *184* (-), 632 - 633.
127. Dong, X. M.; Revol, J.-F.; Gray, D. G., Effect of microcrystallite preparation conditions on the formation of colloid crystals of cellulose. *Cellulose* **1998**, *5* (1), 19 - 32.
128. Hasani, M.; Cranston, E. D.; Westman, G.; Gray, D. G., Cationic surface functionalization of cellulose nanocrystals. *Soft Matter* **2008**, *4* (11), 2238 - 2244.

129. Araki, J.; Wada, M.; Kuga, S.; Okano, T., Influence of surface charge on viscosity behavior of cellulose microcrystal suspension. *Journal of Wood Science* **1999**, *45* (3), 258 - 261.
130. Araki, J.; Wada, M.; Kuga, S.; Okano, T., Birefringent glassy phase of a cellulose microcrystal suspension. *Langmuir* **2000**, *16* (6), 2413 - 2415.
131. Montanari, S.; Roumani, M.; Heux, L.; Vignon, M. R., Topochemistry of carboxylated cellulose nanocrystals resulting from TEMPO-mediated oxidation. *Macromolecules* **2005**, *38* (5), 1665 - 1671.
132. Habibi, Y.; Chanzy, H.; Vignon, M. R., TEMPO-mediated surface oxidation of cellulose whiskers. *Cellulose* **2006**, *13* (6), 679 - 687.
133. Nordenström, M.; Fall, A.; Nyström, G.; Wågberg, L., Formation of colloidal nanocellulose glasses and gels. *Langmuir* **2017**, *33* (38), 9772 - 9780.
134. Azzam, F.; Siqueira, E.; Fort, S.; Hassaini, R.; Pignon, F.; Travelet, C.; Putaux, J.-L.; Jean, B., Tunable aggregation and gelation of thermoresponsive suspensions of polymer-grafted cellulose nanocrystals. *Biomacromolecules* **2016**, *17* (6), 2112 - 2119.
135. Heux, L.; Chauve, G.; Bonini, C., Nonflocculating and chiral nematic self ordering of cellulose nanocrystals in nonpolar solvents. *Langmuir* **2000**, *16* (21), 8310 - 8212.
136. Bonini, C.; Heux, L.; Cavaille, J. Y.; Lindner, P.; Dewhurst, C.; Terech, P., Rodlike cellulose whiskers coated with surfactant: a small-angle neutron scattering characterization. *Langmuir* **2002**, *18* (8), 3311 - 3314.
137. Elazzouzi-Hafraoui, S.; Putaux, J.-L.; Heux, L., Self-assembling and chiral nematic properties of organophilic cellulose nanocrystals. *The Journal of Physical Chemistry B* **2009**, *113* (32), 11069 - 11075.
138. Miao, C.; Hamad, W. Y., Cellulose reinforced polymer composites and nanocomposites: a critical review. *Cellulose* **2013**, *20* (5), 2221 - 2262.

139. Mariano, M.; El Kissi, N.; Dufresne, A., Cellulose nanocrystals and related nanocomposites: Review of some properties and challenges. *Journal of Polymer Science* **2014**, *52* (12), 791 - 806.
140. Revol, J. F.; Bradford, H.; Giasson, J.; Marchessault, R. H.; Gray, D. G., Helicoidal self-ordering of cellulose microfibrils in aqueous suspension. *International Journal of Biological Macromolecules* **1992**, *14* (3), 170 - 172.
141. Khandelwal, M.; Windle, A. H., Self-assembly of bacterial and tunicate cellulose nanowhiskers. *Polmer* **2013**, *54* (19), 5199 - 5206.
142. Dumanli, A. G.; van der Kooij, H. M.; Kamita, G.; Reisner, E.; Baumberg, J. J.; Steiner, U.; Vignolini, S., Digital color in cellulose nanocrystals. *ACS applied materials and interfaces* **2014**, *6* (15), 12302 - 12306.
143. Sugiyama, J.; Chanzy, H.; Maret, G., Orientation of cellulose microcrystals by strong magnetic fields. *Macromolecules* **1992**, *25* (16), 4232 - 4234.
144. Frka-Petesic, B.; Sugiyama, J.; Kimura, S.; Chanzy, H.; Maret, G., Negative diamagnetic anisotropy and birefringence of cellulose nanocrystals. *Macromolecules* **2015**, *48* (24), 8844 - 8857.
145. Bordel, D.; Putaux, J.-L.; Heux, L., Orientation of native cellulose in an electric field. *Langmuir* **2006**, *22* (11), 4899 - 4901.
146. Frka-Petesic, B.; Radavidson, H.; Jean, B.; Heux, L., Dynamically controlled iridescence of cholesteric cellulose nanocrystal suspensions using electric fields. *Advanced Materials* **2017**, *29* (11), - n/a.
147. Lindh, J.; Carlsson, D. O.; Strømme, M.; Mihranyan, A., Convenient one-pot formation of 2,3-dialdehyde cellulose beads via periodate oxidation of cellulose in water. *Biomacromolecules* **2014**, *15* (5), 1928 - 1932.

148. Nevell, T. P., Determination of reducing end-groups. In *Methods in Carbohydrate Chemistry Vol III Cellulose*, Whistler, R. L.; Green, J. W.; BeMiller, J. N.; Wolfrom, M. L., Eds. Academic Press: 1963; Vol. 3, pp 43 - 48.
149. Kim, U.-J.; Kuga, S., Reactive interaction of aromatic amines with dialdehyde cellulose gel. *Cellulose* **2000**, *7*, 287 - 297.
150. Aimin, T.; Hongwei, Z.; Gang, C.; Guohui, X.; Wenzhi, L., Influence of ultrasound treatment on accessibility and regioselective oxidation reactivity of cellulose. *Ultrasonics Sonochemistry* **2005**, *12*, 467- 472.
151. RoyChowdhury, P.; Kumar, V., Fabrication and evaluation of porous 2,3-dialdehydecellulose membrane as a potential biodegradable tissue-engineering scaffold. *Journal of Biomedical Materials Research A* **2006**, *76A* (2), 300 - 309.
152. Amer, H.; Nypelö, T.; Sulaeva, I.; Bacher, M.; Henniges, U.; Potthast, A.; Rosenau, T., Synthesis and characterization of periodate-oxidized polysaccharides: dialdehyde xylan (DAX). *Biomacromolecules* **2016**, *17* (9), 2972 - 2980.
153. Zhao, H.; Heindel, N. D., Determination of degree of substitution of formyl groups in polyaldehyde dextran by the hydroxylamine hydrochloride method. *Pharmaceutical Research* **1991**, *8* (3), 400 - 402.
154. Larsson, P. A.; Gimåker, M.; Wågberg, L., The influence of periodate oxidation on the moisture sorptivity and dimensional stability of paper. *Cellulose* **2008**, *15* (6), 837 - 847.
155. Cervin, N. T.; Johansson, E.; Larsson, P. A.; Wågberg, L., Strong, water-durable, and wet-resilient cellulose nanofibril-stabilized foams from oven drying. *ACS Applied Materials and Interfaces* **2016**, *8* (18), 11682 - 11689.
156. Siller, M.; Amer, H.; Bacher, M.; Roggenstein, W.; Rosenau, T.; Potthast, A., Effects of periodate oxidation on cellulose polymorphs. *Cellulose* **2015**, *22* (4), 2245 - 2261.

157. Sulaeva, I.; Klinger, K. M.; Amer, H.; Henniges, U.; Rosenau, T.; Potthast, A., Determination of molar mass distributions of highly oxidized dialdehyde cellulose by size exclusion chromatography and asymmetric flow field-flow fractionation. *Cellulose* **2015**, *22* (6), 3569 - 3581.
158. Falcoz-Vigne, L.; Ogawa, Y.; Molina-Boisseau, S.; Nishiyama, Y.; Meyer, V.; Petit-Conil, M.; Mazeau, K.; Heux, L., Quantification of a tightly adsorbed monolayer of xylan on cellulose surface. *Cellulose* **2017**, *24* (9), 3725 - 3739.
159. Pääkkö, M.; Ankerfors, M.; Kosonen, H.; Nykänen, A.; Ahola, S.; Österberg, M.; Ruokolainen, J.; Laine, J.; Larsson, P. T.; Ikkala, O.; Lindström, T., Enzymatic hydrolysis combined with mechanical shearing and high-pressure homogenization for nanoscale cellulose fibrils and strong gels. *Biomacromolecules* **2007**, *8* (6), 1934 - 1941.
160. Green, J. W., Determination of carbonyl groups. In *Methods in Carbohydrate Chemistry Vol III Cellulose*, Whistler, R. L.; Green, J. W.; BeMiller, J. N.; Wolfrom, M. L., Eds. Academic Press: 1963; Vol. 3, pp 49 - 54.
161. Von Ströle, U., Bestimmung der carbonylgruppen in oxydierter cellulose. *Macromolecular Chemistry and Physics* **1956**, *20* (1), 19 - 36.
162. Cantley, M.; Hough, L.; Pittet, A. O., The non-malapradian oxidation of carbohydrates and related compounds by periodate. *Journal of the Chemical Society* **1963**, - (-), 2527 - 2535.
163. Münster, L.; Vícha, J.; Klofáč, J.; Masař, M.; Kucharczyk, P.; Kuřitka, I., Stability and aging of solubilized dialdehyde cellulose. *Cellulose* **2017**, *24* (7), 2753 - 2766.
164. Fumagalli, M.; Ouhab, D.; Molina-Boisseau, S.; Heux, L., Versatile gas-phase reactions for surface to bulk esterification of cellulose aerogels. *Biomacromolecules* **2013**, *14* (9), 3246 - 3255.

165. Fumagalli, M.; Sanchez, F.; Boisseau, S. M.; Heux, L., Gas-phase esterification of cellulose nanocrystal aerogels for colloidal dispersion in apolar solvents. *Soft Matter* **2013**, *9* (47), 11309 - 11317.
166. Benítez, A. J.; Walther, A., Cellulose nanofibril nanopapers and bioinspired nanocomposites: a review to understand the mechanical property space. *Journal of Materials Chemistry A* **2017**, *5* (31), 16003 - 16024.
167. Matsumura, H.; Sugiyama, J.; Glasser, W. G., Cellulosic nanocomposites. 1. Thermally deformable cellulose hexanoates from heterogeneous reaction. *Journal of Applied Polymer Science* **2000**, *78* (13), 2242 - 2253.
168. Leguy, J.; Nishiyama, Y.; Jean, B.; Heux, L., Accurate degree of oxidation measurement of periodate oxidized cellulose by CP/MAS <sup>13</sup>C NMR. *ACS Sustainable Chemistry and Engineering* **2018**, *To be published*.
169. Kim, U.-J.; Kuga, S.; Wada, M.; Okano, T.; Kondo, T., Periodate oxidation of crystalline cellulose. *Biomacromolecules* **2000**, *1*, 488 - 492.
170. Larsson, P. A.; Berglund, L. A.; Wågberg, L., Highly ductile fibres and sheets by core-shell structuring of the cellulose nanofibrils. *Cellulose* **2014**, *21*, 323 - 333.
171. Schmidt-Rohr, K.; Spiess, H. W., *Multidimensional solid-state NMR and polymers*. Academic Press: 1994.
172. Schmidt-Rohr, K.; Spiess, H. W., Correlation of structure, mobility, and morphological information in heterogeneous polymer materials by two-dimensional wideline-separation NMR spectroscopy. *Macromolecules* **1992**, *25* (12), 3273 - 3277.
173. Landfester, K.; Boeffel, C.; Lambla, M.; Spiess, H. W., Characterization of interfaces in core-shell polymers by advanced solid-state NMR methods. *Macromolecules* **1996**, *29* (18), 5972 - 5980.

174. Radloff, D.; Boeffel, C.; Spiess, H. W., Cellulose and cellulose/poly (vinyl alcohol) blends. 2. Water organization revealed by solid-state NMR spectroscopy. *Macromolecules* **1996**, *29* (5), 1528 - 1534.
175. Leguy, J.; Diallo, A.; Putaux, J.-L.; Nishiyama, Y.; Heux, L.; Jean, B., Periodate oxidation followed by NaBH<sub>4</sub> reduction converts microfibrillated cellulose into sterically-stabilized neutral cellulose nanorod suspensions. *Langmuir* **2018**, *To be published*.
176. Berriot, J.; Montes, H.; Lequeux, F.; Long, D.; Sotta, P., Evidence for the shift of the glass transition near the particles in silica-filled elastomers. *Macromolecules* **2002**, *35* (26), 9756 - 9762.
177. Molberg, M.; Crespy, D.; Rupper, P.; Nüesch, F.; Månson, J.-A. E.; Löwe, C.; Opris, D. M., High breakdown field dielectric elastomer actuators using encapsulated polyaniline as high dielectric constant filler. *Advance Functional Materials* **2010**, *20* (19), 3280 - 3291.
178. Huang, X.; Jiang, P., Core-shell structured high-k polymer nanocomposites for energy storage and dielectric applications. *Advanced Materials* **2015**, *27* (3), 546 - 554.
179. Klemm, D.; Kramer, F.; Moritz, S.; Lindstrom, T.; Ankerfors, M.; Gray, D.; Dorris, A., Nanocelluloses: a new family of nature-based materials. *Angewandte Chemie-International Edition* **2011**, *50* (24), 5438 - 5466.
180. Moon, R. J.; Martini, A.; Nairn, J.; Simonsen, J.; Youngblood, J., Cellulose nanomaterials review: structure, properties and nanocomposites. *Chemical Society Reviews* **2011**, *40* (7), 3941 - 3994.
181. Eichhorn, S. J., Cellulose nanowhiskers: promising materials for advanced applications. *Soft Matter* **2011**, *7* (2), 303 - 315.
182. Cherhal, F.; Cousin, F.; Capron, I., Structural description of the interface of pickering emulsions stabilized by cellulose nanocrystals. *Biomacromolecules* **2016**, *17* (2), 496 - 502.

183. Kalashnikova, I.; Bizot, H.; Cathala, B.; Capron, I., New pickering emulsions stabilized by bacterial nanocrystals. *Langmuir* **2011**, *27* (12), 7471 - 7479.
184. Frka-Petesic, B.; Jean, B.; Heux, L., First experimental evidence of a giant permanent electric-dipole moment in cellulose nanocrystals. *Europhysics Letters* **2014**, *107* (2), 28006-1 - 28006-5.
185. De France, K. J.; Yager, K. G.; Hoare, T.; Cranston, E. D., Cooperative ordering and kinetics of cellulose nanocrystal alignment in a magnetic field. *Langmuir* **2016**, *32* (30), 7564 - 7571.
186. Frka-Petesic, B.; Guidetti, G.; Kamita, G.; Vignolini, S., Controlling the photonic properties of cholesteric cellulose nanocrystal films with magnets. *Advanced Materials* **2017**, *29* (32), - n/a.
187. Lagerwall, J. P. F.; Schutz, C.; Salajkova, M.; Noh, J.; Park, J. H.; Scalia, G.; Bergstrom, L., Cellulose nanocrystal-based materials: from liquid crystal self-assembly and glass formation to multifunctional thin films. *Npg Asia Materials* **2014**, *6* (80), 1 - 12.
188. Chauve, G.; Fraschini, C.; Jean, B., Separation of cellulose nanocrystals. In *Handbook of green materials: 1 Bionanomaterials: separation processes, characterization and properties*, World Scientific: 2014; pp 73 - 87.
189. Zhou, Q.; Brumer, H.; Teeri, T. T., Self-organization of cellulose nanocrystals adsorbed with xyloglucan oligosaccharide–poly(ethylene glycol)–polystyrene triblock copolymer. *Macromolecules* **2009**, *42* (15), 5430 - 5432.
190. Ljungberg, N.; Bonini, C.; Bortolussi, F.; Boisson, C.; Heux, L.; Cavaille, J. Y., New nanocomposite materials reinforced with cellulose whiskers in atactic polypropylene: effect of surface and dispersion characteristics. *Biomacromolecules* **2005**, *6* (5), 2732 - 3739.
191. Ljungberg, N.; Cavallé, J. Y.; Heux, L., Nanocomposites of isotactic polypropylene reinforces with rod-like cellulose whiskers. *Polymer* **2006**, *47* (18), 6285 - 6292.

192. Winter, H. T.; Cerclier, C.; Delorme, N.; Bizot, H.; Quemener, B.; Cathala, B., Improved colloidal stability of bacterial cellulose nanocrystal suspensions for the elaboration of spin-coated cellulose-based model surfaces. *Biomacromolecules* **2010**, *11* (11), 3144 - 3151.
193. Dammak, A.; Quémener, B.; Bonnin, E.; Alvarado, C.; Bouchet, B.; Villares, A.; Moreau, C.; Cathala, B., Exploring architecture of xyloglucan cellulose nanocrystal complexes through enzyme susceptibility at different adsorption regimes. *Biomacromolecules* **2015**, *16* (2), 589 - 596.
194. Araki, J.; Mishima, S., Steric stabilization of “charge-free” cellulose nanowhiskers by grafting of poly (ethylene glycol). *Molecules* **2014**, *20* (1), 169 - 184.
195. Habibi, Y.; Goffin, A.-L.; Schiltz, N.; Duquesne, E.; Dubois, P.; Dufresne, A., Bionanocomposites based on poly([varepsilon]-caprolactone)-grafted cellulose nanocrystals by ring-opening polymerization. *Journal of Materials Chemistry* **2008**, *18* (41), 5002 - 5010.
196. Lonnberg, H.; Fogelstrom, L.; Berglund, M.; Malmstrom, E.; Hult, A., Surface grafting of microfibrillated cellulose with poly(epsilon-caprolactone) - Synthesis and characterization. *European Polymer Journal* **2008**, *44* (9), 2991 - 2997.
197. Goussé, C.; Chanzy, H.; Excoffier, G.; Soubeyrand, L.; Fleury, E., Stable suspensions of partially silylated cellulose whiskers dispersed in organic solvents. *Polymer* **2002**, *43* (9), 2645 - 2651.
198. Sheikhi, A.; van de Ven, T. G., Colloidal aspects of Janus-like hairy cellulose nanocrystalloids. *Current Opinion in Colloid & Interface Science* **2017**, *29* (-), 21 - 31.
199. Shimizu, M.; Saito, T.; Nishiyama, Y.; Iwamoto, S.; Yano, H.; Isogai, A.; Endo, T., Fast and robust nanocellulose width estimation using turbidimetry. *Macromolecular Rapid Communications* **2016**, *37* (19), 1581 - 1586.

200. Tanaka, R.; Kuribayashi, T.; Ogawa, Y.; Saito, T.; Isogai, A.; Nishiyama, Y., Ensemble evaluation of polydisperse nanocellulose dimensions: rheology, electron microscopy, X-ray scattering and turbidimetry. *Cellulose* **2017**, *24* (8), 3231 - 3242.
201. Corrêa, A. C.; de Moraes Teixeira, E.; Pessan, L. A.; Mattoso, L. H. C., Cellulose nanofibers from curaua fibers. *Cellulose* **2010**, *17* (6), 1183 - 1192.
202. Navon, Y.; Radavidson, H.; Putaux, J.-L.; Jean, B.; Heux, L., pH-sensitive interaction between cellulose nanocrystals and DOPC liposomes. *Biomacromolecules* **2017**, *18* (9), 2918 - 2927.
203. Borch, R. F.; Bernstein, M. D.; Durst, H. D., The cyanohydridoborate anion as a selective reducing agent. *Journal of the American Chemical Society* **1971**, *93* (12), 2897 - 2904.
204. Chimpibul, W.; Nagashima, T.; Hayashi, F.; Nakajima, N.; Hyon, S.-H.; Matsumura, K., Dextran oxidized by a malaprade reaction shows main chain scission through a maillard reaction triggered by schiff base formation between aldehydes and amines. *Polymer Chemistry* **2016**, *54* (14), 2254 - 2260.
205. Matsumura, K.; Nakajima, N.; Sugai, H.; Hyon, S.-H., Self-degradation of tissue adhesive based on oxidized dextran and poly-l-lysine. *Carbohydr Polym* **2014**, *113* (-), 32 - 38.
206. Wang, H.-Y.; Qian, H.; Yao, W.-R., Melanoidins produced by the Maillard reaction: Structure and biological activity. *Food Chemistry* **2011**, *128* (3), 573 - 584.
207. Huang, T.-C.; Soliman, A. A.; Rosen, R. T.; Ho, C.-T., Studies on the Maillard browning reaction between aspartame and glucose. *Food Chemistry* **1987**, *24* (3), 187 - 196.
208. Leguy, J.; Nishiyama, Y.; Jean, B.; Heux, L., Synthesis an characterization of all-cellulose thermoplastics. *Macromolecules* **2018**, *To be published*.

## **Résumé**

La cellulose, abondante et renouvelable, offre une alternative biosourcée intéressante pour remplacer les thermoplastiques pétrosourcés très présents dans la vie courante. Cependant, elle ne peut être utilisée dans les procédés de thermoformage de l'industrie de la plasturgie car sa température de fusion est supérieure à sa température de dégradation. Des dérivés comme l'acétate de cellulose montrent un caractère thermoplastique plus affirmé, avec des températures de transition vitreuse et de fusion plus basses que celles de la cellulose, mais nécessitent néanmoins l'usage de plastifiants externes pour être mis en forme. Ces plastifiants peuvent à terme migrer en dehors des matériaux, provoquant une dégradation des propriétés et des problèmes environnementaux si ces molécules sont dangereuses.

Le travail présenté ici propose de remplacer la plastification externe par une plastification interne qui consiste à greffer les plastifiants sur les macromolécules, évitant ainsi toute migration. Pour cela, une modification en deux étapes de la cellulose a été imaginée : une oxydation au périodate pour augmenter la flexibilité du squelette cellulosique et introduire des groupements aldéhyde donnant lieu à la cellulose oxydée périodate (POC), suivie d'un greffage des molécules plastifiantes sur ces aldéhydes.

Une étude complète de l'oxydation de la cellulose au périodate a d'abord été réalisée en faisant varier de nombreux paramètres tels que la quantité d'oxydant, le temps de réaction ou la température. Elle a permis de préciser les conditions optimales de contrôle du degré d'oxydation (DO) qui est un paramètre clé dans la compréhension des relations structure-propriétés au sein des matériaux réalisés à partir de POC. En particulier, une méthode de caractérisation fiable et précise du DO par résonance magnétique nucléaire du solide ( $^{13}\text{C}$  CP-MAS RMN) a été développée et comparée aux méthodes de la littérature. Une réduction de la POC a ensuite permis de générer des nanobâtonnets colloïdaux chevelus, non chargés mais stables en suspension aqueuse, qui ont été caractérisés par une combinaison de techniques (diffusion de rayonnement, microscopie électronique en transmission et turbidimétrie). Par ailleurs, le séchage de ces suspensions produit des films thermoplastiques avec une structuration nanocomposite de type cœur-écorce. Enfin, grâce à des réactions d'amination réductrice avec différentes amines, de nouveaux matériaux thermoplastiques ont été obtenus. Les propriétés ultrastructurales et thermomécaniques de ces différents matériaux ont été caractérisées par des méthodes telles que la RMN, l'analyse mécanique dynamique, la calorimétrie différentielle à balayage ou l'analyse thermogravimétrique (ATG). Ces résultats montrent que les matériaux issus de ces modifications possèdent une  $T_g$  inversement proportionnelle au DO, comprise entre 122 et 65 °C selon le DO et le type de modification. Notre stratégie est donc prometteuse pour la fabrication de matériaux thermoplastiques transformables élaborés à partir de cellulose.

## **Summary**

Cellulose, an abundant and renewable polymer, offers an interesting biosourced alternative to replace petrosourced thermoplastics commonly used in our everyday life. However, cellulose cannot be used in industrial thermoforming processes since its melting temperature is higher than its degradation temperature. Derivatives such as cellulose acetate show glass transition and melting temperatures below the thermal decomposition but still require the addition of external plasticizers to be processable. These plasticizers can exude over time, making the materials brittle and causing environmental issues due to the release of potentially toxic molecules.

The present work proposes to introduce internal plasticization of cellulose, by increasing both the flexibility of the chains and the free volume using a grafting strategy, thus preventing exudation. To achieve this goal, a two-steps strategy was followed: first, a periodate oxidation was performed to cleave the glucose ring and generate aldehyde groups, resulting in periodate oxidized cellulose (POC). Second, the highly reactive aldehyde groups were used to graft plasticizing agents.

The periodate oxidation of cellulose was first studied by varying parameters such as the amount of oxidant, the reaction time or the temperature, in order to precisely map the reaction conditions leading to a controlled degree of oxidation. To characterize POC samples, an accurate and reliable quantification method based on solid-state nuclear magnetic resonance ( $^{13}\text{C}$  CP-MAS NMR) has been developed and compared to other methods from the literature. The reduction of POC led to colloiddally stable hairy neutral nanorods suspensions, which were characterized by a combination of structural investigation techniques (light and X-ray scattering, transmission electron microscopy and turbidimetry). Casting of the suspensions led to thermoplastic films with a core-shell nanocomposite structure. Reductive amination of POC with different amines also led to thermoplastic materials. The thermo-mechanical properties of all these materials were studied by solid-state NMR, dynamic mechanical analysis, differential scanning calorimetry and thermogravimetric analysis. Results show that materials produced from this strategy have a  $T_g$  inversely proportional to DO, between 122 and 65 °C, depending on the DO and the modification. This strategy is promising for the synthesis of processable thermoplastic materials from cellulose.